DEPARTMENT OF THE NAVY
NAVAL SHIP RESEARCH AND DEVELOPMENT CENTER
WASHINGTON, D. C. 20007

EXPERIMENTAL PERFORMANCE AND STEERING CHARACTERISTICS OF CYCLOIDAL PROPELLERS

by

N.L. Ficken and Mary C. Dickerson

July 1969 Report 2983

TABLE OF CONTENTS

LIST OF FIGURES

Page

NOTATION

Symbol	Definition	Dimensions
b	Blade length	feet
c	Blade chord	feet
D	Orbit diameter	feet
F	Magnitude of resultant force vector	pounds
J	Speed coefficient V_A/nD	
K_Q	Torque coefficient $Q/\rho n^2 bD^4$	
K_S	Side force coefficient $S/\rho n^2 bD^3$	
K_T	Thrust coefficient $T/\rho n^2 bD^3$	
n	Rotational speed	$rev\text{-}sec^{-1}$
p	Propeller pitch	feet
P/D	Pitch ratio	
Q	Torque	pound-foot
R_n	Reynolds number $c\sqrt{V_A^2+(\pi nD)^2}/\nu$	
S	Side force	pounds
T	Thrust	pounds
V_A	Inflow velocity	$feet\text{-}second^{-1}$
β	Blade angle	degrees
δ	Angle of resultant force vector	degrees
η_o	Propeller efficiency $K_T/K_Q \cdot J/2\pi$	
θ	Orbit angle	degrees
ν	Kinematic viscosity	$feet^2\text{-}second^{-1}$
ρ	Density	$pounds\text{-}sec^2\text{-}ft^{-4}$
ϕ	Steering angle	degrees

ABSTRACT

This report presents performance and steering characteristics of cycloidal propellers obtained from model tests for a series of cycloidal motions with pitch ratios ranging from 0.4π to 0.9π. Measured quantities included the thrust, torque, and side force. The tests showed that the direction and magnitude of the resultant force varies with loading and steering. For small steering angles, no significant effect of steering was observed on thrust or on efficiency. Most of the results presented here are for a six-bladed cycloidal propeller. Some performance characteristic curves obtained for a propeller with two and three blades are also included for comparison.

ADMINISTRATIVE INFORMATION

The work reported herein was conducted under the auspices of the Ship Powering Division, Propeller Branch, at the Naval Ship Research and Development Center and was funded by the Naval Ship Systems Command Subproject S-F013 07 10, Task 3744, and S4632001, Task 12499.

INTRODUCTION

The cycloidal, or vertical axis, propeller is characterized by a number of blades projecting from the surface of a ship hull into the flow and orbiting about an axis normal to the hull surface. The angle of attack of the blades is varied in a programmed manner to produce a resultant force in any direction normal to the axis of rotation. The name cycloidal propeller derives from the cycloidal path of the blades, which results from the combined orbital motion of the blades and straight-line motion of the vessel.[1]

In the most familiar case, the propeller is installed in the bottom of a ship hull. A number of ships also use cycloidal propellers installed in transverse tunnels through the hull as lateral thrust units.[2] Suggestions have also been made to use cycloidal propellers for propulsion and control,

---

[1]References are listed on page 65.

or control only, of submersible vehicles. In this case, the axis of rotation could be either vertical to develop transverse controlling forces or horizontal for vertical control.

The history of the cycloidal propeller dates back to 1870,[3-8] although reference to similar devices appeared as early as 1681.[8] Little was accomplished however until the development of the Kirsten-Boeing propeller in the United States[9] and the Voith-Schneider propeller in Germany. In both designs, the direction of the resultant force can be changed without changing rotation. The Voith-Schneider propeller can also change pitch and thus vary the magnitude of the resultant force available at a given rpm whereas the Kirsten-Boeing propeller has fixed pitch. The Voith-Schneider propeller has found wide application in European lake and river vessels, but the Kirsten-Boeing propeller has received only limited use.

Variable-pitch cycloidal propellers have been used extensively in Europe on minesweepers, tugs, river ferries, and other vessels that require good maneuvering qualities or the ability to develop large forces in any direction at low or high speed. The principal applications in the United States have been the Army LTI and BDL and the Navy LCU 1620 and 1625, as well as the forthcoming T-AGOR.[10] They are also potentially useful for auxiliary control or for propulsion and control of submerged vehicles.

In recent years, the theory of cycloidal propellers has been investigated by Isay[11-14] in Germany, by Taniguchi[15-17] in Japan, by Haberman[18-19] in the United States, and more recently by Sparenberg[20] in the Netherlands. Experimental work has been conducted by Nakonechny[5-7] and by Ficken and Dickerson[7] in the United States, and by Van Manen[21] in the Netherlands.

This report presents the results of tests with a systematic cycloidal propeller series. These tests were an outgrowth of the tests conducted by Nakonechny in 1960.[5,6] Reference 5 presented open-water curves obtained in tests using a six-bladed, 6.3-in., orbit-diameter model propeller. The modified cycloidal and sinusoidal blade motions were generated by various sets of cams which had been constructed for prior evaluation test programs. For the blade motions and blade configurations used, those tests showed that the cycloidal propeller achieved lower efficiency than comparably loaded screw propellers; like the screw propeller, however, their increased pitch produced higher peak efficiency.

The present results were obtained from a series of tests which began in 1965. Use of a 9-in., orbit-diameter model[6] extended the range of test variables obtainable with the 6.3-in. model in that a greater range of pitch capability and a higher Reynolds number range were achieved. Six pure cycloidal blade motions were tested with six, three, and two blades.

Application of cycloidal propellers has been limited because they are less efficient than screw propellers under free-running conditions. Most theoretical and experimental work undertaken has been to predict and improve the efficiency of free-running cycloidal propellers. Very little has been done, however, to determine what forces other than forward thrust are available, or to demonstrate how best to use cycloidal propellers for maneuvering. The Voith Company has presented an approximate graphical method[22] for determining the direction of the resultant force as a function of the pitch, steering angle, and speed coefficient. The effectiveness of this method will be discussed later in this report. There is no indication, however, in Reference 22 or elsewhere of the magnitude of the resultant force at nonzero steering angles. To fill this gap and furnish information to prospective users, the cycloidal propeller investigations at this Center have included measurements of side force as well as the usual thrust and torque.

The results of the test series are presented as curves of thrust, torque, and side force coefficients as functions of pitch ratio, speed coefficient, and steering angle. Curves of efficiency as a function of pitch ratio, speed coefficient, and number of blades are presented for the case of zero steering angle. Polar diagrams are included for each pitch ratio to show the magnitude and direction of the resultant force coefficient at any combination of speed and steering angle.

CYCLOIDAL PROPELLER BLADE MOTIONS

Figure 1a illustrates the cycloidal path of a blade when the peripheral speed ωR is twice the speed of advance V_A. The advance coefficient ($J=V_A/nD$), which corresponds to the advance per revolution of the propeller, is 1.571 for this case (i.e., 0.5π). If the blade angles are programmed as a function of the orbit angle θ to be always tangent to that cycloidal path, the resulting program is then designated a cycloidal blade motion

with pitch ratio equal to 0.5π. The physical criterion for the cycloidal motion, as shown in Figure 1b, is that a normal to the blade at all times intersects a point on the 0-180 deg reference axis. This point is referred to here as the control center. For this example (pitch ratio = 0.5π), the control center is located at a radius of one-half that of the orbit circle. The propeller would produce nearly zero thrust in the zero slip condition depicted here. The operating J for cruising would be smaller and thus the blades would not be tangent to the shortened cycloidal path, but would be at an angle of attack to the path.

The blade motions of full-scale cycloidal propellers are developed by linkages which permit the control center radius and angular position to be varied continuously. Steering is accomplished by varying the angular position of the control center. Note that the control center is a geometrical center and need not have any direct connection with the linkage. Linkages for cycloidal blade motion are possible, and the first few propellers produced by the Voith Company had such a linkage. However it was not practical for pitch ratios above 0.62π because of mechanical problems. All present-day cycloidal propellers therefore have motions which differ slightly from the true cycloidal motion. The motion is modified by effectively reducing the pitch during that part of the cycle where the blade angle changes from positive to negative. In some designs, the blade angles are increased in the negative half of the cycle to compensate for the accelerated flow in the wake of the forward blades. Neither of these effects has been evaluated in this test series, but in general it seems that the modification to reduce mechanical loading on the linkage tends to decrease efficiency, whereas compensation tends to increase efficiency. The net effect is probably quite small.

The blade motion of the model propeller is controlled by a set of cams. The operation of the model will be described in detail in the next section. This test series was conducted with six sets of cams to produce unmodified cycloidal blade motion at six pitch ratios from 0.4π to 0.9π. Curves of blade angle versus orbit angle are shown in Figure 2.

Figure 3a shows how steering angle is defined for cycloidal motions and the approximate direction of the resultant force. In the nominal zero condition shown on Figure 1, the control center is on the reference

(0-180 deg) axis. By the definition of cycloidal motion given previously, the chord of each blade is always normal to a line connecting its axis and the control center. Pitch ratio is defined as π times the ratio of control center radius to orbit radius. To apply a steering force, the control center is moved off the reference axis. The resultant force is then rotated by roughly the steering angle ϕ in the same direction. The pitch ratio is still defined in terms of the control center radius, and the blades are normal to the line connecting their axes and the control center. The resulting motion is then that which results from a horizontal shift of the blade motion curve as shown in Figure 3b.

EXPERIMENTAL EQUIPMENT AND PROCEDURES

The construction of the 9-in., orbit-diameter propeller model used for these tests is shown in Figure 4. This model was designed and built by Nakonechny. A full description of the device can be found in Reference 6. The major components of the propeller include a rotor which carries the blades; two circular housings, one secured to the test vehicle, the other supported by the first and adjustable to vary steering angle although it is stationary while the propeller is operating; and two cams which control the blade angles as a function of orbit angle. The rotor, (Figure 5) contains six ball-bearing supported blade spindles. The blade angle, which is defined in Figure 1b, depends on the angular position of the cam follower crank arm secured to the upper end of each spindle.

Two flat cams are installed in the stationary (not revolving) propeller housing (see Figures 6 and 7). The rollers at the end of each cam follower arm ride in the track between the two cams. The instantaneous angle of the follower arm, and hence the blade angle, is governed by the radial distance from the main shaft axis to the center of the track at the rollers (about 17 deg behind the orbital position of the blade spindle axis). Six sets of cams were used in these tests to produce the cycloidal blade motions shown in Figure 2. The curves of blade angle versus orbit angle shown in Figure 2 represent the nominal zero steering angle condition. Steering is accomplished on the model by rotating the propeller housing away from this position by an angle equal to the steering angle and in the same direction. This causes a corresponding shift in the blade motion

curve as indicated in Figure 3b. The sign convention used is shown in Figure 3. Positive steering angle represents rotation of the housing in a direction opposite the direction of rotation of the rotor, or counterclockwise for this right-hand rotating propeller model.

The blades are readily removable. This facilitates the variation of blade shape and number of blades and also permits the measurement of tare loads with the model in the water and the entire mechanism operating, except that the blades are removed. The propeller is shown with a full complement of six blades in Figure 8. As indicated in Figure 9, when the blades are removed for measurement of tare loads, or when the propeller is running with less than six blades, flat disks with the dimensions of the blade palms are inserted to smooth out the surface of the rotor. The blades used for this series of tests (Figure 10) had slightly tapered rectangular planform and airfoil sections with a 4.5-in. circular arc camber corresponding to the orbit circle of the model.

Historically, two different test vehicles have been used to test the 9-in. propeller model. The test boat used for earlier tests conducted in 1961 is shown in Figures 11 and 12. This was the same boat used in the tests described in Reference 5, but the aperture in the bottom was enlarged to accommodate the larger model, as reported in Reference 6.

The propeller was driven through bevel gears, and torque was measured on a differential-reluctance electronic dynamometer. Thrust was measured by two 4-in. modular force gages (block gages) which supported the propeller housing. To permit deflection of the modular force gages, a free space of 1/4 in. was provided between the boat and the periphery of the cylindrical housing. A thin rubber diaphragm was installed in the lower part of this free space to prevent water from entering the boat around the propeller housing. Water was kept out of the propeller during the tests by a teflon ring-and-slot seal arrangement in the propeller.

Tests of the 6.3-in.-diameter propeller were run with the bottom of the boat barely touching the water surface to minimize the effect of the hull on the inflow to the propeller.[5] In addition to an increased diameter for the propeller aperture, the boat was altered for the tests of the 9-in.-diameter model[6] by the addition of a stepped bottom; this allowed the propeller to be submerged slightly while the ends of the hull were kept out

of the water. The mid portion of the boat was immersed to a nominal depth of 1/8-in. in an attempt to avoid drawing air from the water surface down to the blades.

The test results reported here were obtained with a new test vehicle (Figures 13 and 14) designed and constructed in 1964 to eliminate any air-drawing problem and to facilitate measuring side forces.

The propeller rotor surface was mounted flush with the plane bottom of the vehicle. The surface water was encouraged to flow over the top of the horizontal surface through tunnels running the length of the boat and exhausting at the stern. The depth was set to between 1/2 and 1 in. No air drawing was observed through the plexiglass bottom, which was installed for this purpose, and no symptoms of air drawing were apparent in the performance curves.

Sheet rubber was used here also to prevent water from entering the boat through the clearance gap which was necessary so that thrust and side force could be measured. The propeller was run completely flooded with water. An evacuated reservoir above the propeller was used to ensure that the housing was full of water at all times. This technique led to larger torque tare readings than with the housing empty. However, consistently high tare readings were considered preferable to the inconsistent tare which would have resulted from partial filling.

Both thrust and side force were measured using two block gages for each component (see Figure 15). A new 250-in.-lb differential reluctance torque dynamometer was constructed for use with the new test vehicle. The earlier tests[6] of the 0.8π and 0.9π pitch ratios were run at Reynolds numbers (based on average blade chord) from about 0.5×10^5 to 1.5×10^5. The tests of the 0.8π pitch ratio using the new torque dynamometer were run at Reynolds numbers from 1.3×10^5 to 2.1×10^5 and the 0.9π pitch ratio, at Reynolds numbers from 1.2×10^5 to 2.0×10^5. Tests at the lower pitch ratios, where higher Reynolds numbers were obtained, gave consistent results at values of Reynolds numbers higher than 1.0×10^5; at lower Reynolds number, the tests tended to predict lower thrust and erratic, mostly higher torque.

During the tests, tare readings were made with the rotor immersed and blades removed. This effectively removed from the final results the

losses due to the mechanism and those due to the rotor plate drag. The rotor plate drag, that is the hydrodynamic drag of the surface of the rotating disk, was measured and found to produce a torque coefficient approximately equal to 0.06, with rpm and speed having little effect. No attempt was made to evaluate the losses related to the machinery or rotating masses since the model construction bears no relation to any full-scale unit.

TEST PROGRAM AND RESULTS

The major part of the test program was run with six rectangular blades (Figure 10). Each of the six sets of cams, representing the six pitch ratios (0.4π, 0.5π, 0.6π, 0.7π, 0.8π, and 0.9π) was tested over a wide range of steering angle and speed coefficient. A portion of these results, presented in Figures 16 through 18, show K_T and K_Q, and η_o versus J at very low values of steering angle, where side force is approximately zero.

Tests were also run with two and three blades at zero steering angle. Comparative results are shown in Figures 19 and 20 for 0.7π and 0.8π pitch ratios.

Figures 21 through 26 give the cycloidal propeller characteristics over the full range of steering angles. For a pitch ratio of 0.4π, the thrust, torque, and side force coefficients are plotted against speed coefficient in Figure 21 with steering angle as a parameter. The legends on these figures indicate steering angles in the first and fourth quadrants only. The plots, however, apply to all four quadrants since both positive and negative ranges of speed coefficient are plotted, and changing the sign of J is equivalent to a 180-deg change in steering angle. For example, in Figure 21a with a 30-deg steering angle and J=0.5, the thrust coefficient $K_T = 0.54$ whereas for a 210-deg steering angle and J=0.5, $K_T = -1.14$ which is found using the $\phi = 30$ deg curve at $J = -0.5$. The sign of K_T must be reversed in this case because the positive thrust shown on the curve is now measured from the $\phi = 180$ deg line, or opposite the direction of motion. The same principle holds for the torque and side force coefficients except

that the sign of the torque coefficient is not changed. Thus, for J=0.5, Figures 21b and 21c give $K_Q = 0.20$ and $K_S = 0.83$ at $\phi = 30$ deg and $K_Q = 0.24$ and $K_S = -0.46$ at $\phi = 210$ deg.

The thrust and side force coefficients are plotted in polar form in Figures 21d and 21e. A vector representation of the resultant force magnitude and direction at any operating condition specified by the curves can be obtained by drawing a line from the origin to the appropriate point.

Curves in Figure 21d are for constant steering angle only, except for the semicircle separating the positive and negative ranges of speed coefficient. As in Figures 21a through 21c, only angles in the forward quadrants (half-circle) are shown.

The base graph of Figure 21e contains curves for constant speed coefficient, and the overlay contains curves for constant steering angle, except that the circle for J = 0 is included to facilitate alignment. In this figure, steering angles cover all four quadrants (full-circle) but for positive values of J only.

Similar plots are presented for the other five pitch ratios in Figures 22 through 26.

DISCUSSION

The open-water curves for zero steering angle (Figures 16 through 18) resemble the characteristic curves of a screw propeller series except that the peak efficiencies are lower than the six-bladed B series.[3] Lower efficiency is to be expected since the angle of attack of the cycloidal propeller blades varies throughout the cycle between relatively large positive and negative values. Although the blade produces a positive thrust component at negative as well as positive angles of attack, the lift-drag ratios suffer at very high angles of attack and near zero angle of attack. This effect is complicated by the fact that in the downstream quadrants of the orbit, the blades pass through the wake of the blades in the upstream quadrants. Figures 19 and 20 suggest that this blade interference is considerable since the effect of varying number of blades is much more pronounced than for the screw propeller. With two blades, the peak efficiency with 0.8π pitch ratio was 0.79; this compares favorably with the screw propeller.

Preliminary investigation of the effect of blade shape on performance has indicated that this effect is not significant. The experiments conducted in 1961 by Nakonechny[6] using two sets of elliptical blades (same mean chord but differing in length) and two sets of rectangular blades (one with symmetrical sections, the other cambered) indicated small differences in performance when compared to the estimated accuracy of the tests. The comparison of rectangular versus elliptical blades derived from these tests is reported in Reference 7.

In light of these preliminary results, the emphasis of test program reported here was on the effect of steering angle and number of blades. Most of the new data for zero steering angle agree reasonably well with results given in Reference 7. However, the new tests at 0.9π pitch ratio, which were run at higher Reynolds number, produced significantly higher values of K_T and K_Q at low values of J.

The steering characteristics are best illustrated by the polar diagrams (Figures 21e, 22e, 23e, 24e, 25e, and 26e) which show the resultant force vector as a function of advance coefficient J and steering angle ϕ. The diagram for the bollard condition (J=0) is nearly a perfect circle for all pitches. The magnitude of the resultant force is independent of steering angle, except for small interference effects when water is drawn in from the sides or stern of the test vehicle. The direction of the resultant force was found to be about 3 deg negative (in direction of rotation) from the nominal steering angle setting for all pitches above 0.5π. This small angular difference is attributed to blade shape and asymmetry of the flow field. The photographs in References 23 and 24 illustrate the asymmetry and apparent confusion of the flow through a cycloidal propeller.

When the speed is not zero, the angle of the resultant force is, in general, rotated toward the downstream direction except for steering angles near zero, and the force is larger than the thrust with zero steering angle and the same value of J.

Figure 27 illustrates an approximate method for predicting the vector angle of the resultant force on the basis of blade kinematics. This method predicts the direction of the resultant force vector to be normal to a line connecting Points N and N'_ϕ. Point N is located on a radius normal to

the direction of motion at a distance J/π from the center, and represents the position of the steering center for nominal no-slip condition. The radius of the steering center N'_ϕ is determined by the pitch ratio. For example, it is 0.8 for 0.8π pitch ratio. ϕ is the steering angle and δ is the angle of the resultant force vector.

Figures 28 through 33 compare the measured value of the resultant force vector angle δ with that predicted from the kinematic approximation.[22] The kinematic approximation predicts that at zero speed, the vector angle will equal the steering angle ϕ; actually, as mentioned earlier, the measured angles were about 3 deg different. The measured change in direction of the resultant force vector (due to change in the speed coefficient) was generally within 10 deg of that predicted for J values below that corresponding to the peak of the zero steering angle efficiency curve for the pitch in question (Figure 18). This is the normal range for ahead propulsion although higher values of J may be useful for maneuvering. The kinematic approximation cannot predict the magnitude of the resultant force, but it may be useful for obtaining preliminary estimates of the vector angle.

The polar diagrams demonstrate the value of the cycloidal propeller for maneuvering. For example, with the propeller operating at a pitch ratio of 0.8π and J = 2.0, pure side force approximately equal to the bollard thrust can be obtained without change in rpm; see Figure 25e. With the propeller rotating clockwise as viewed from above, larger side forces were obtained to port than to starboard. Most of this discrepancy is probably accounted for by the acceleration of the flow in the downstream quadrants or by deceleration for some steering angles. The effect can possibly be reduced by suitable compensation of the blade motion.

If it is desired to maintain ahead thrust while side force is applied, vector angles of 45 deg can be obtained with small loss in thrust or with no loss in thrust and only slight increase in rpm. The steering angle required for 45-deg vector angle is slightly less than 30 deg at J = 1 and about 10 deg at J = 2. Figure 25b indicates that between a 5- and 10-percent increase in torque would be required for this condition if rpm is unchanged.

The foregoing remarks are applicable to all types of ships using cycloidal propulsion. It should be noted that they apply either to ahead motion with steering angles in the forward quadrants or to backing with steering angles in the after quadrants. This is distinctly different from screw propellers whose backing effectiveness is considerably less than when propelling ahead.

It should be noted in connection with these diagrams that the steering angle and resultant force vector angle are measured from the direction of motion of the propeller rather than from the ship centerline. Thus, if the combined translational and rotational (yaw) motion of the ship hull are such that the propeller is advancing in a direction 30 deg to port of the ship centerline, then a steering angle of 60 deg to port relative to the hull represents an effective steering angle of 30 deg. If the vector angle, which depends also on pitch ratio and advance coefficient, is shown by the diagrams to be 45 deg to port relative to the direction of motion, then the force is directed at an angle of 75 deg relative to the hull centerline.

The left side of Figure 25e, where $K_T < 0$, represents the crashback condition when a ship is moving ahead, or the crashahead condition when the ship is backing and steering angles are reversed. For example, if the ship is moving ahead with $J = 2$ and $\phi = -2$ deg, K_T is about 1.0 and K_S is zero. If the steering angle is changed to about 178 deg without changing rpm, the thrust coefficient will be about -2.3 and will tend to stop the ship. As the ship slows down, the negative thrust approaches the bollard thrust. This happens also with the screw propeller except that the bollard thrust for reverse rotation is generally less than that for ahead rotation and the available crashback thrust and stopping ability are less.

Considerably higher crashback thrusts can be obtained with twin propulsion arrangements such as those on the BDL and LCU's. Starting at the same ahead condition, if the steering angle of both propellers (which are assumed to be rotating in opposite directions) were changed to about 90 deg, the crashback thrust would be more than double that available at 180 deg, while the large side forces would be in opposite directions on the two propellers and would cancel. As the ship slowed down, the steering angle would be gradually increased to 180 deg. To utilize this feature,

the propulsion plant would have to be designed to absorb almost twice the bollard torque at the start of the crashback maneuver and the blades designed to withstand twice their bollard loading. On the other hand, if the propulsion system is not designed to withstand these conditions, limits must be imposed on the control system to prevent their occurrence.

Effective use of the maneuvering crashback capabilities of the cycloidal propeller would be enhanced by using a computer to select the most effective operating point. The computer memory would contain characteristics, such as those presented here, in whatever format is most effective. Sensors would determine the direction of motion at any instant. The helmsman would then indicate the direction and magnitude of the desired force relative to the ship, and the computer would control the steering angle, pitch, and engine rpm to produce the desired force vector most effectively. The computer would also account for changes in ship speed and direction to maintain that force vector until the helm settings are changed. It could also be programmed to consider the limiting values of torque and blade loading in choosing the operating conditions as well as the desired thrust and side force.

CONCLUSION

Performance and steering characteristics are presented for a cycloidal propeller series. The basic series comprised six pure cycloidal blade motions with pitch ratios between 0.4π and 0.9π. The series was characterized with six rectangular blades, but several tests were run with two and three blades and zero steering angle to determine the effect of number of blades. The effect of blade number was similar to the effect of changing the number of blades of a screw propeller, but it was more pronounced. Specifically, the peak efficiency of the cycloidal propeller with six blades was 10 to 15 points lower than the Troost six-bladed B series; with two blades, the cycloidal propeller was very nearly as efficient as the two-bladed B series propeller.

Side force was measured as well as thrust and torque, and steering characteristics are presented as curves of K_T, K_Q, and K_S versus J and in the form of polar diagrams. An approximate kinematic method for predicting

the direction of the resultant force as a function of pitch ratio, steering angle, and advance coefficient was examined. The approximation is adequate for preliminary estimates of the vector angle, but it does not predict the magnitude of the force.

The cycloidal propeller can develop maneuvering, backing, and crash-back forces that are much larger than those available from a screw propeller. The propulsion system should be designed to make effective use of these forces or to protect against their inadvertent occurrence. Consideration should be given to the use of an on-board computer to use the cycloidal propeller most effectively.

ACKNOWLEDGMENTS

The NSRDC experimental program for cycloidal propellers was initiated by Dr. Basil Nakonechny, who was also responsible for development of the 9-in., orbit-diameter propeller model. The assistance of Messrs. James Peck and Garnell Belt in the testing and analysis is gratefully acknowledged.

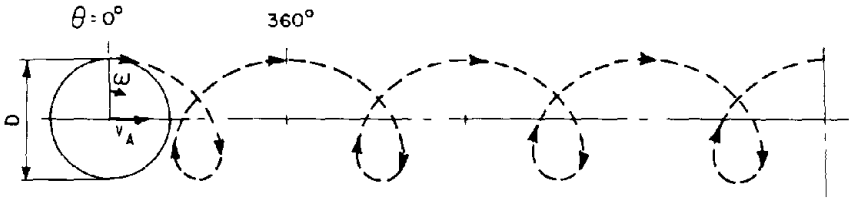

(a)

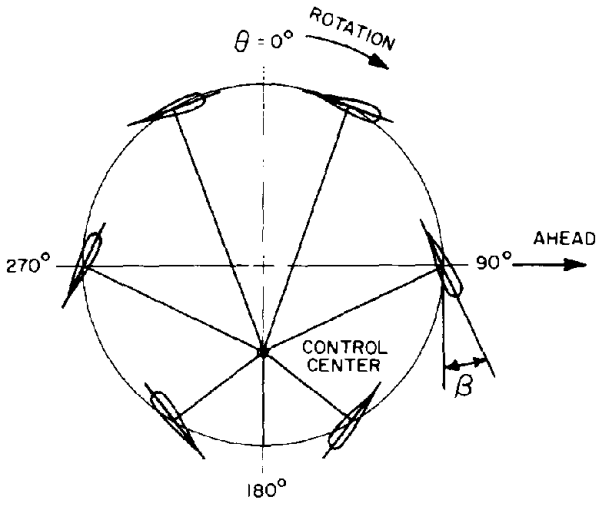

(b)

Figure 1 - Schematic Illustration of Cycloidal Blade Motion

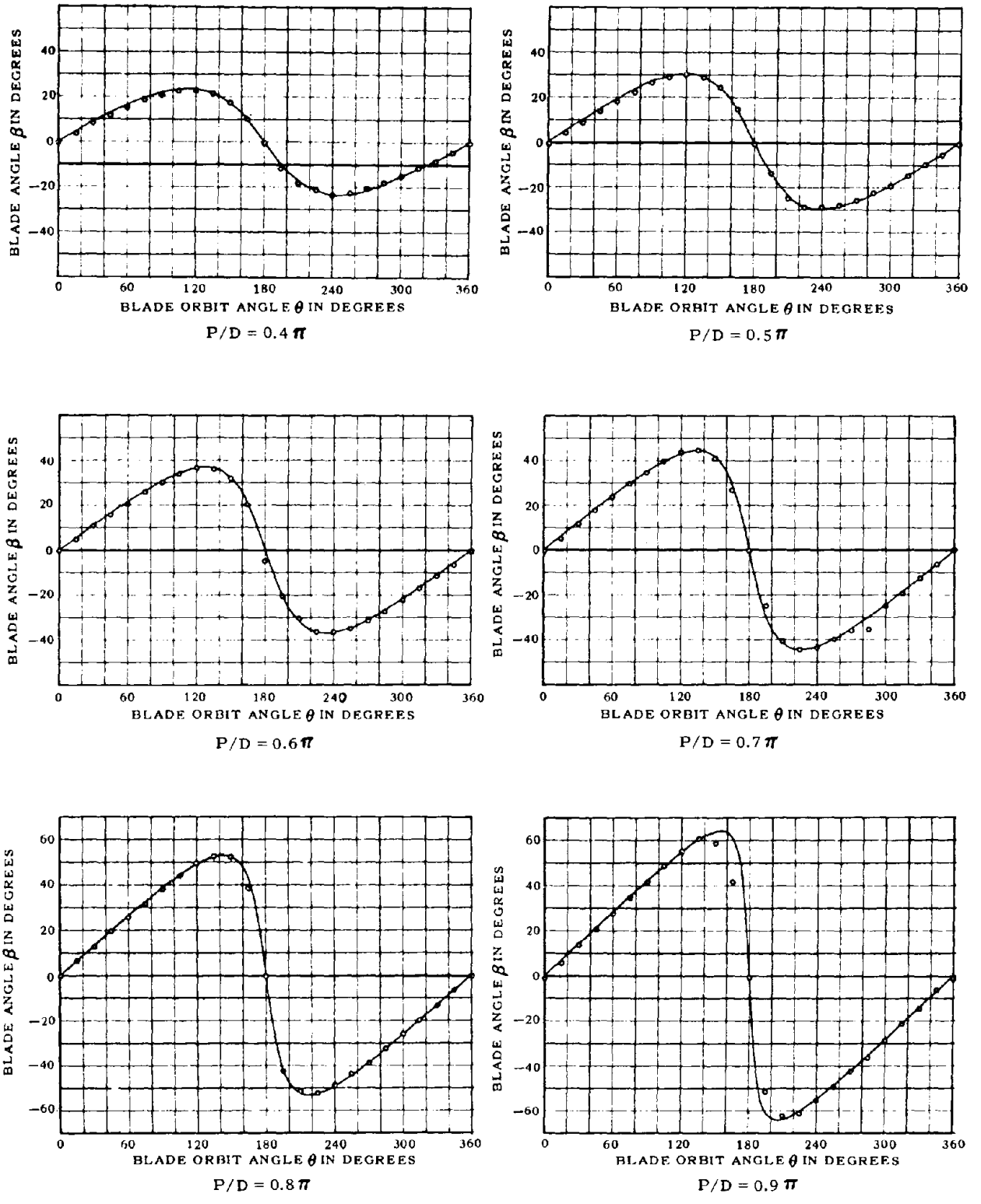

Figure 2 - Blade Motion Curves for the Test Series

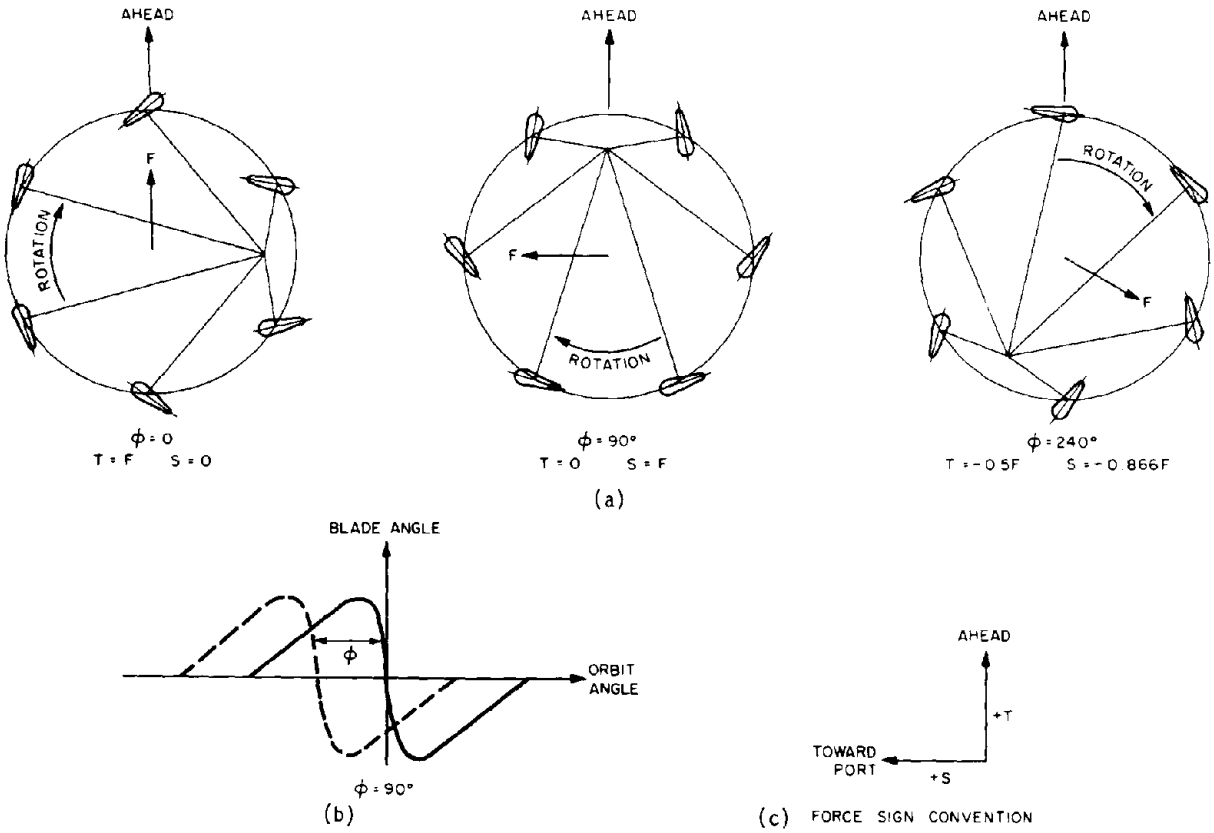

Figure 3 - Schematic Illustration Showing Sign Convention, Steering Angle, and Direction of Force under Bollard Conditions

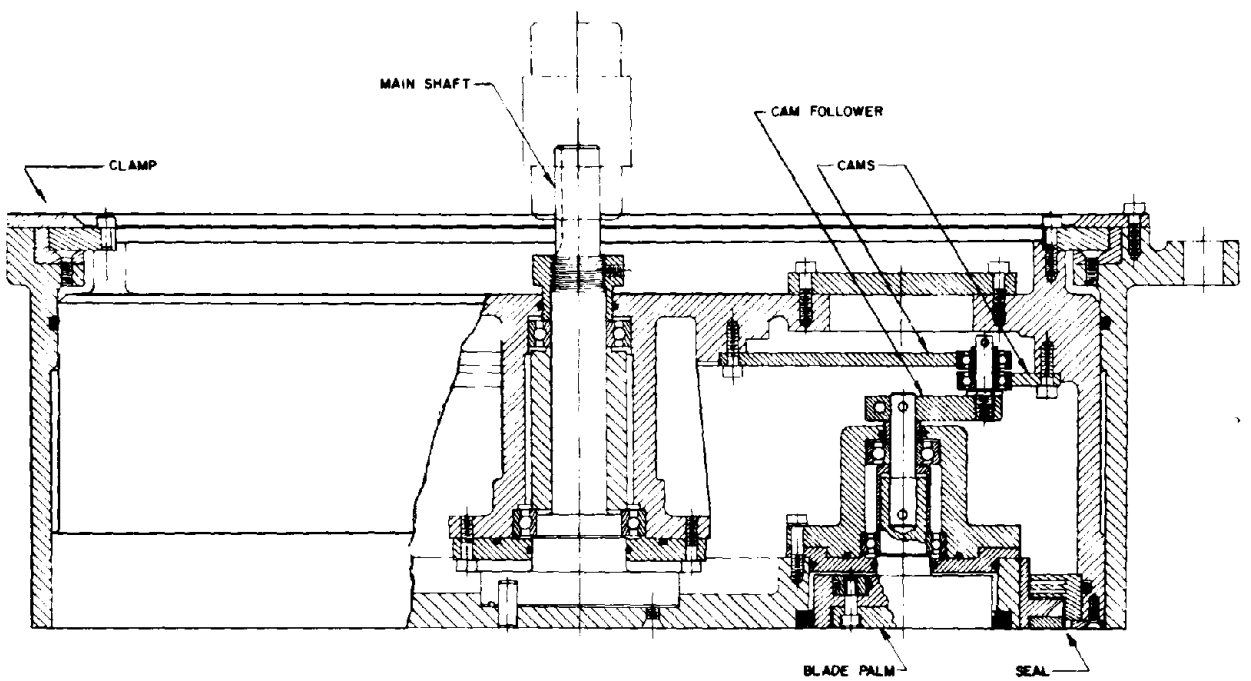

Figure 4 - Nine-Inch Orbit Diameter Cycloidal Propeller Model

Figure 5 - Propeller Rotor

PSD 304168

Figure 6 - Propeller Stationary Housing

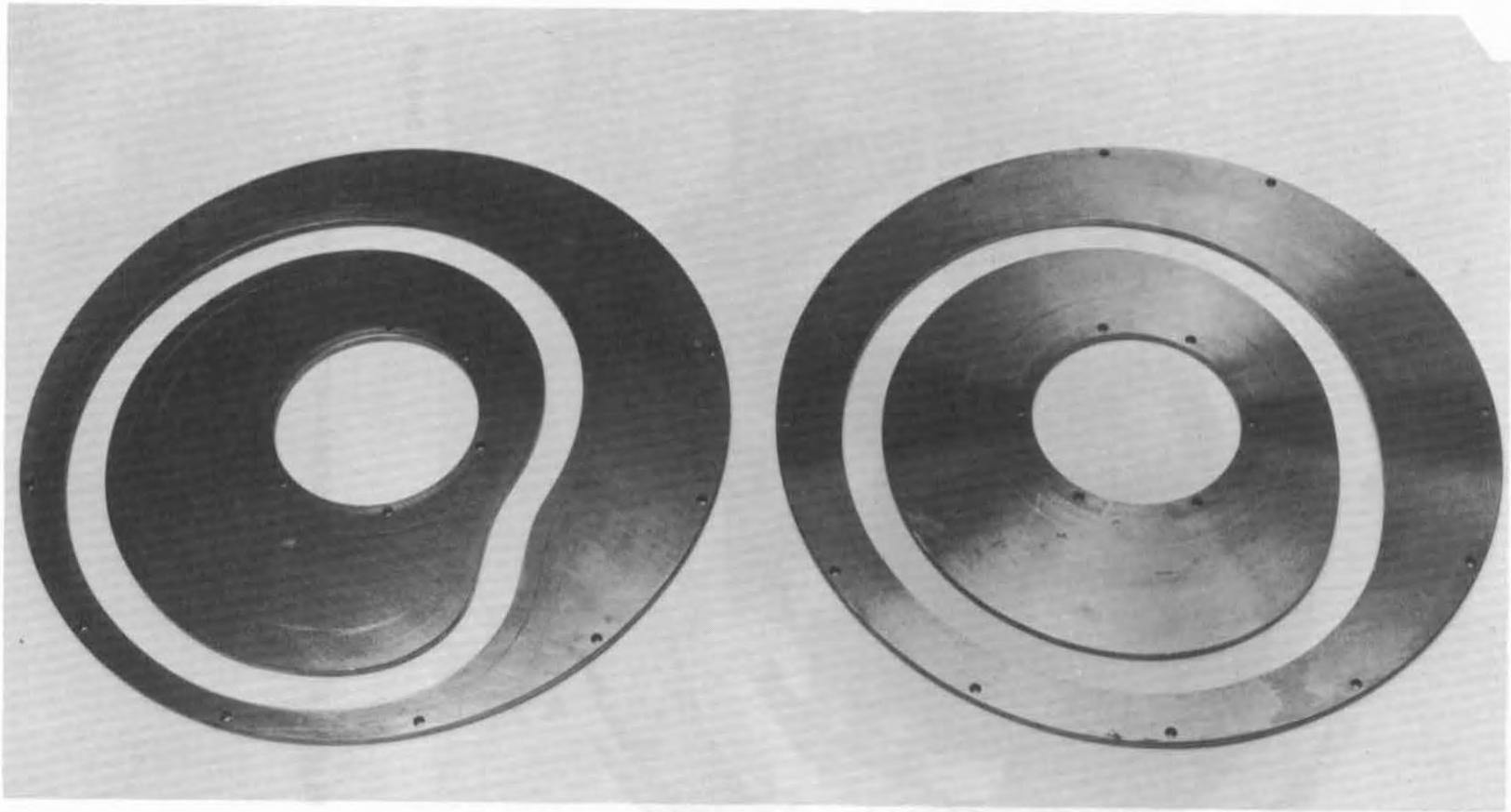

PSD 326667

(P/D = 0.8π) (P/D = 0.5π)

Figure 7 - Cams for Cycloidal Propeller Model

Figure 8 - Cycloidal Propeller Model with Rectangular Blades

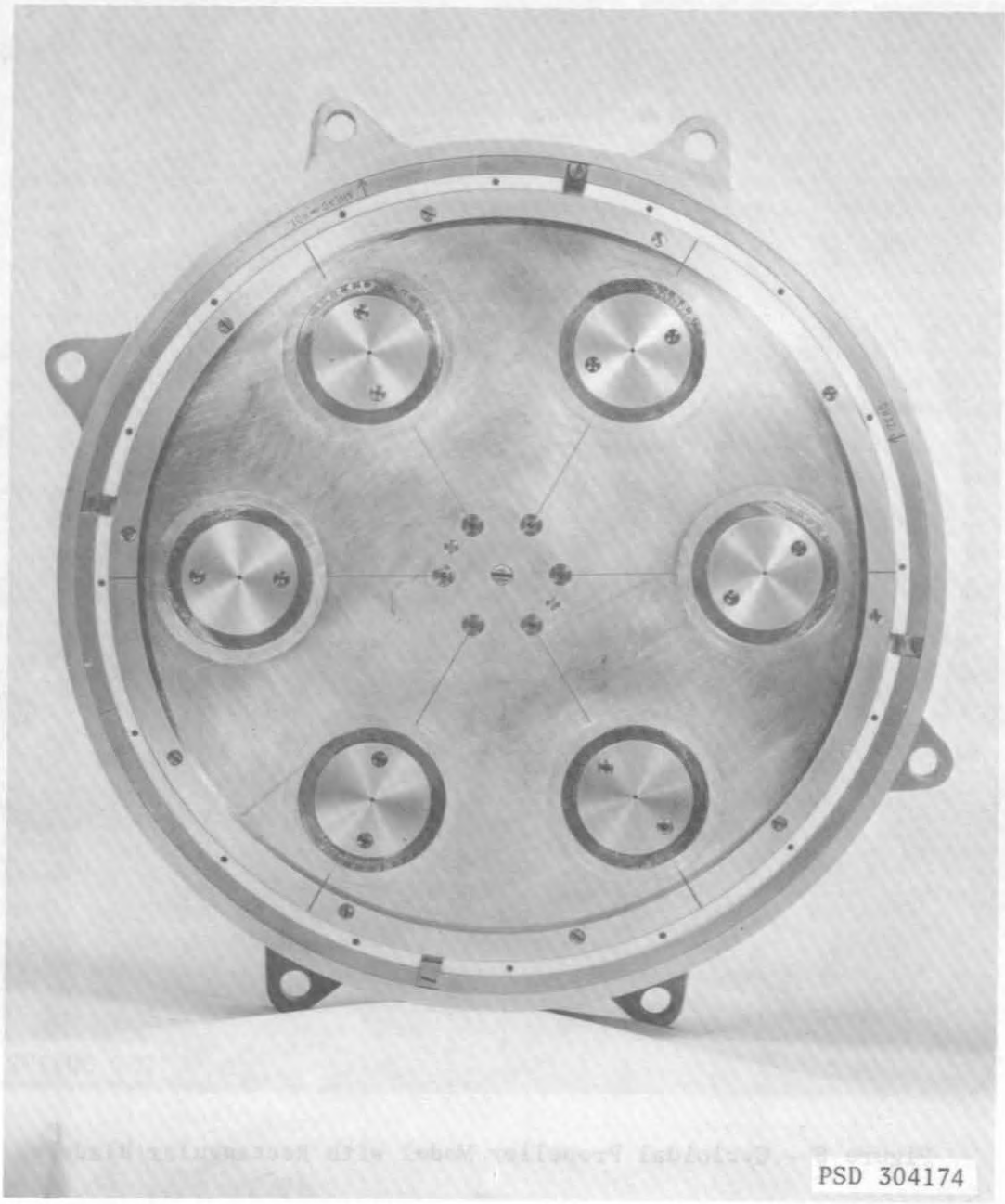

Figure 9 - Cycloidal Propeller Model without Blades

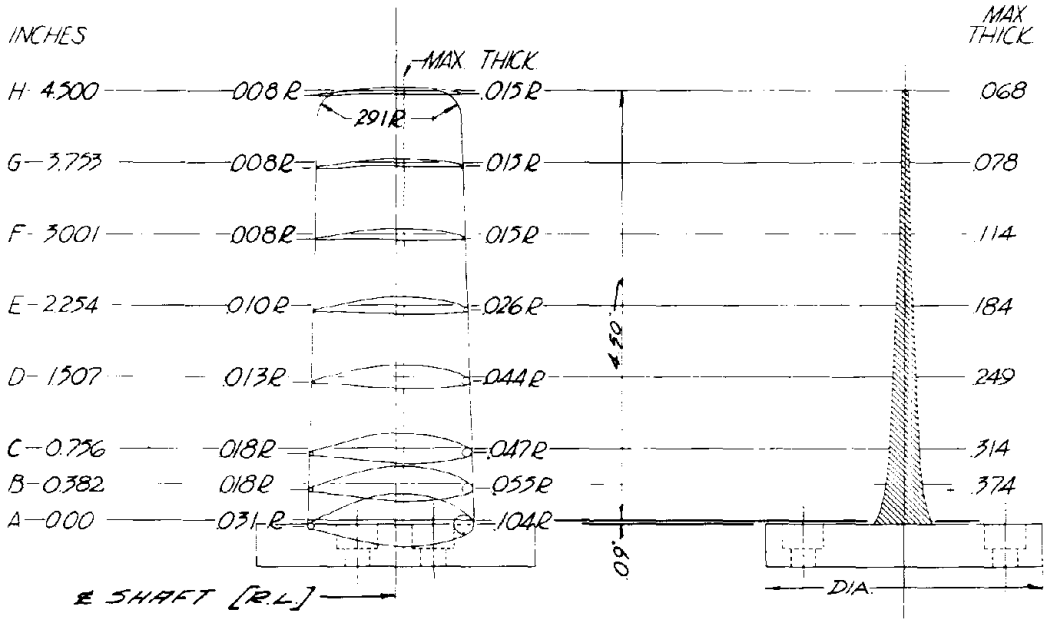

Length	4.500 in.	L/D	0.500
Max. Chord	1.704 in.	C/D	0.176 (avg)
Avg. Chord	1.585 in.	Aspect Ratio	5.7
Blade Area	7.13 sq. in.	Blade Area Ratio	1.06 (6 Blades)

Figure 10 Rectangular Blades

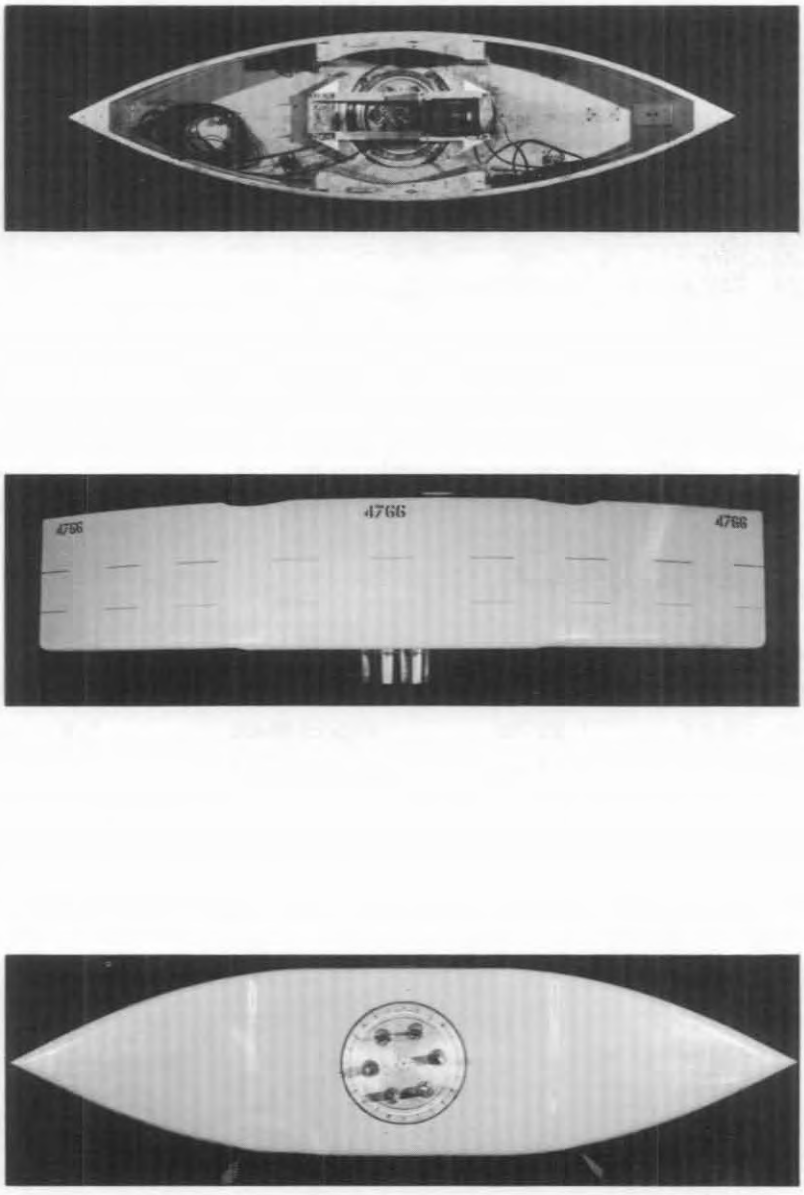

Figure 11 - Boat-Shaped Test Vehicle

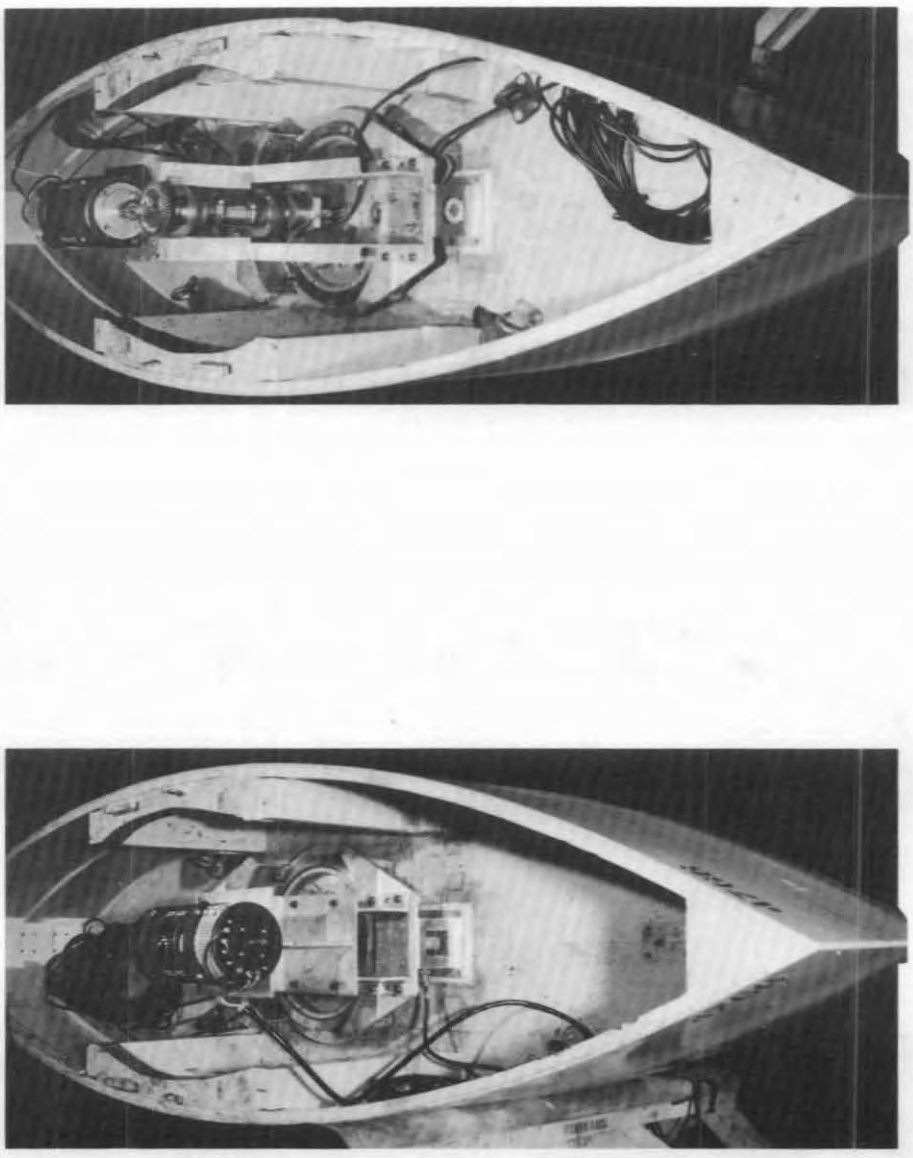

Figure 12 - Closeup of Boat-Shaped Test Vehicle

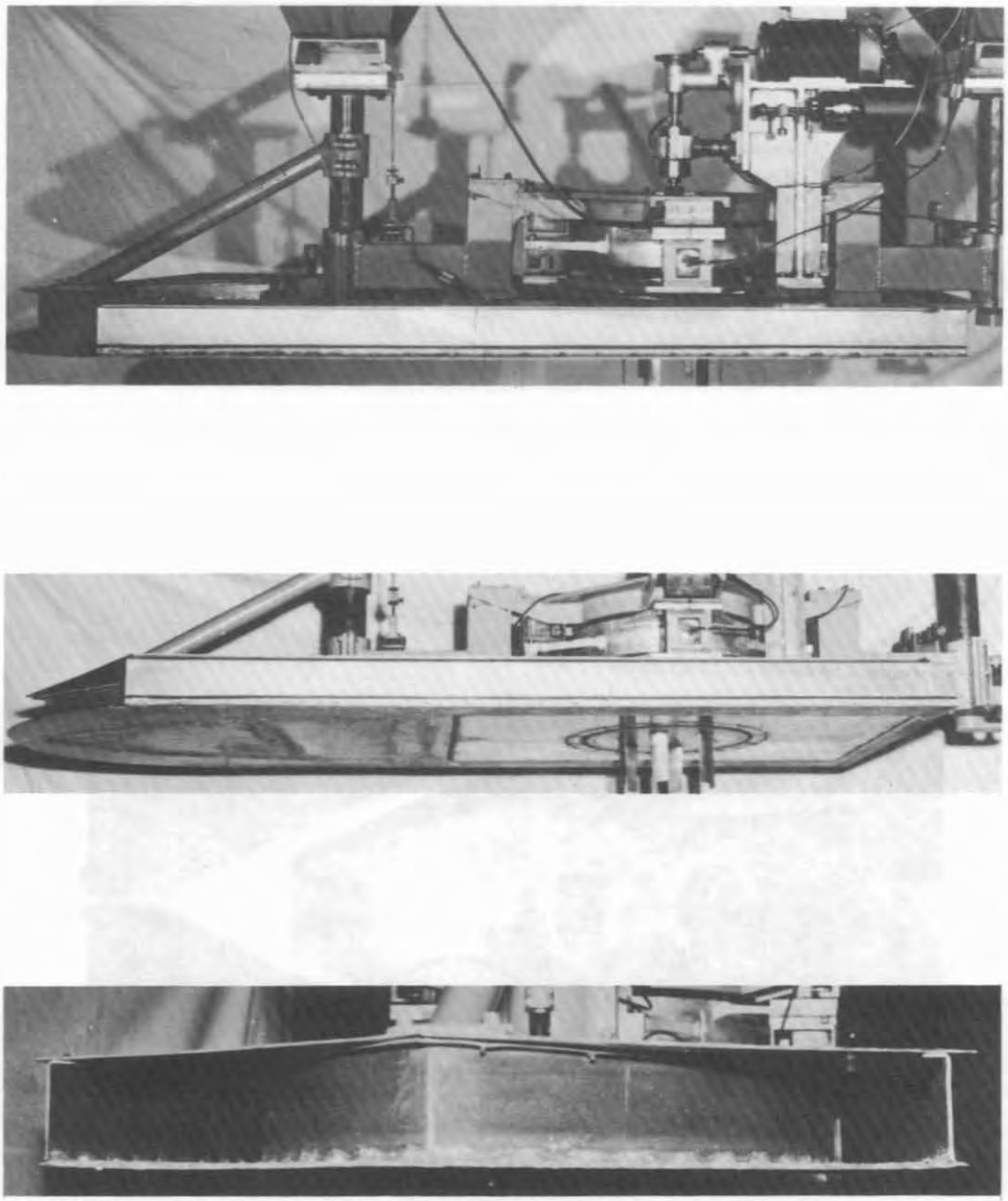

Figure 13 - Plane-Bottom Test Vehicle

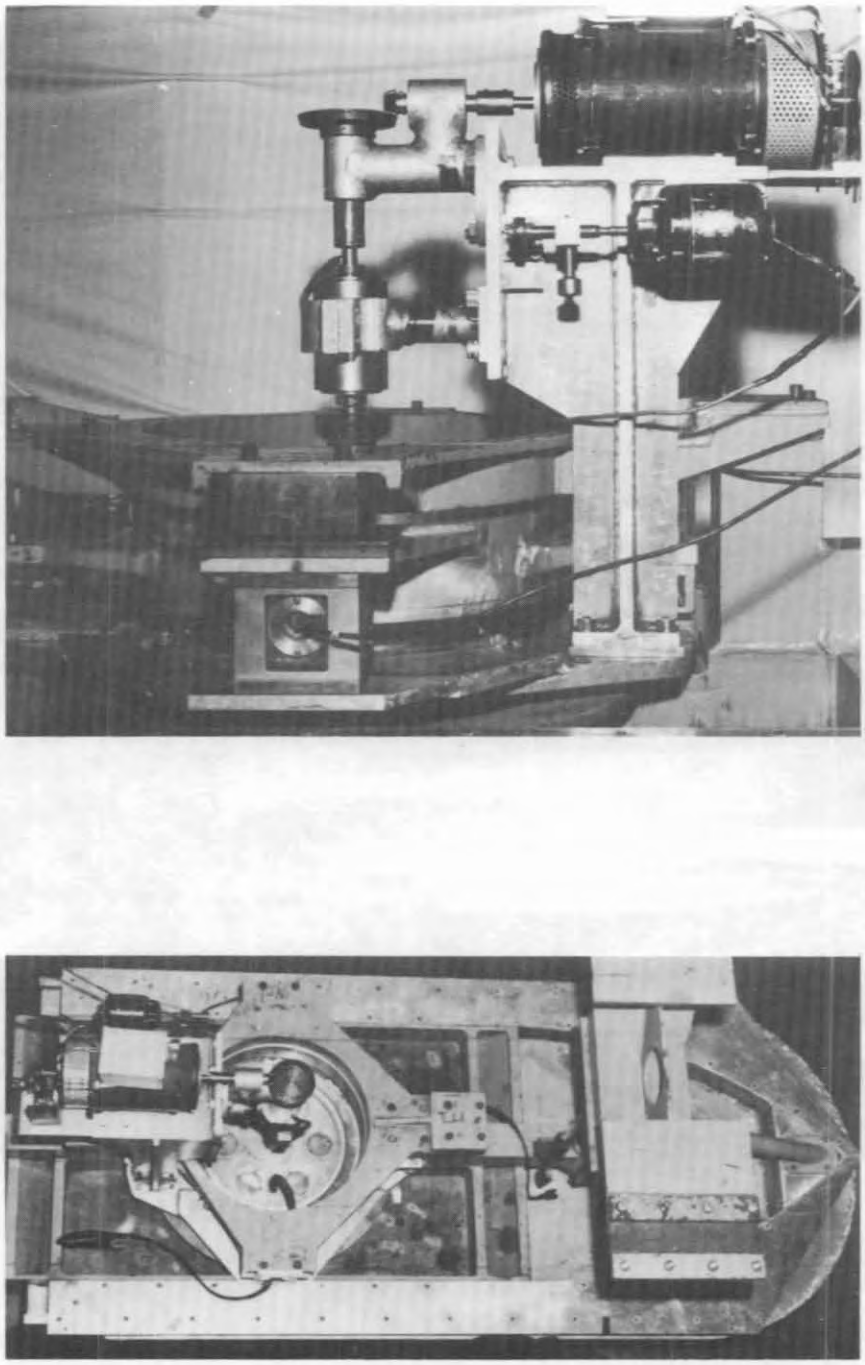

Figure 14 - Closeup of Plane-Bottom Test Vehicle

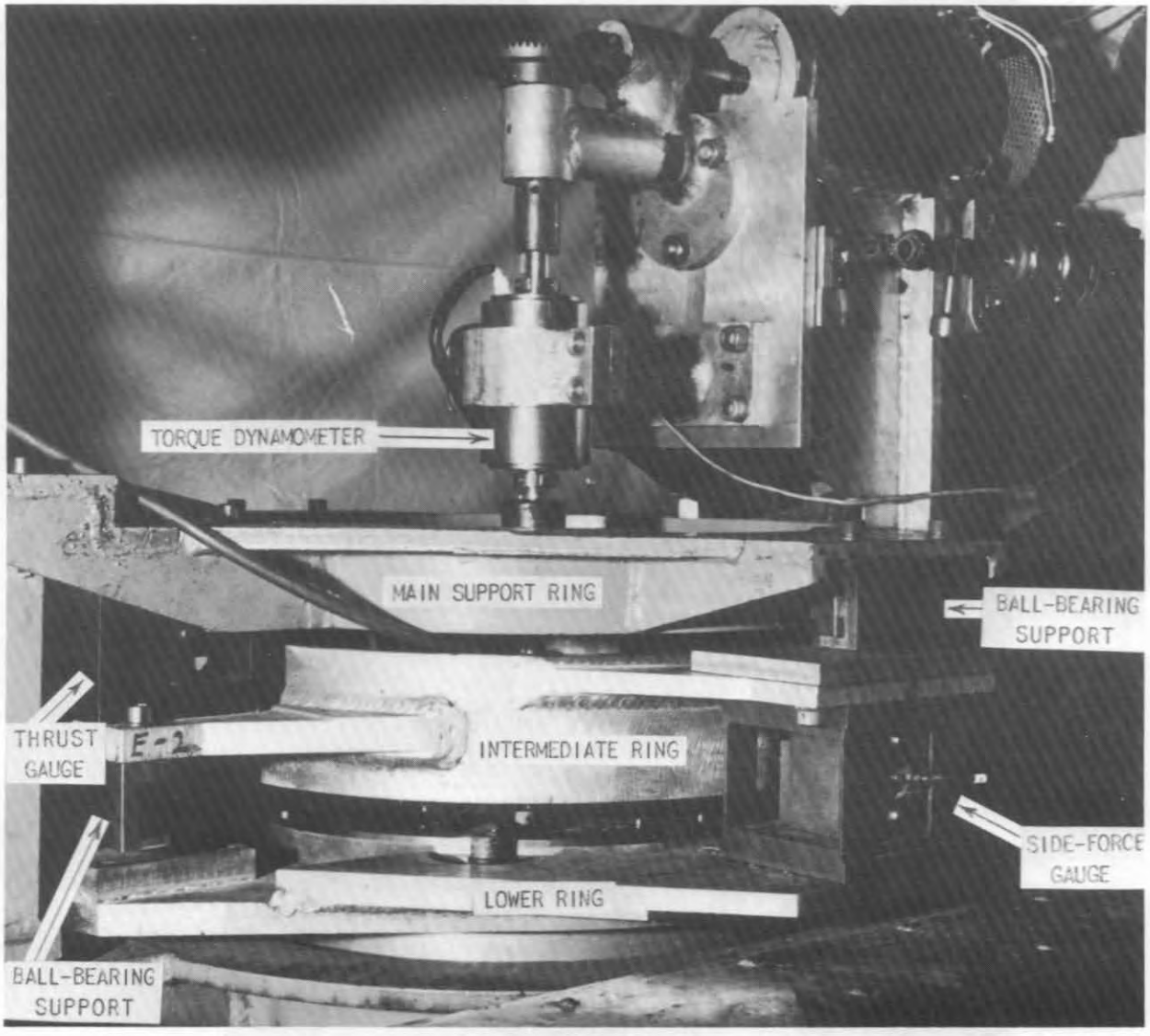

Figure 15 - Force Measuring System

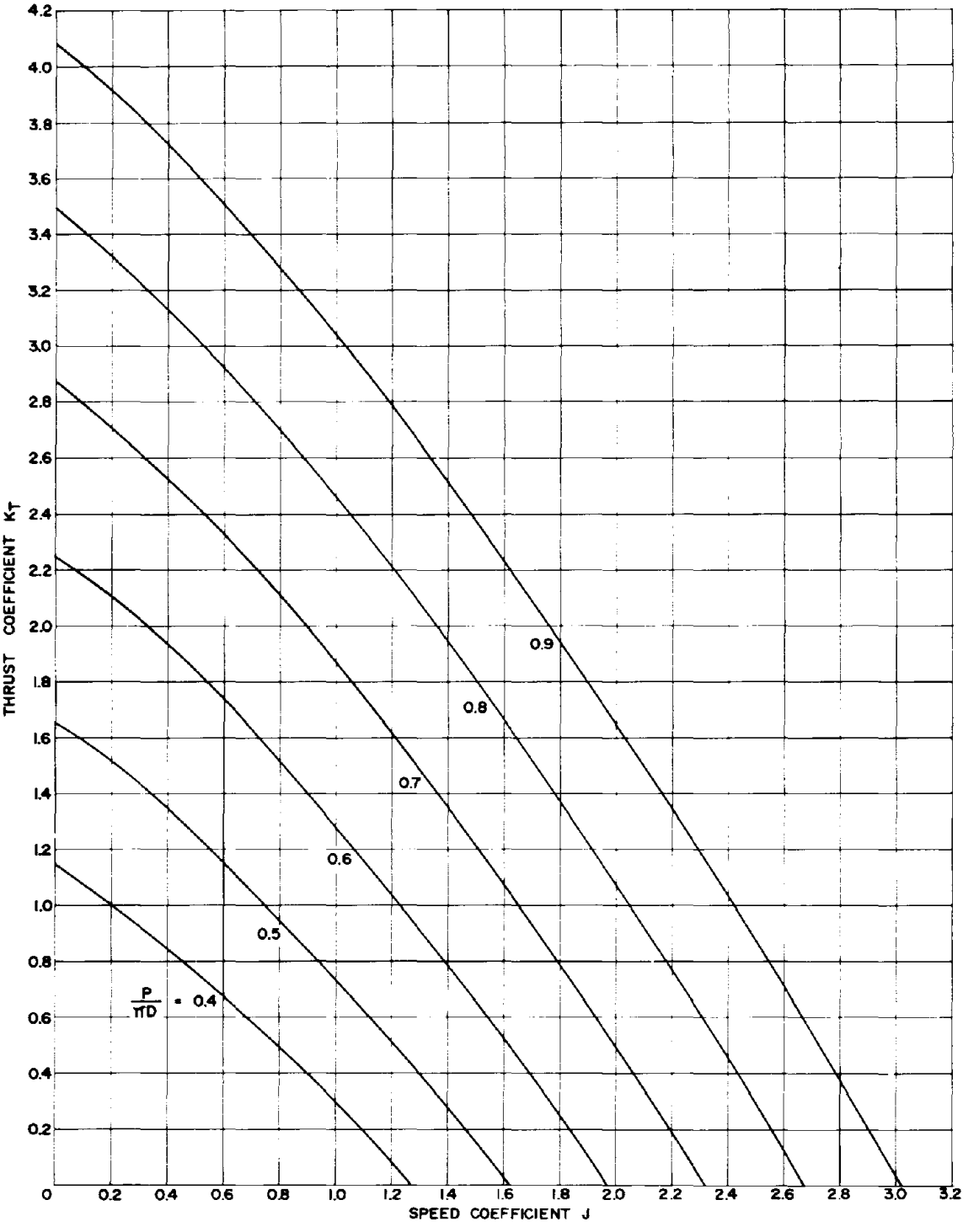

Figure 16 - Thrust Characteristics with Six Rectangular Blades at Zero Steering Angle

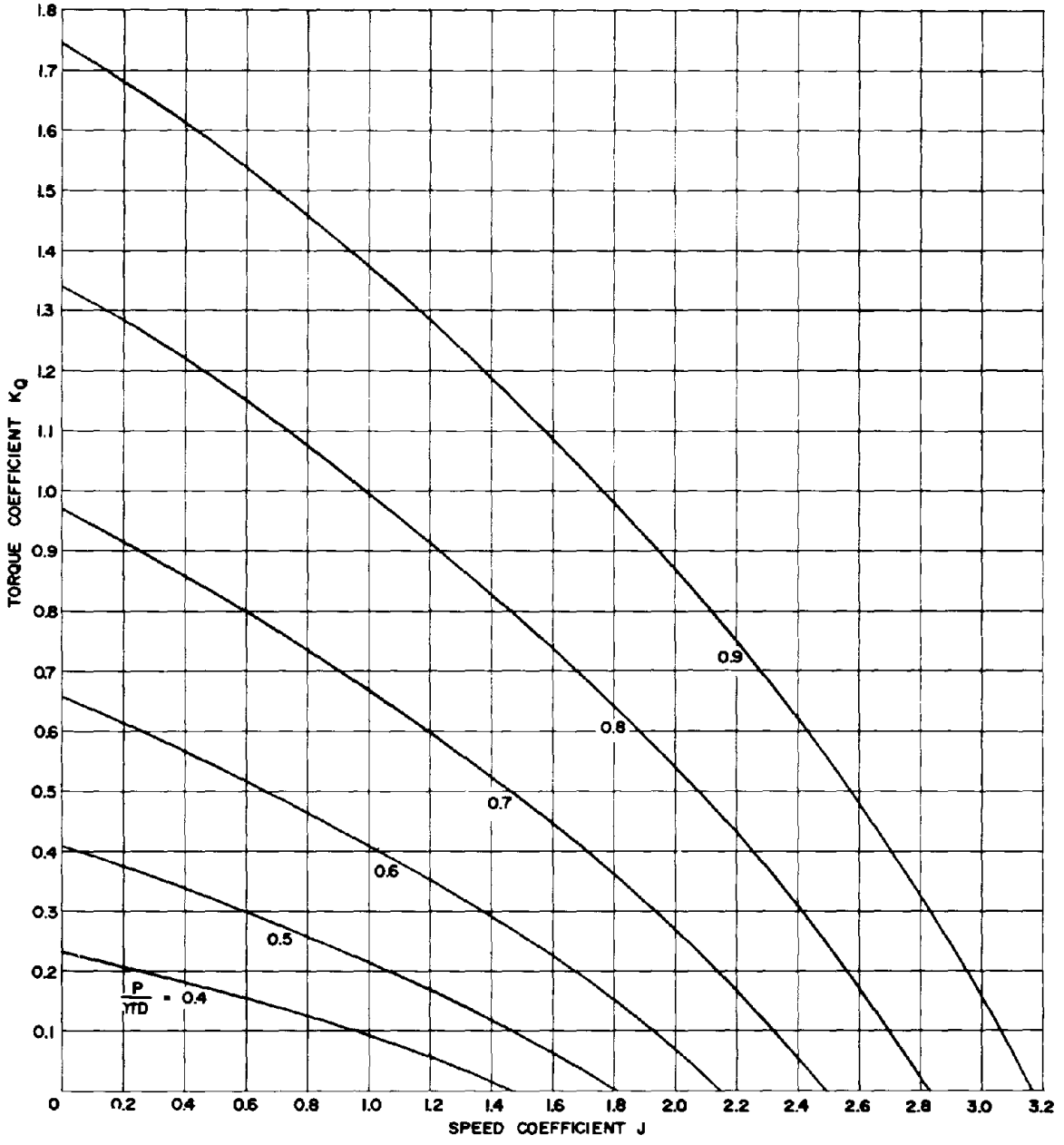

Figure 17 - Torque Characteristics with Six Rectangular Blades at Zero Steering Angle

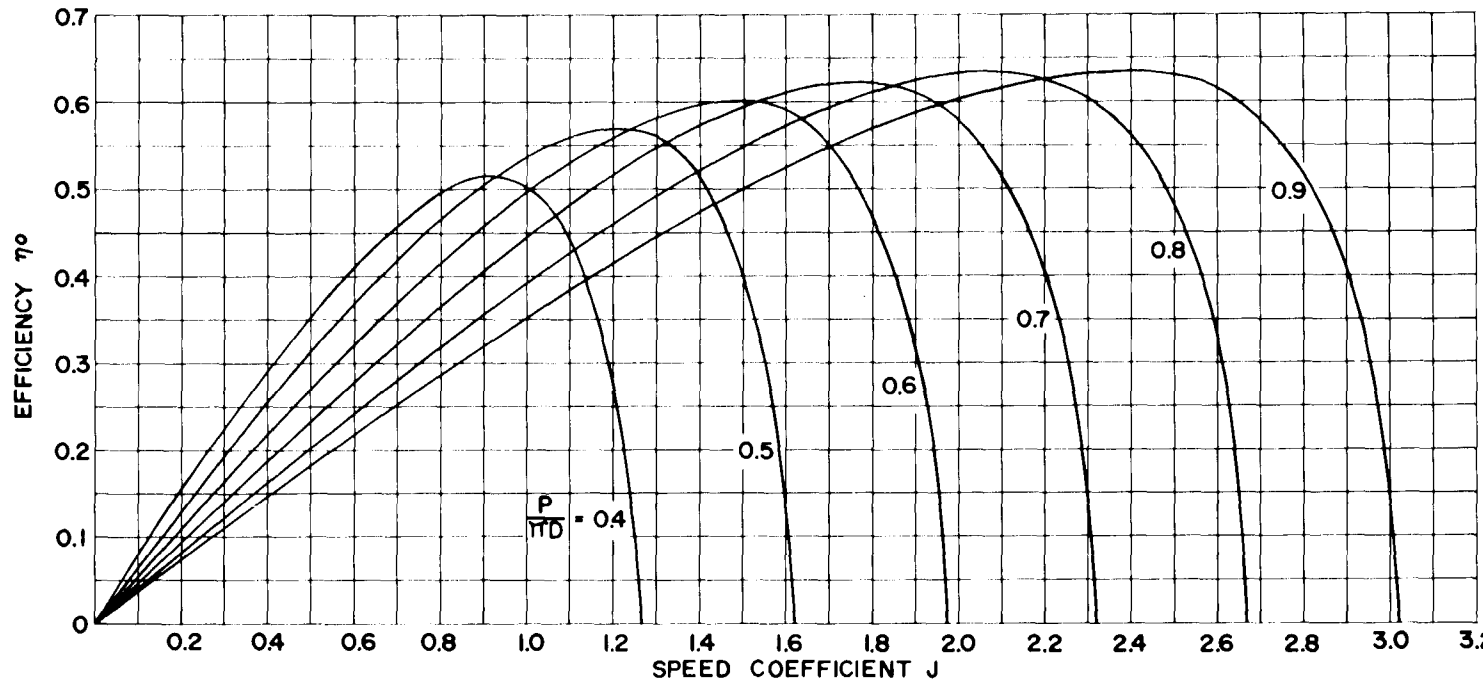

Figure 18 - Propeller Efficiencies with Six Rectangular Blades at Zero Steering Angle

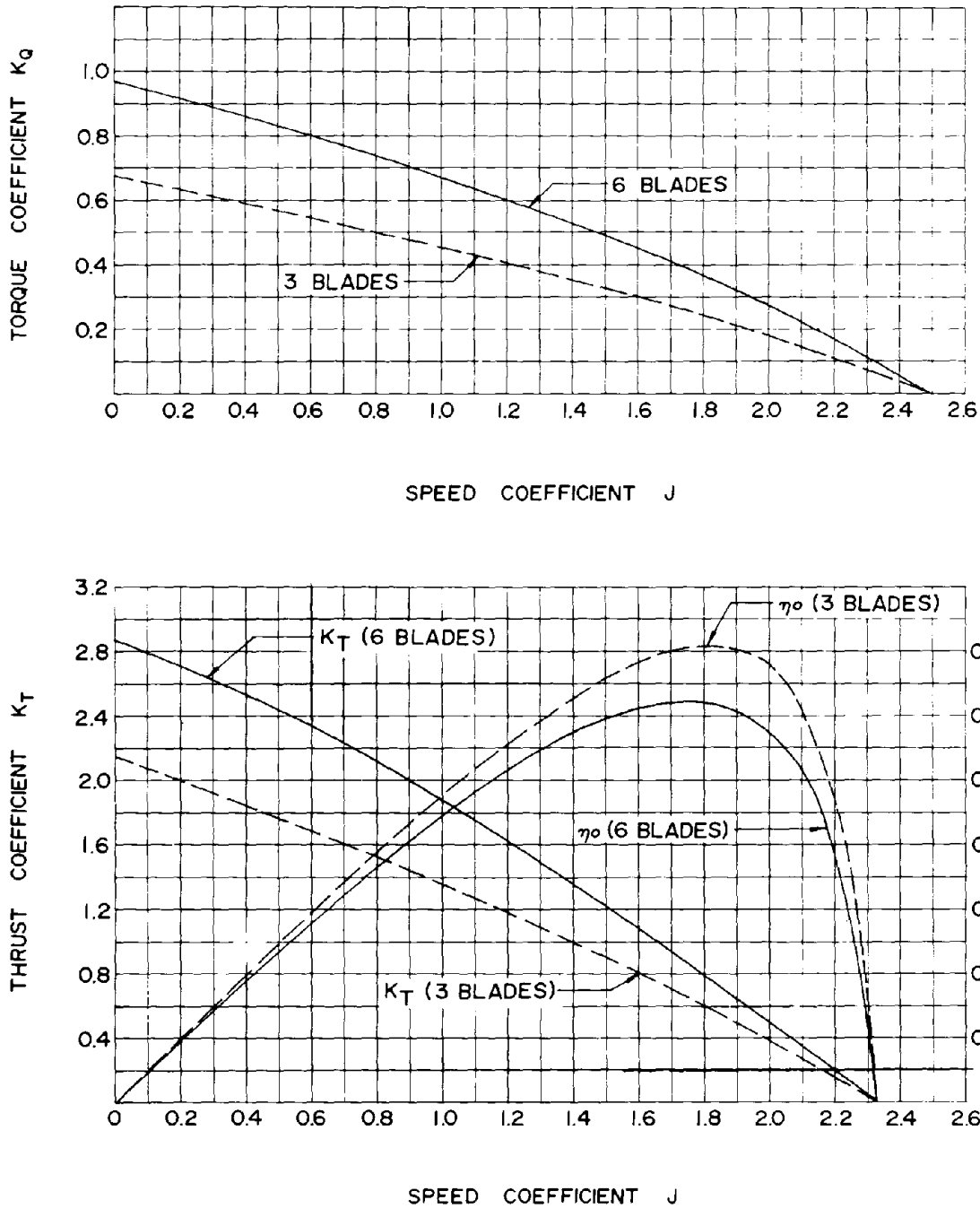

Figure 19 - Effect of Number of Blades on Propeller Characteristics at 0.7π Pitch Ratio

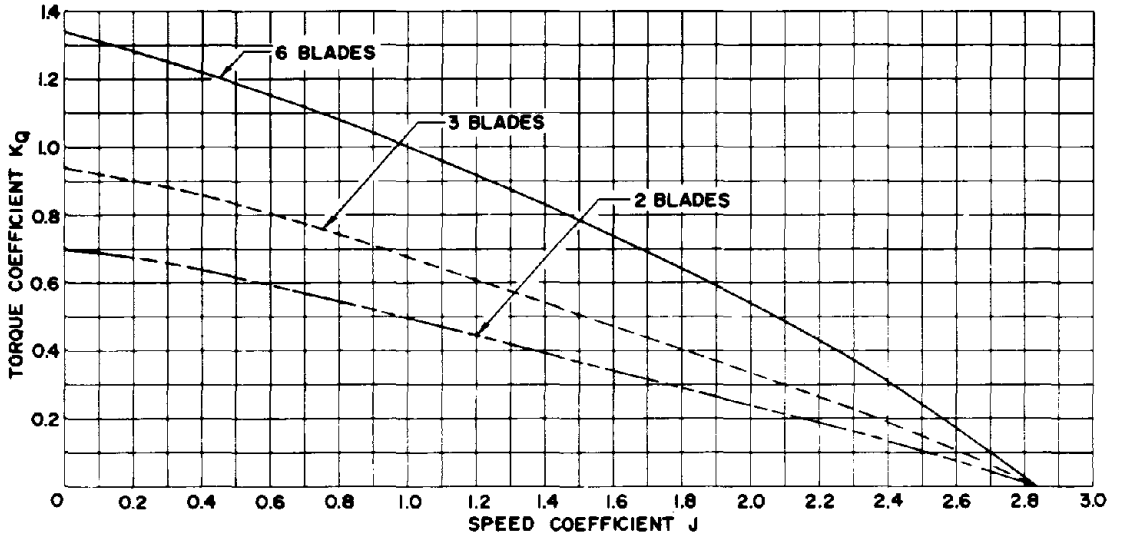

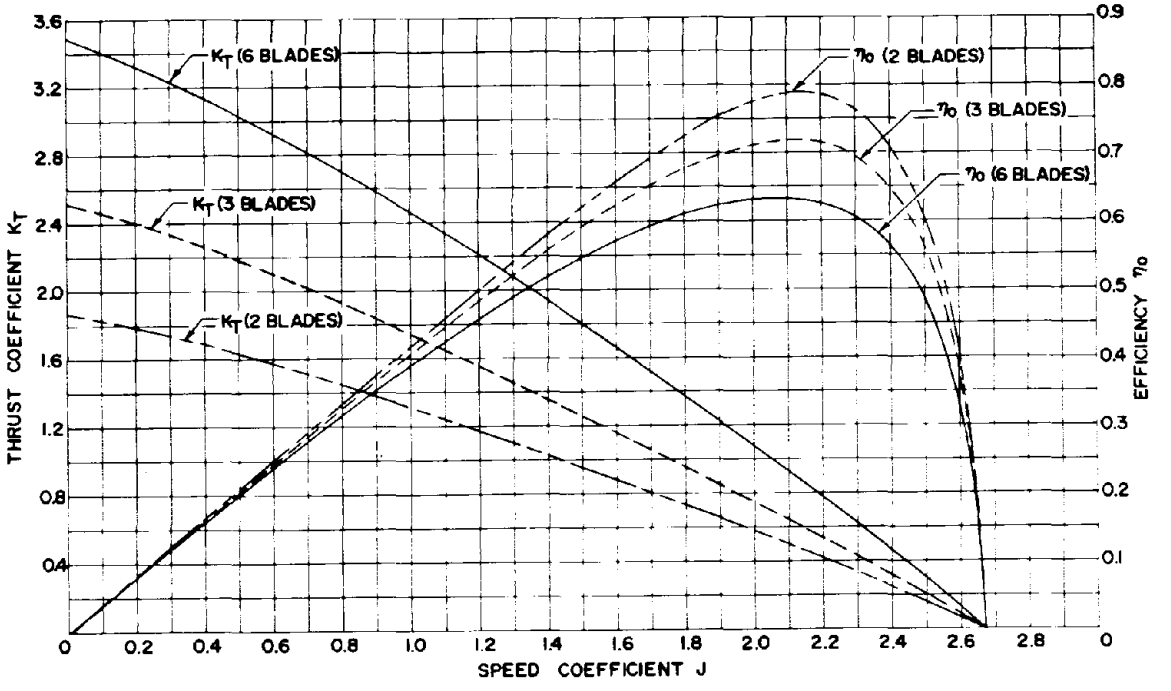

Figure 20 - Effect of Number of Blades on Propeller Characteristics at 0.8π Pitch Ratio

Figure 21 - Propeller Characteristics with Variation of Steering Angle for 0.4π Pitch Ratio

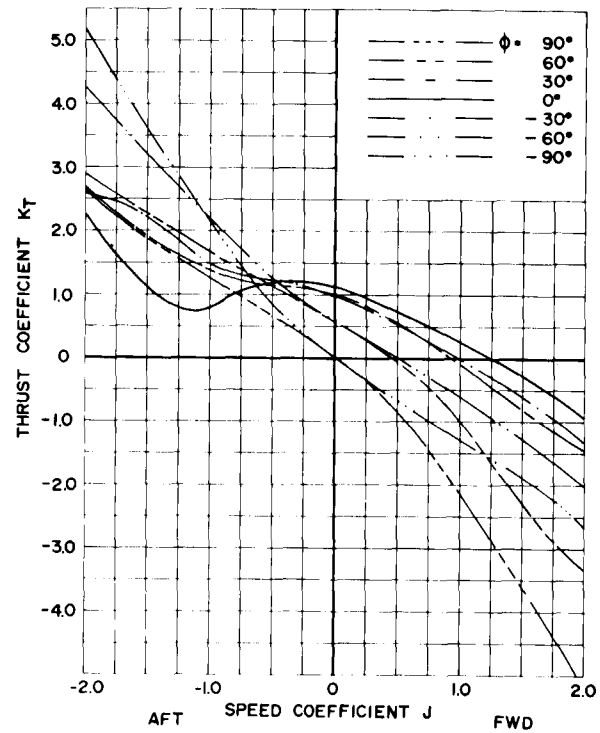

Figure 21a - Thrust Characteristic Curves

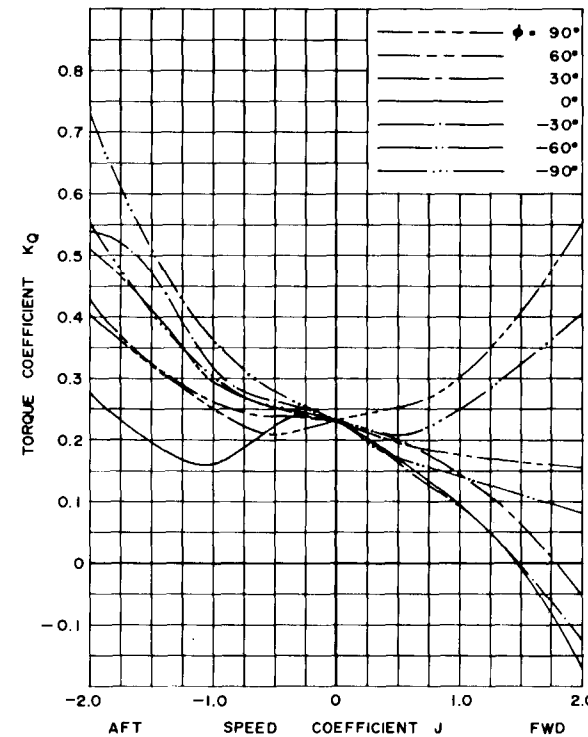

Figure 21b - Torque Characteristic Curves

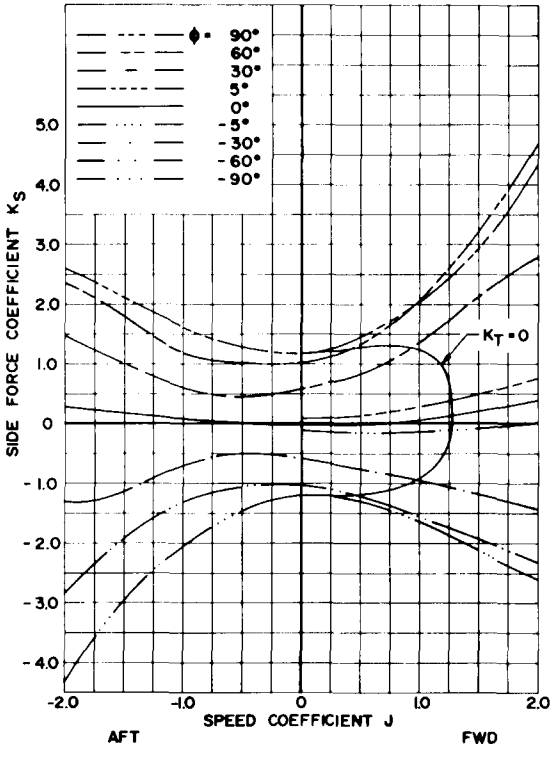

Figure 21c - Side Force Characteristics

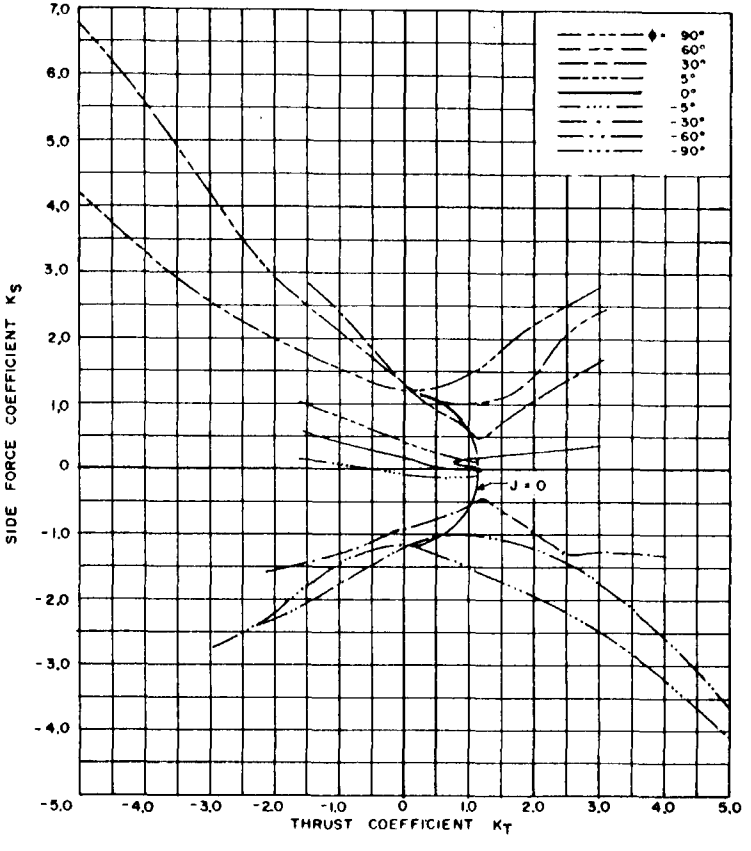

Figure 21d - Half-Circle Polar Diagram

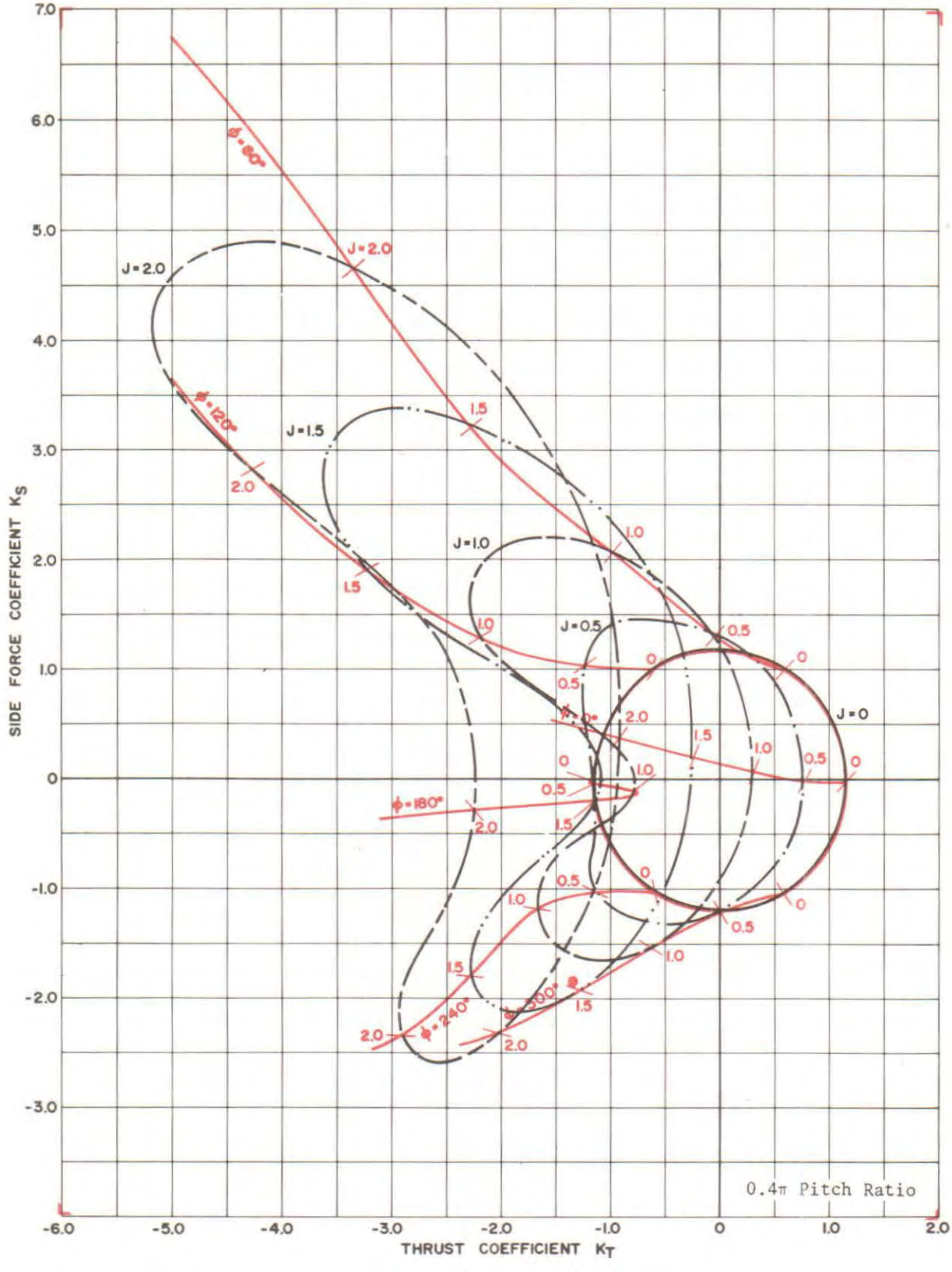

Figure 21e - Full-Circle Polar Diagram

Figure 22 - Propeller Characteristics with Variation of Steering Angle for 0.5π Pitch Ratio

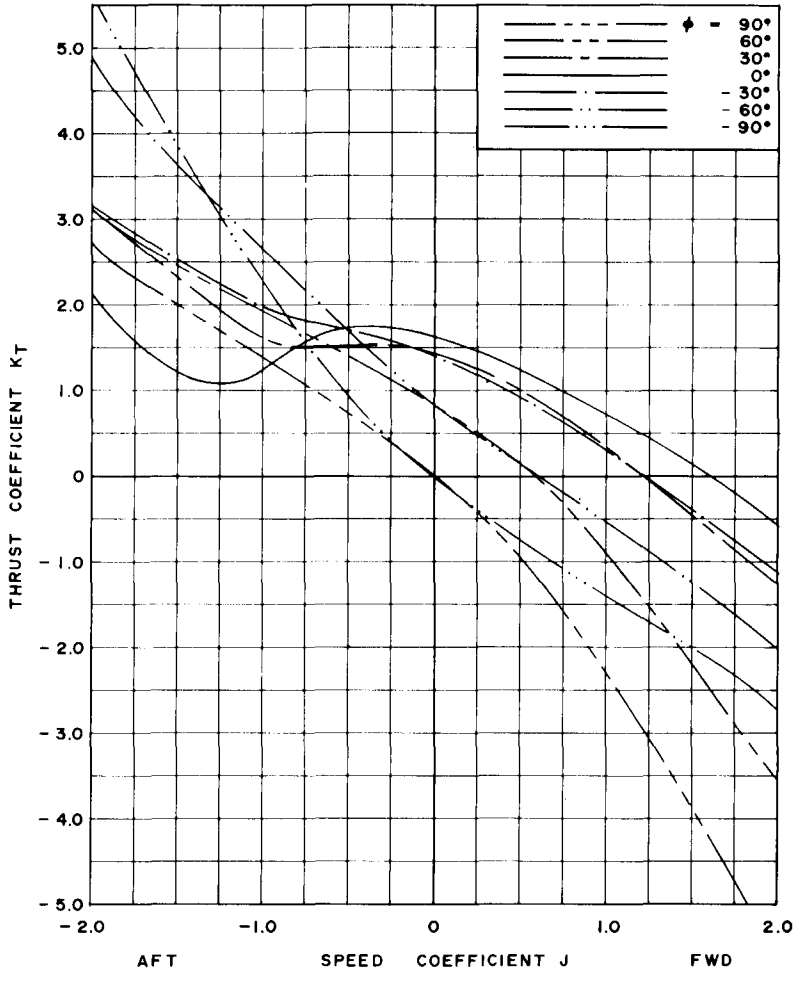

Figure 22a - Thrust Characteristic Curves

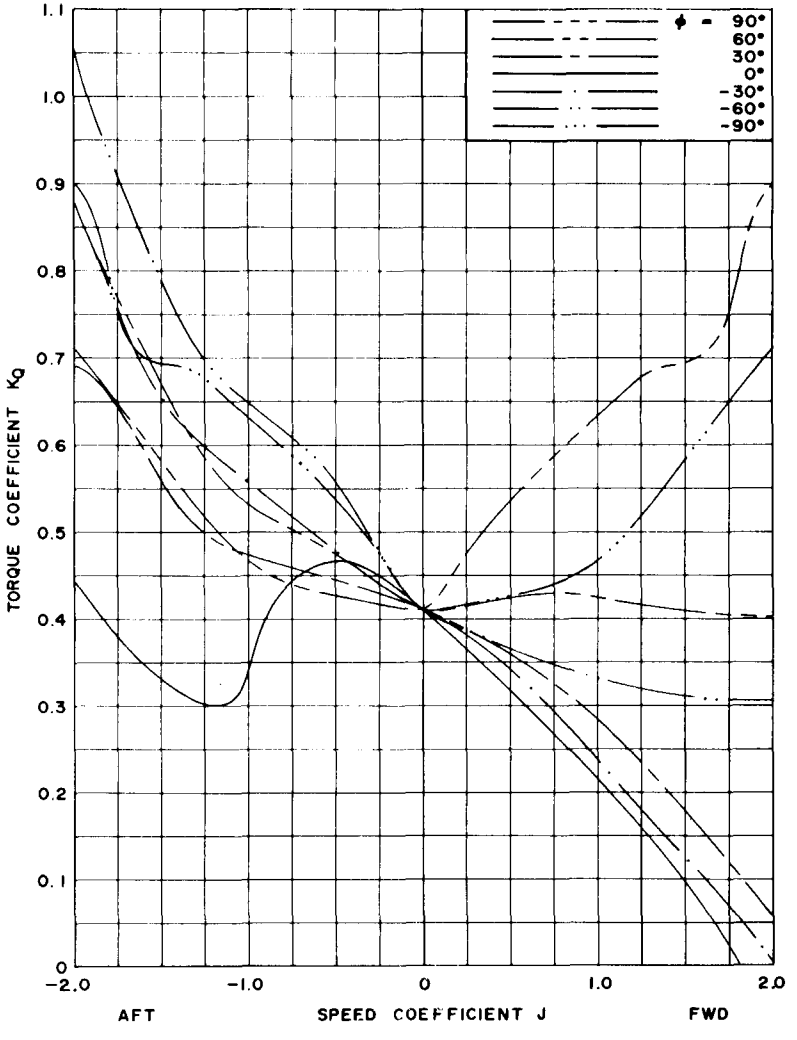

Figure 22b - Torque Characteristic Curves

0.5π Pitch Ratio

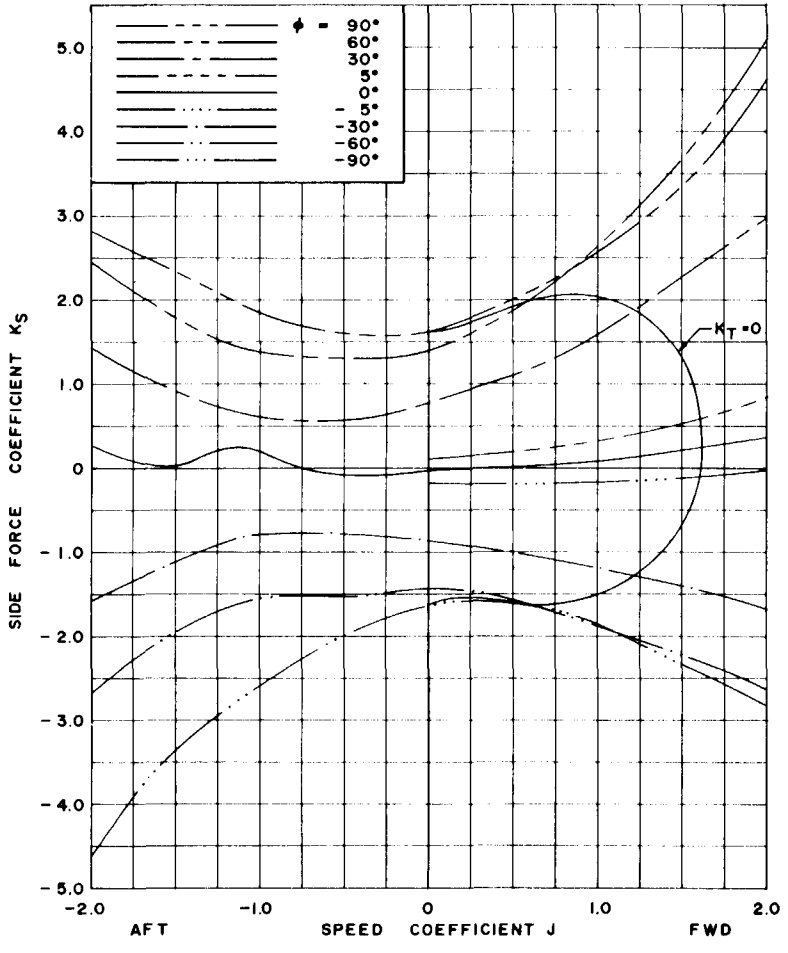

Figure 22c - Side Force Characteristics

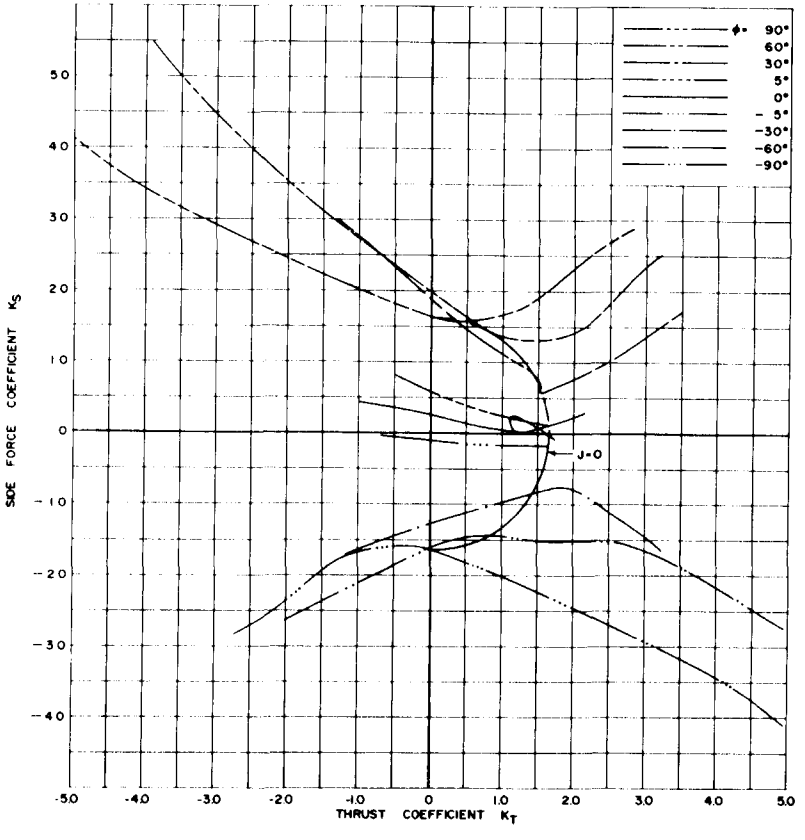

Figure 22d - Half-Circle Polar Diagram

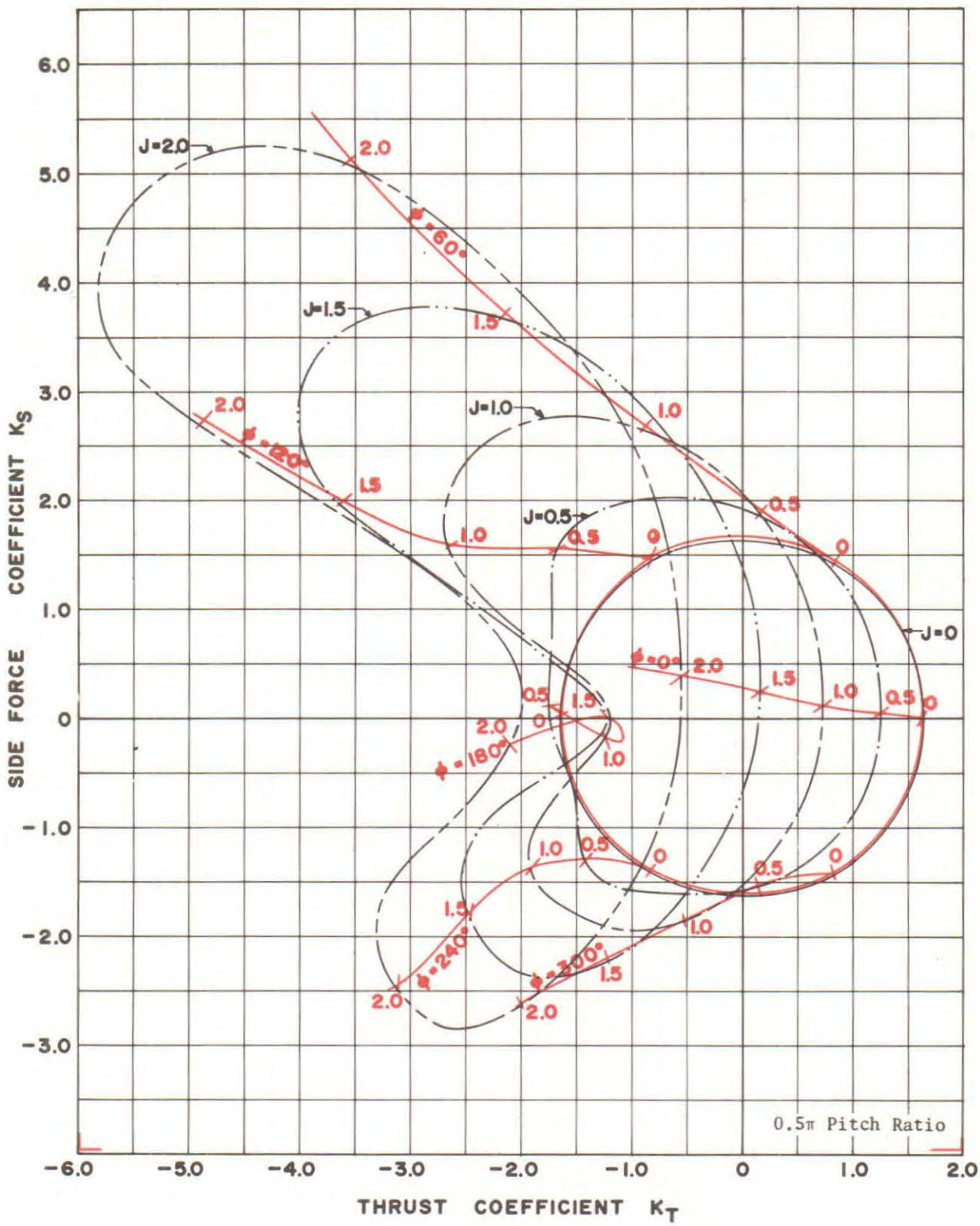

Figure 22e - Full-Circle Polar Diagram

Figure 23 - Propeller Characteristics with Variation of Steering Angle for 0.6π Pitch Ratio

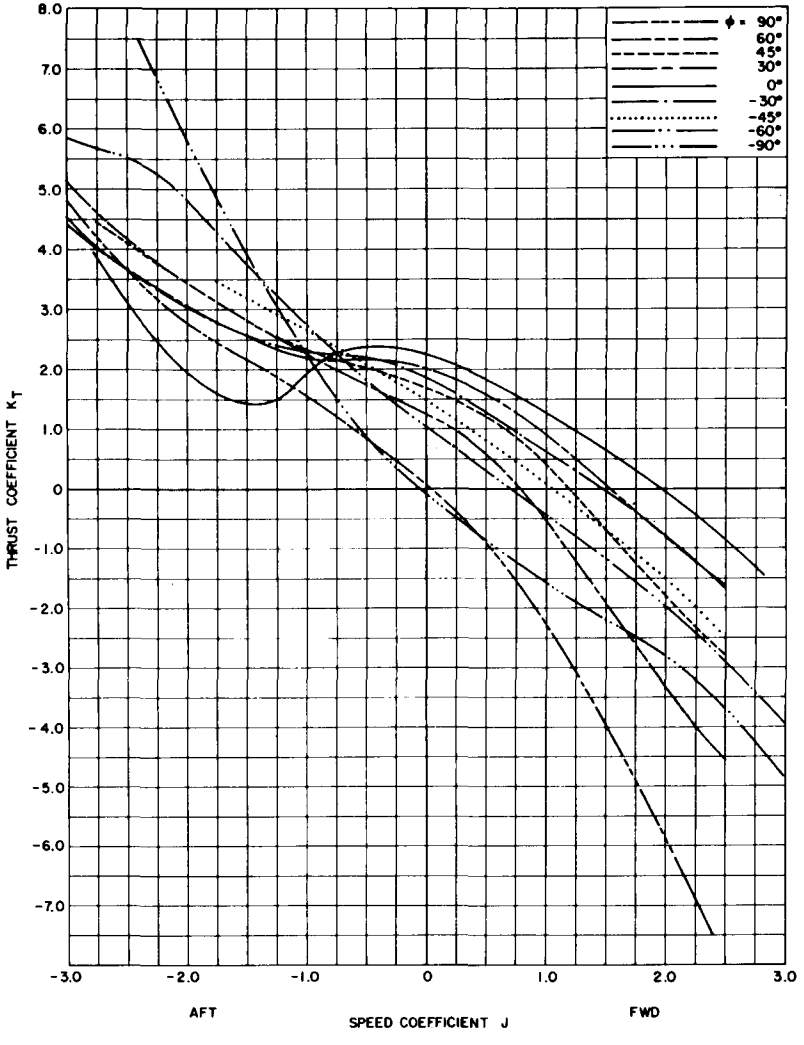

Figure 23a - Thrust Characteristic Curves

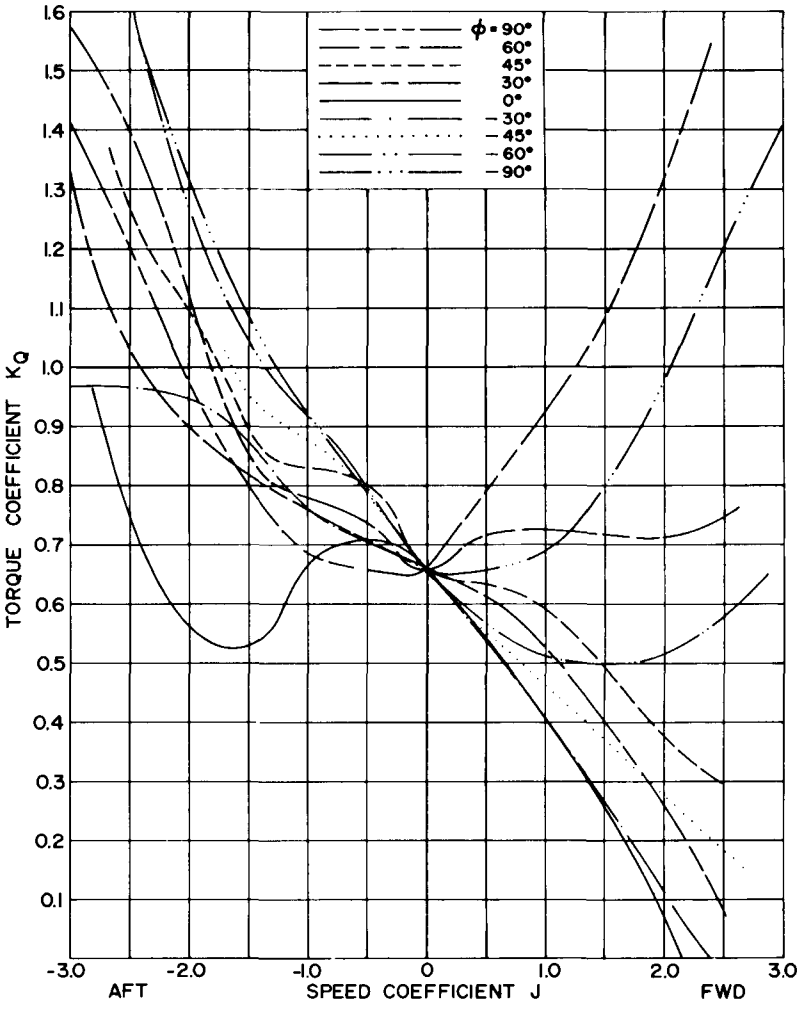

Figure 23b - Torque Characteristic Curves

0.6π Pitch Ratio

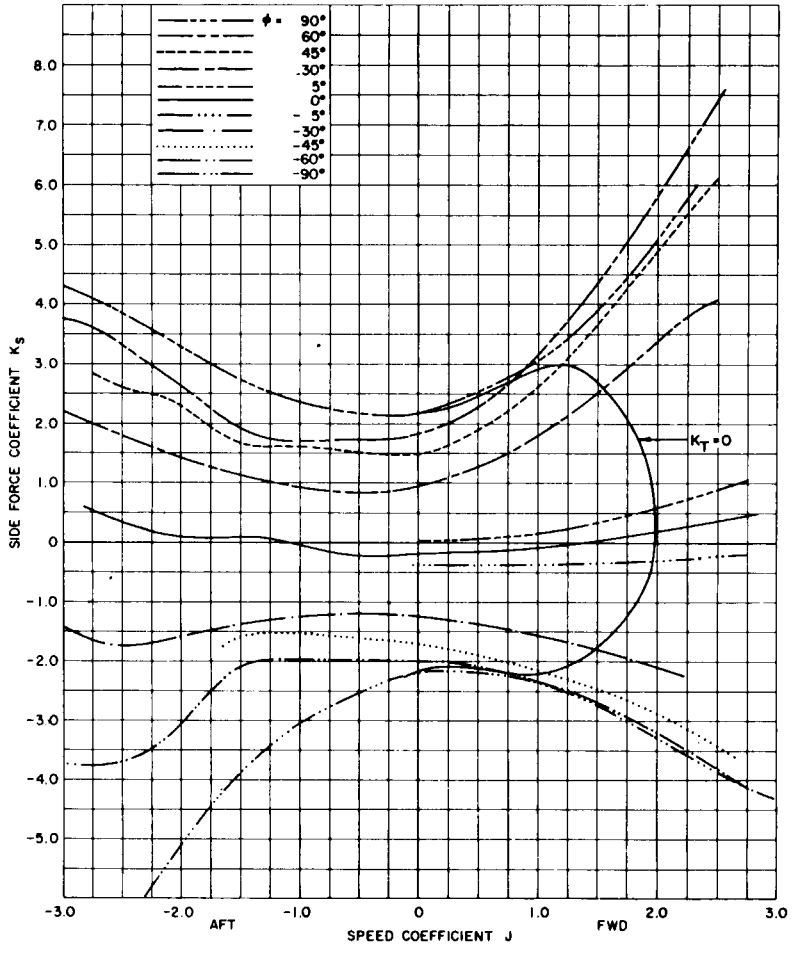

Figure 23c - Side Force Characteristics

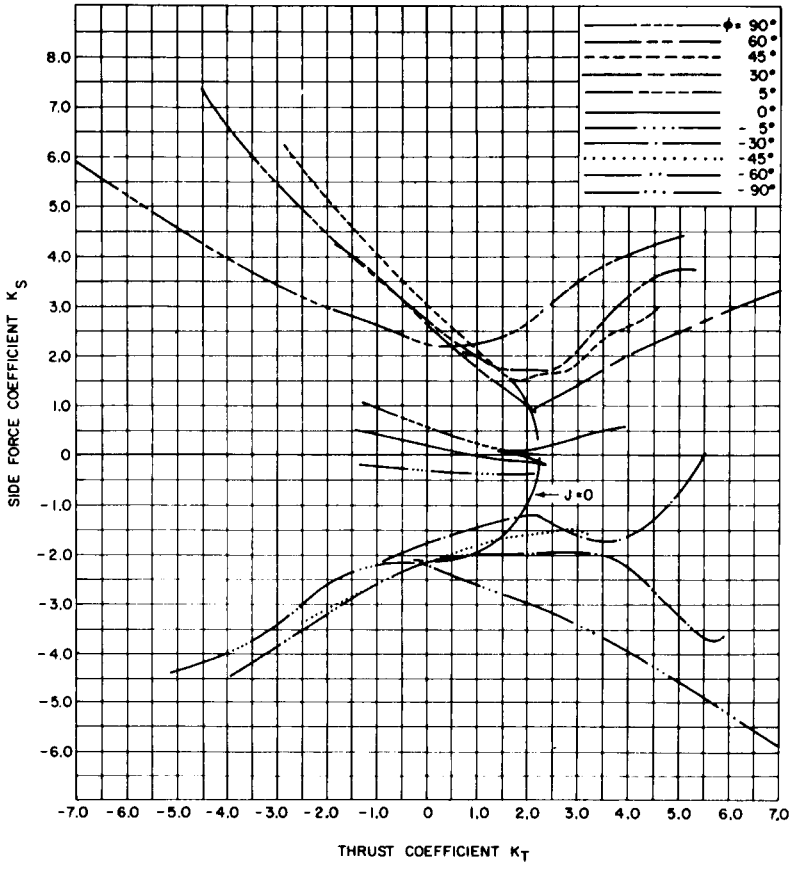

Figure 23d - Half-Circle Polar Diagram

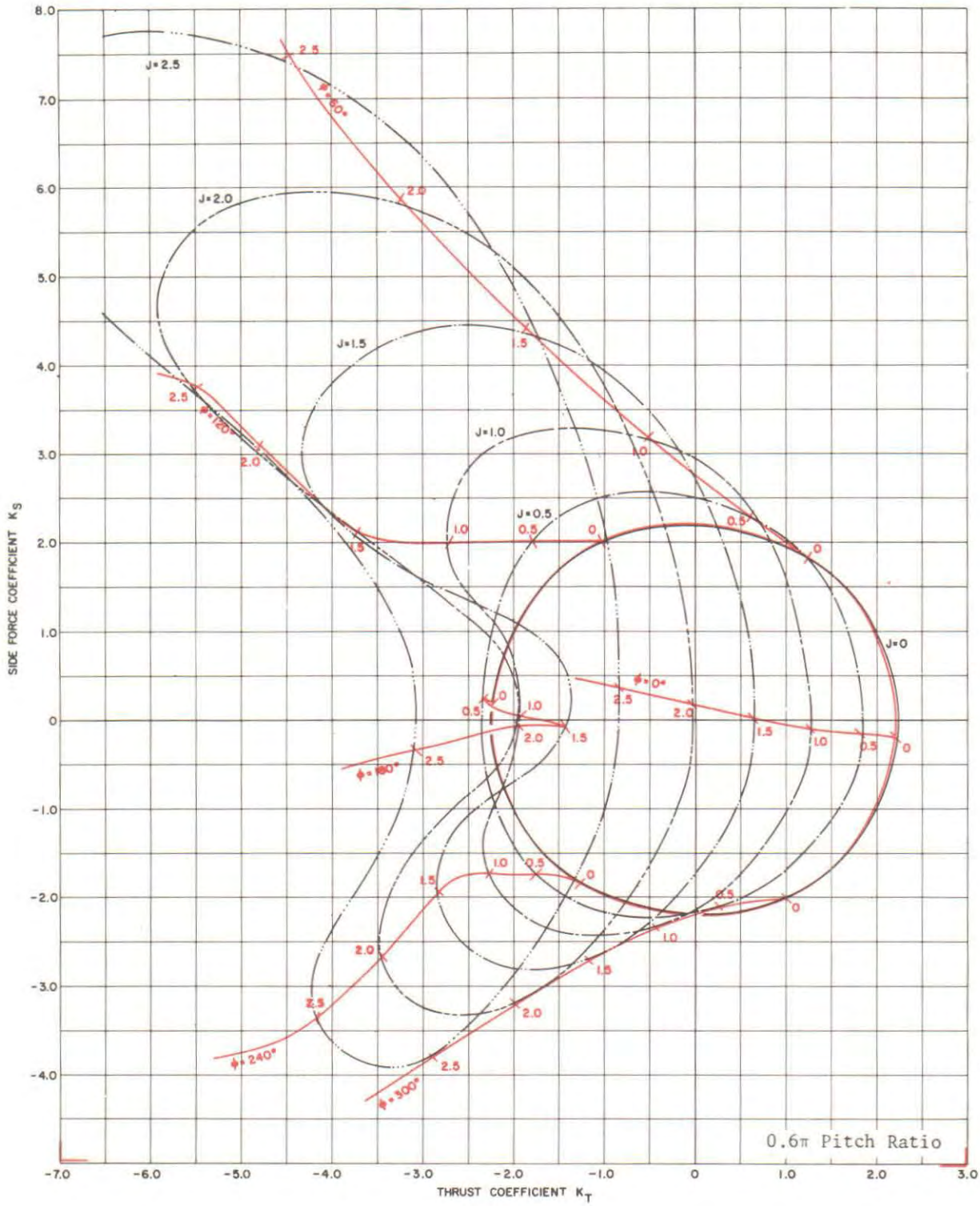

Figure 23e - Full-Circle Polar Diagram

Figure 24 - Propeller Characteristics with Variation of Steering Angle for 0.7π Pitch Ratio

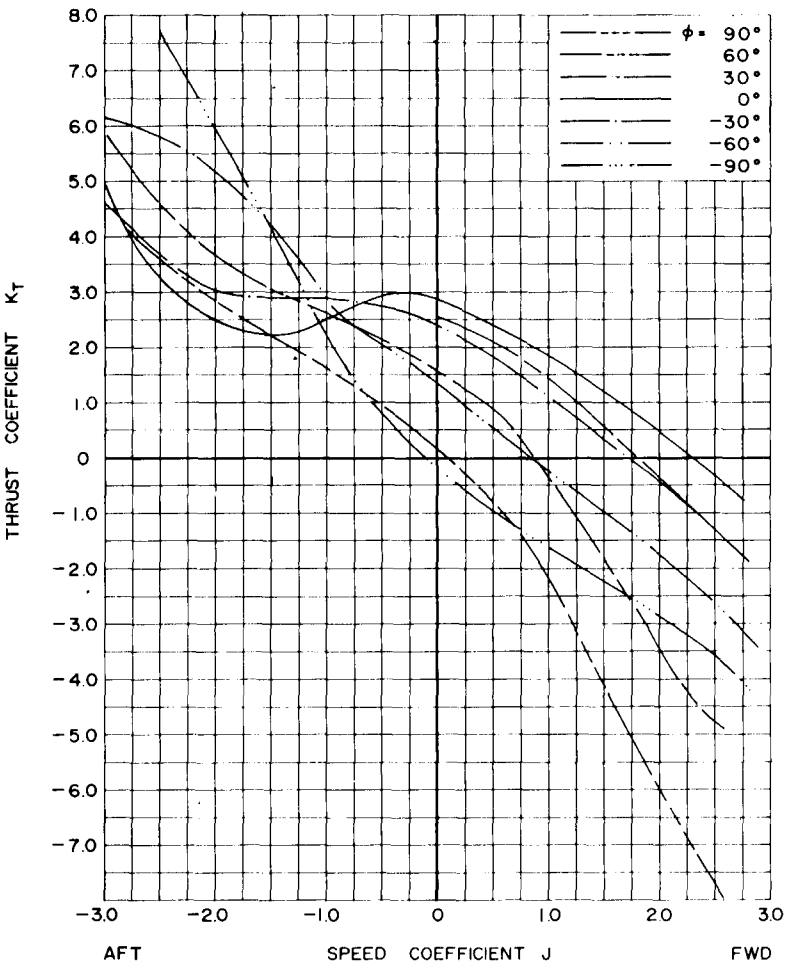

Figure 24a - Thrust Characteristic Curves

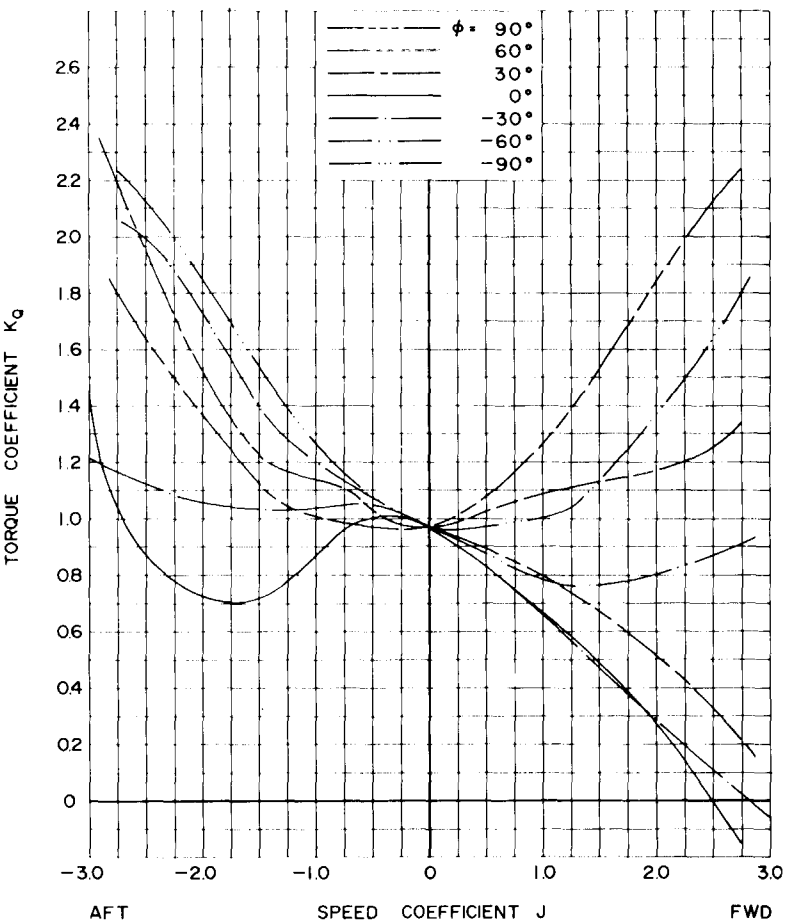

Figure 24b - Torque Characteristic Curves

0.7π Pitch Ratio

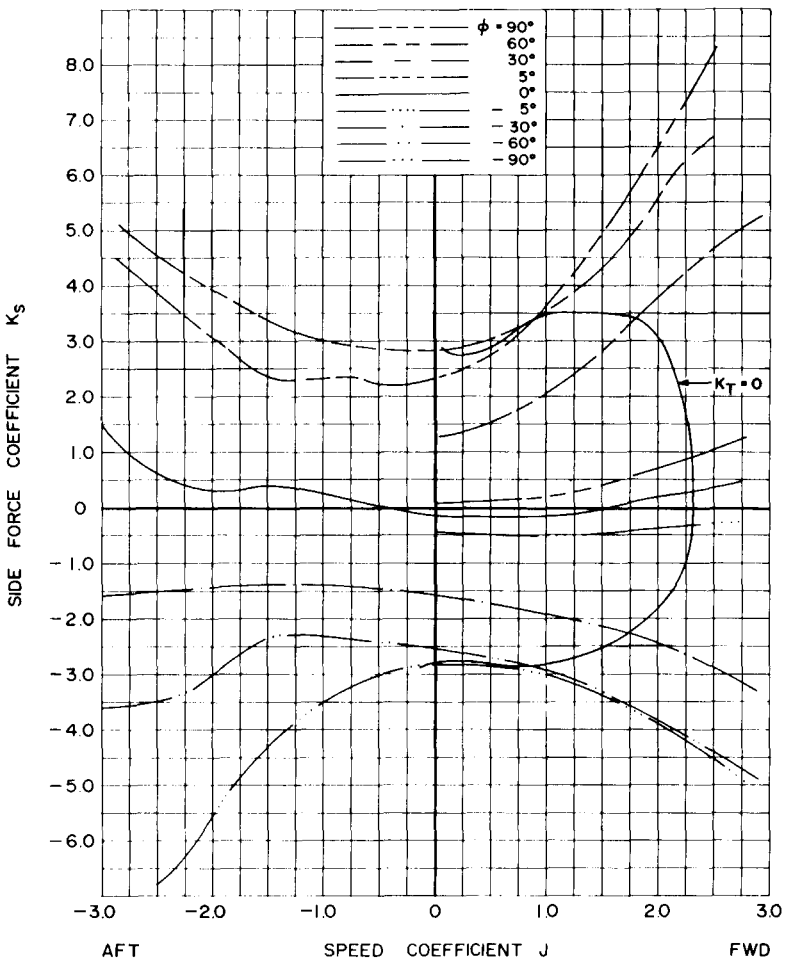

Figure 24c - Side Force Characteristics

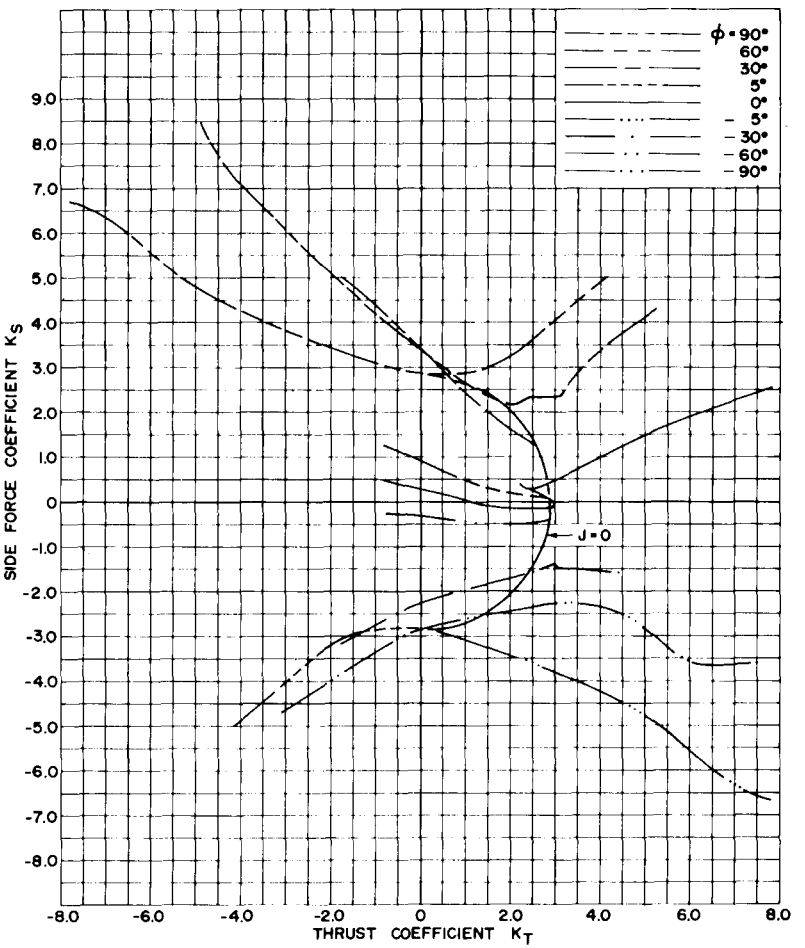

Figure 24d - Half-Circle Polar Diagram

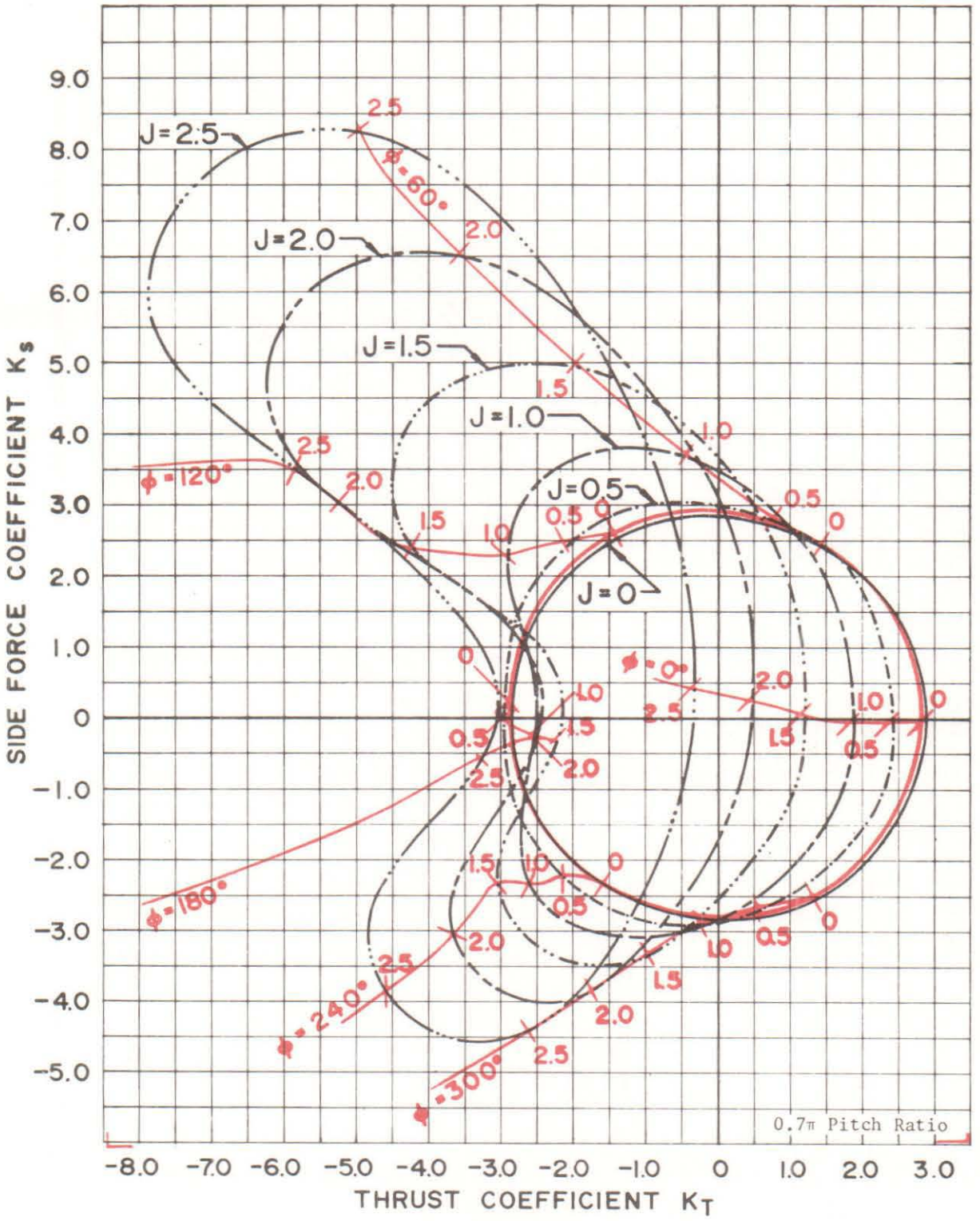

Figure 24e - Full-Circle Polar Diagram

Figure 25 - Propeller Characteristics with Variation of Steering Angle for 0.8π Pitch Ratio

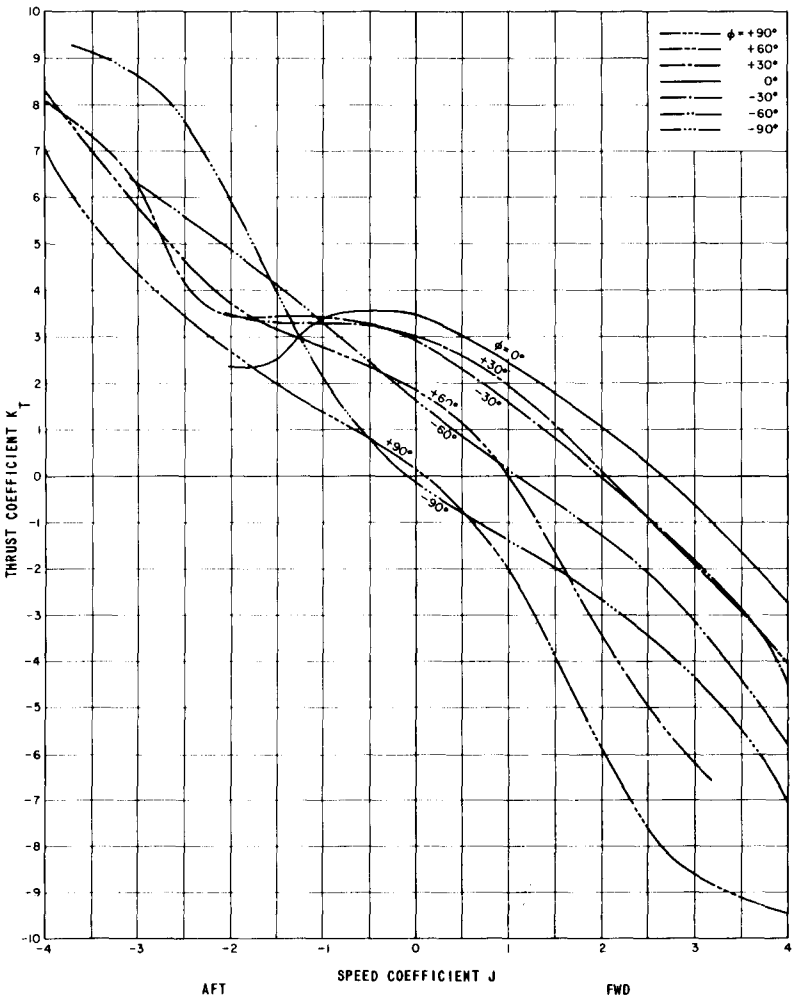

Figure 25a - Thrust Characteristic Curves

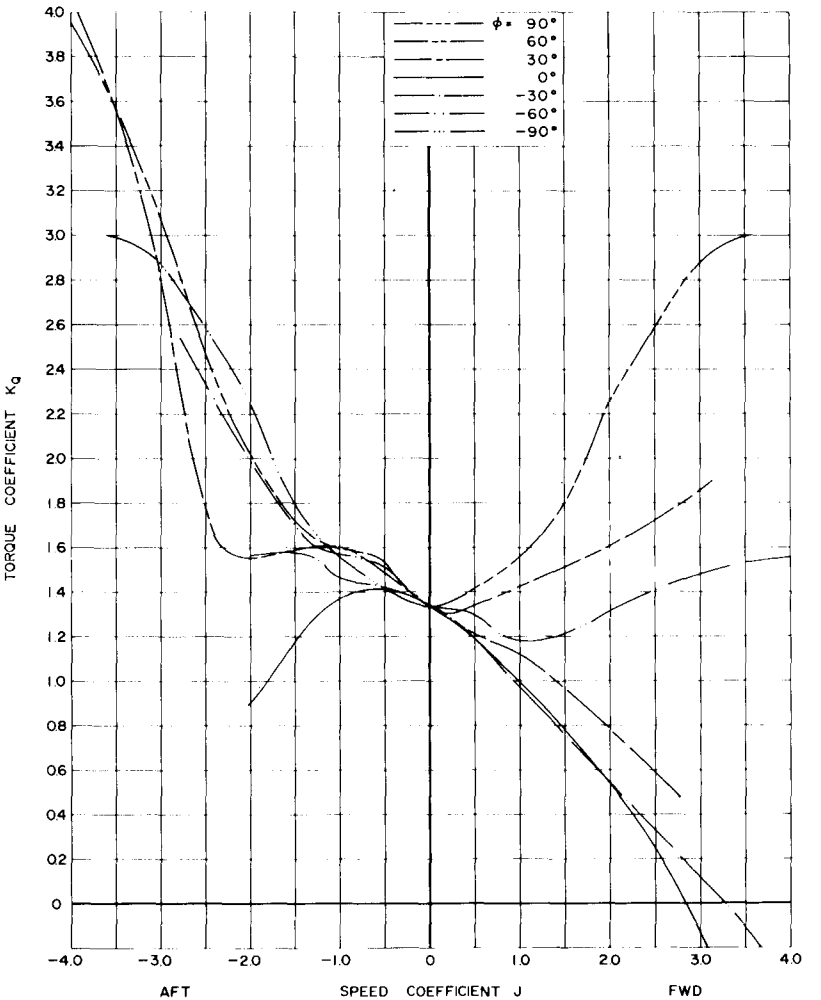

Figure 25b - Torque Characteristic Curves

0.8π Pitch Ratio

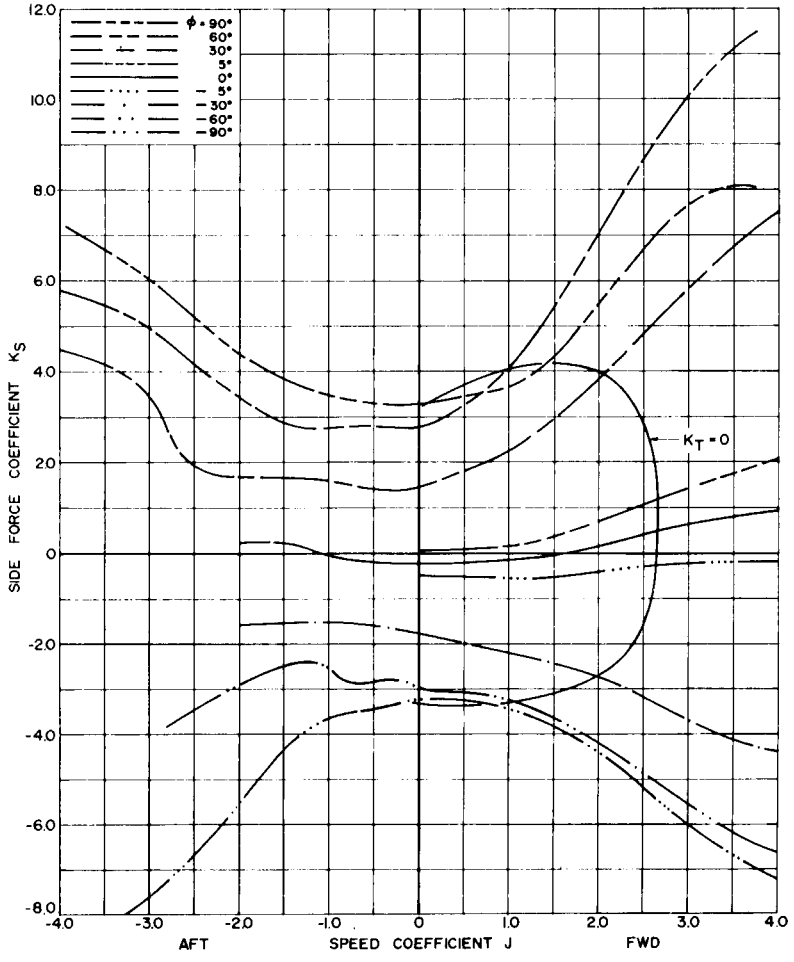

Figure 25c - Side Force Characteristics

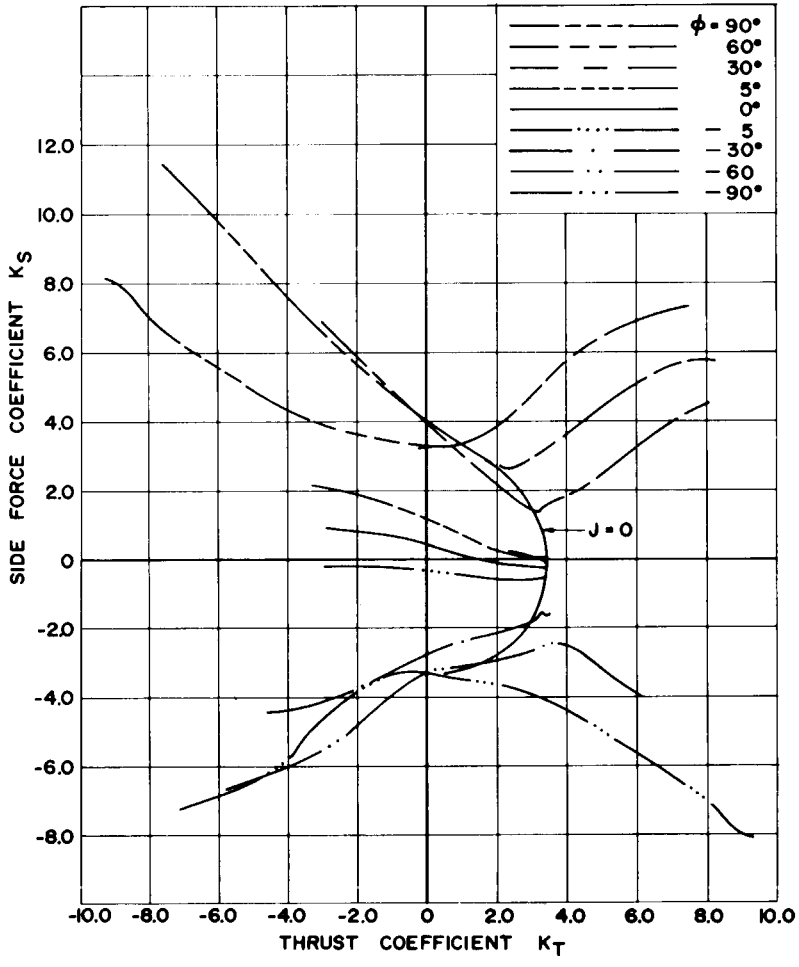

Figure 25d - Half-Circle Polar Diagram

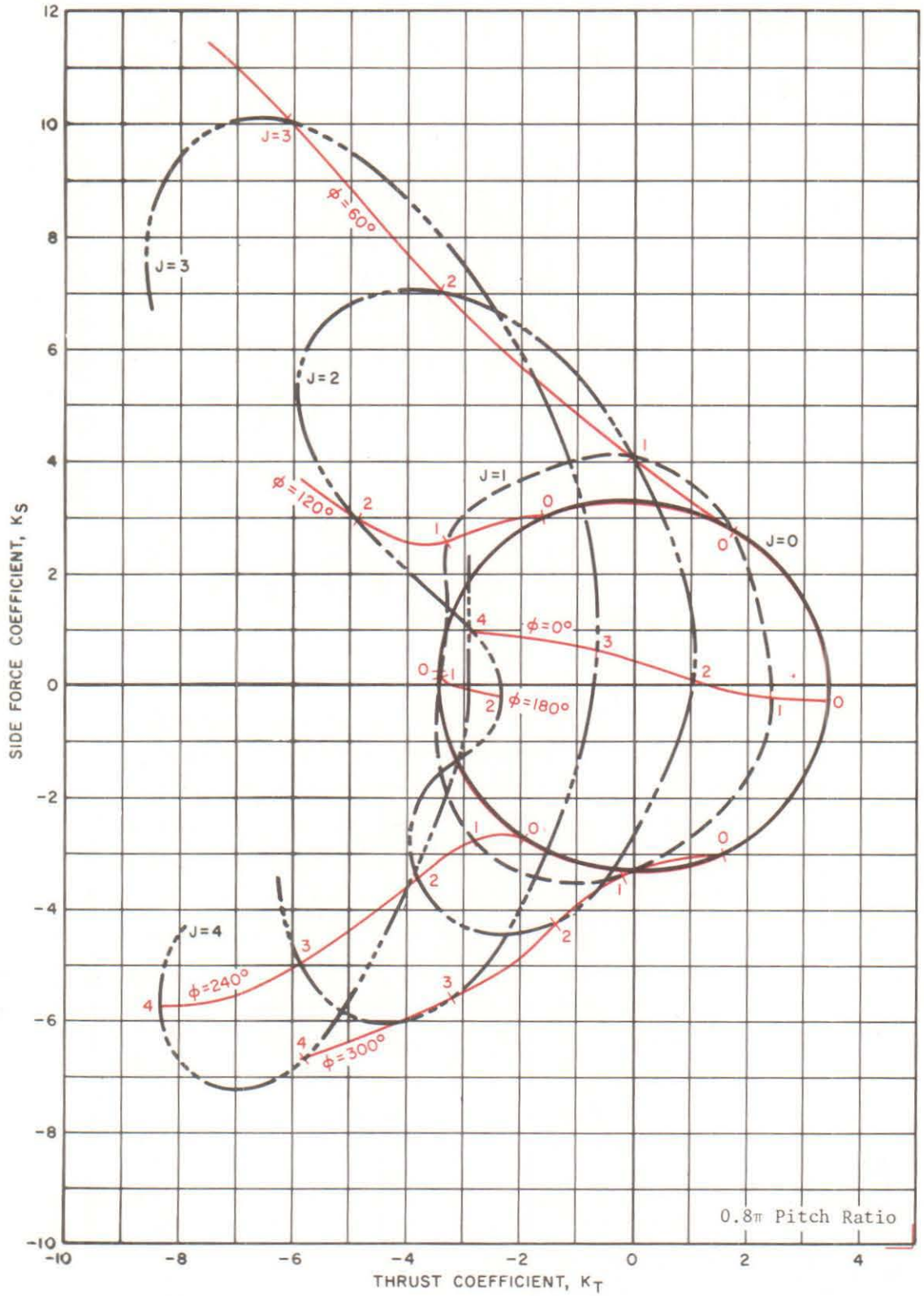

Figure 25e - Full-Circle Polar Diagram

Figure 26 - Propeller Characteristics with Variation of Steering Angle for 0.9π Pitch Ratio

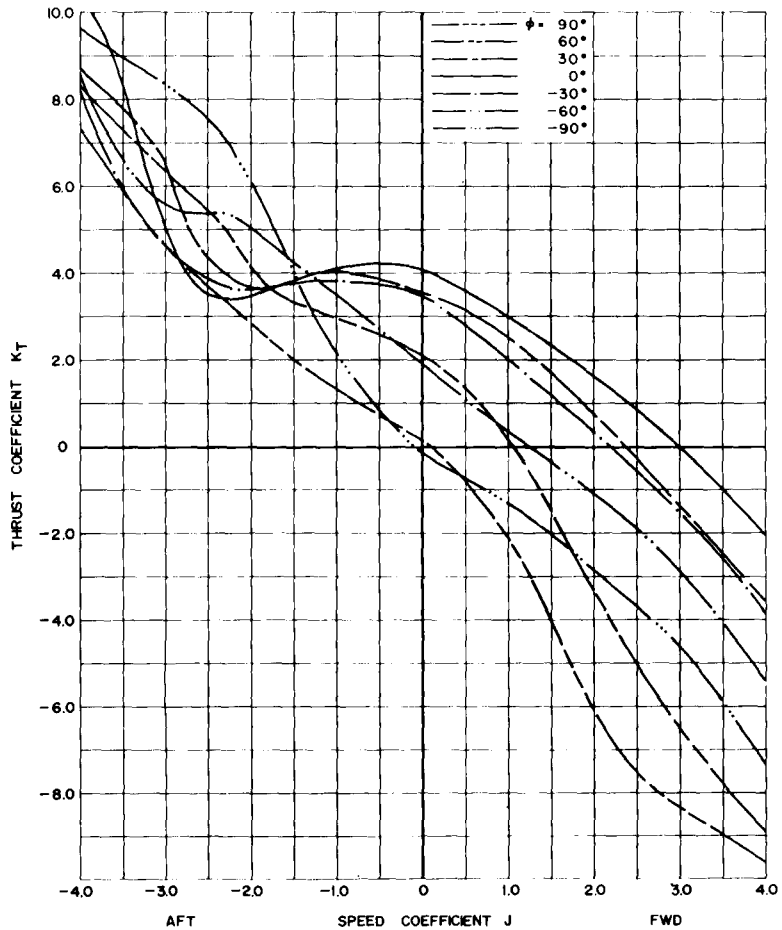

Figure 26a - Thrust Characteristic Curves

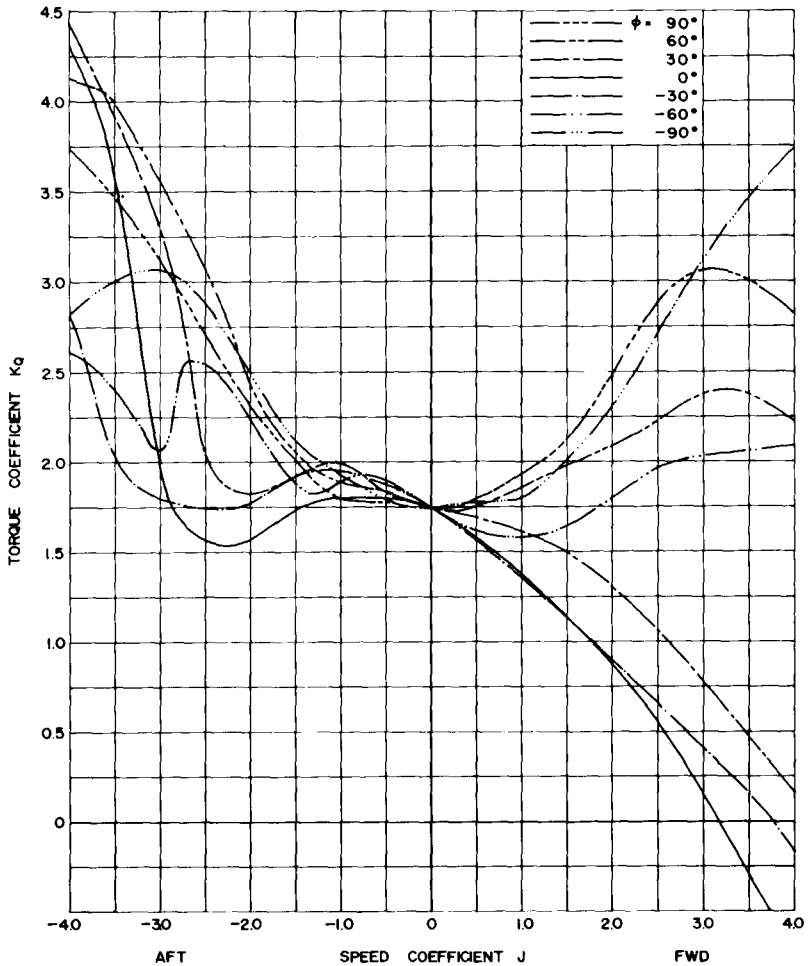

Figure 26b - Torque Characteristic Curves

0.9π Pitch Ratio

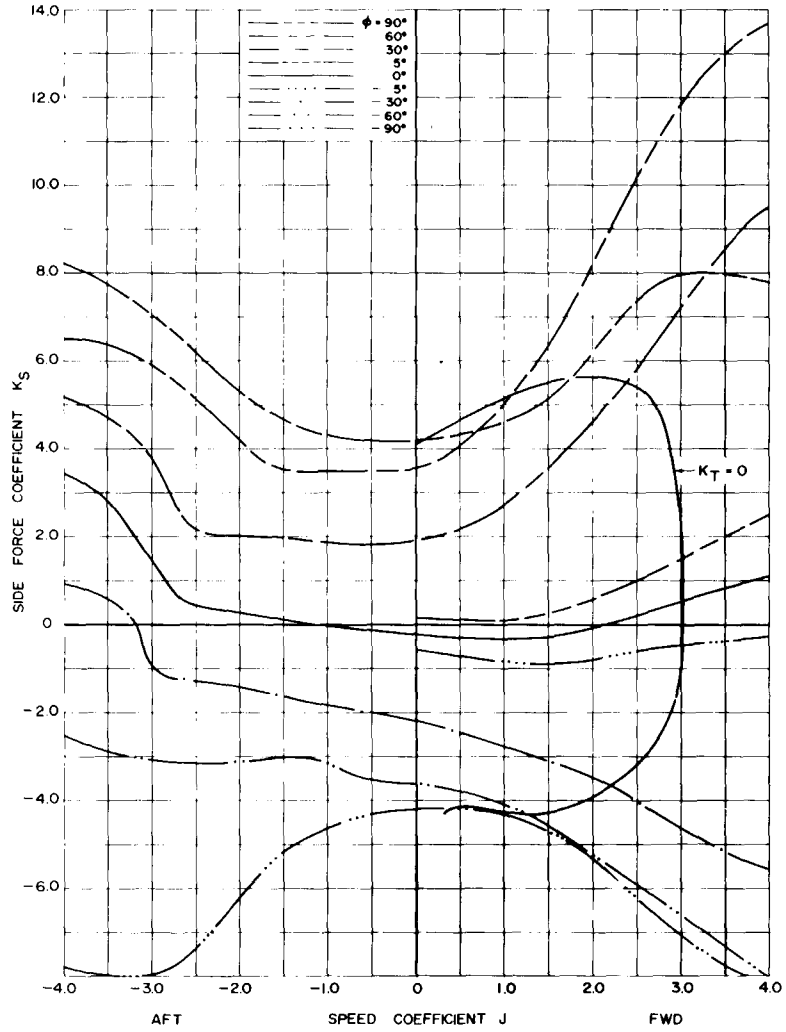

Figure 26c - Side Force Characteristics

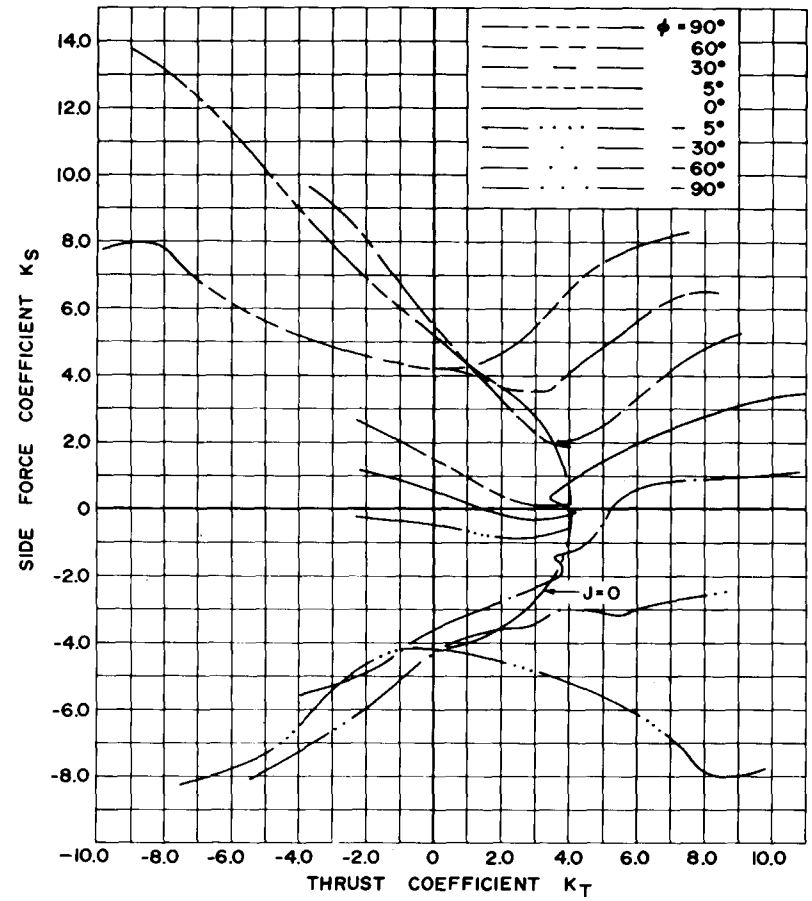

Figure 26d - Half-Circle Polar Diagram

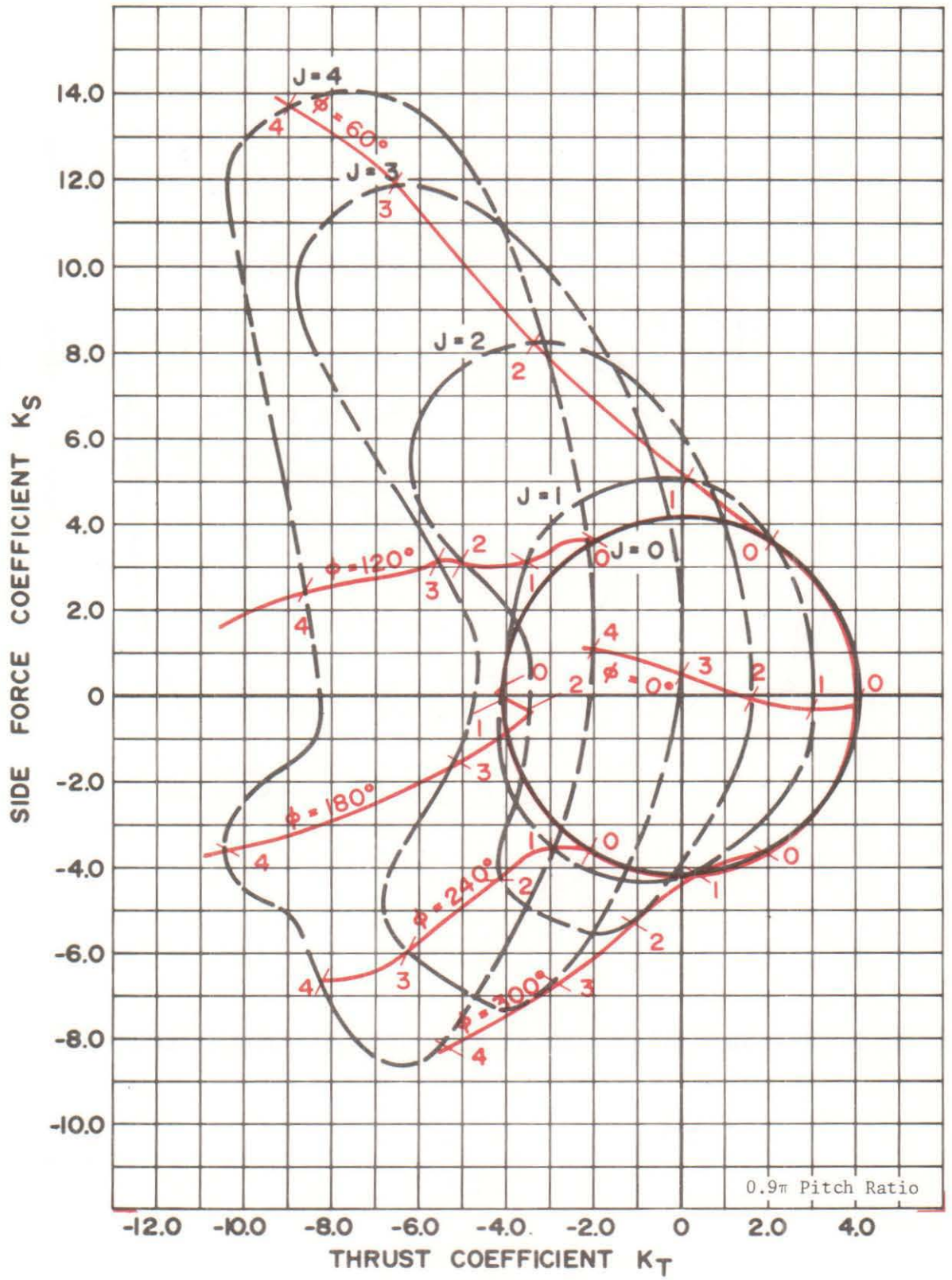

Figure 26e - Full-Circle Polar Diagram

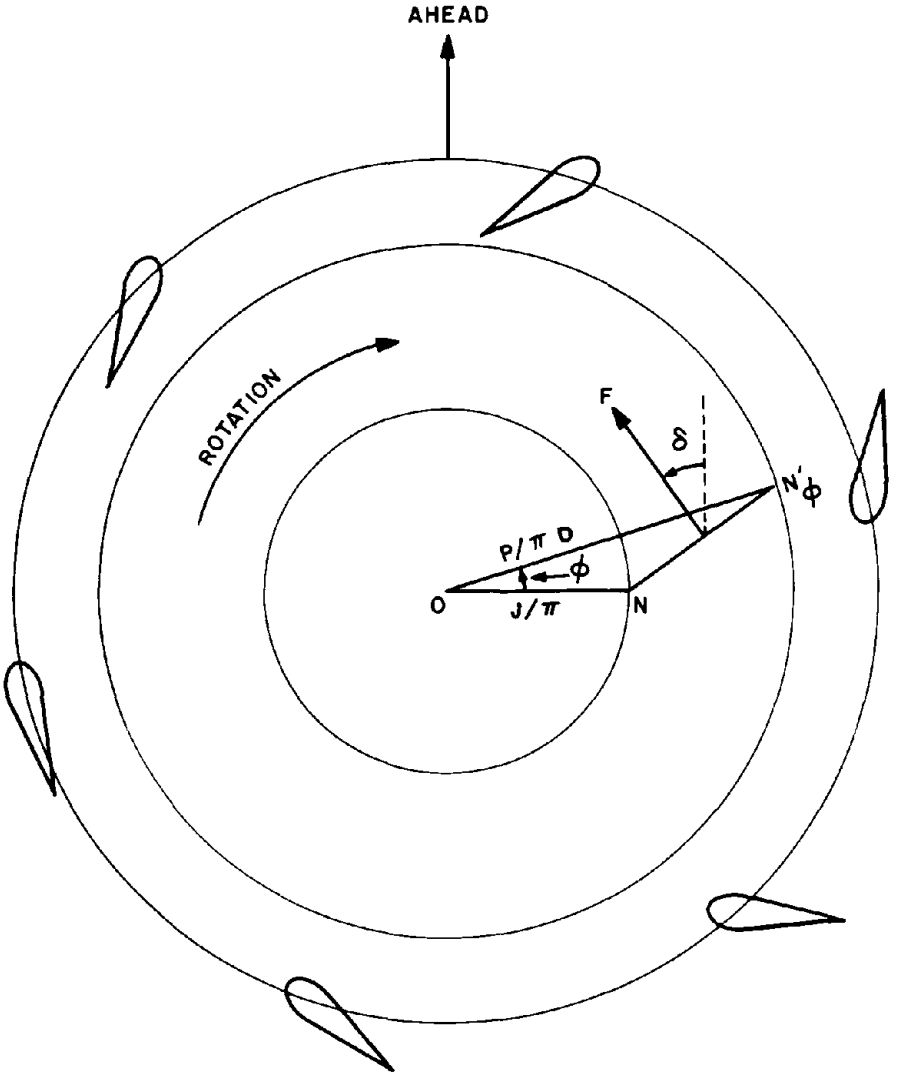

Figure 27 - Graphical Prediction of the Direction of Resultant Force

Figure 28 - Angle of Resultant Force Vector for 0.4π Pitch Ratio

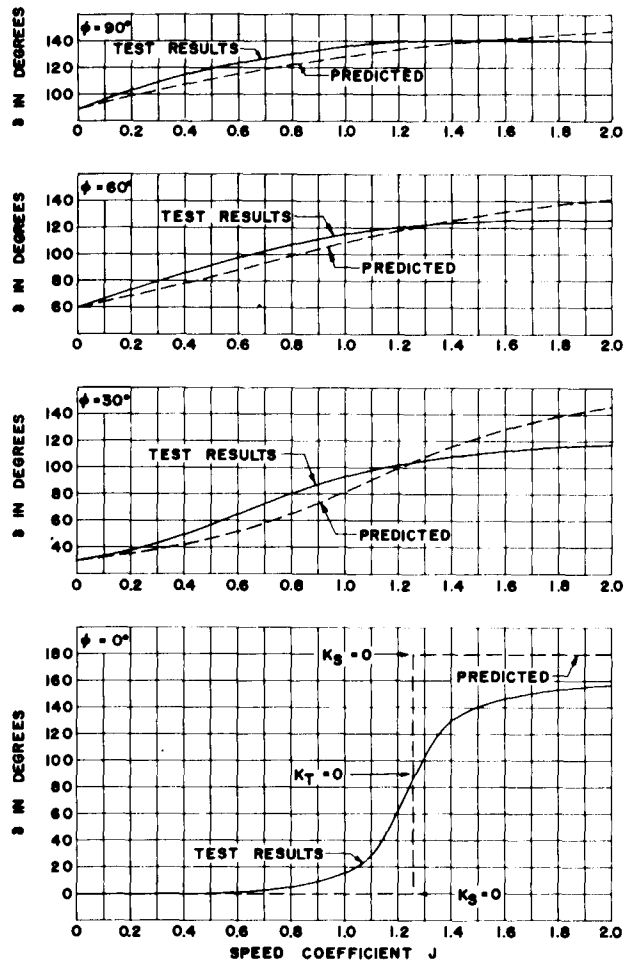

Figure 28a - Steering Angles in First Quadrant

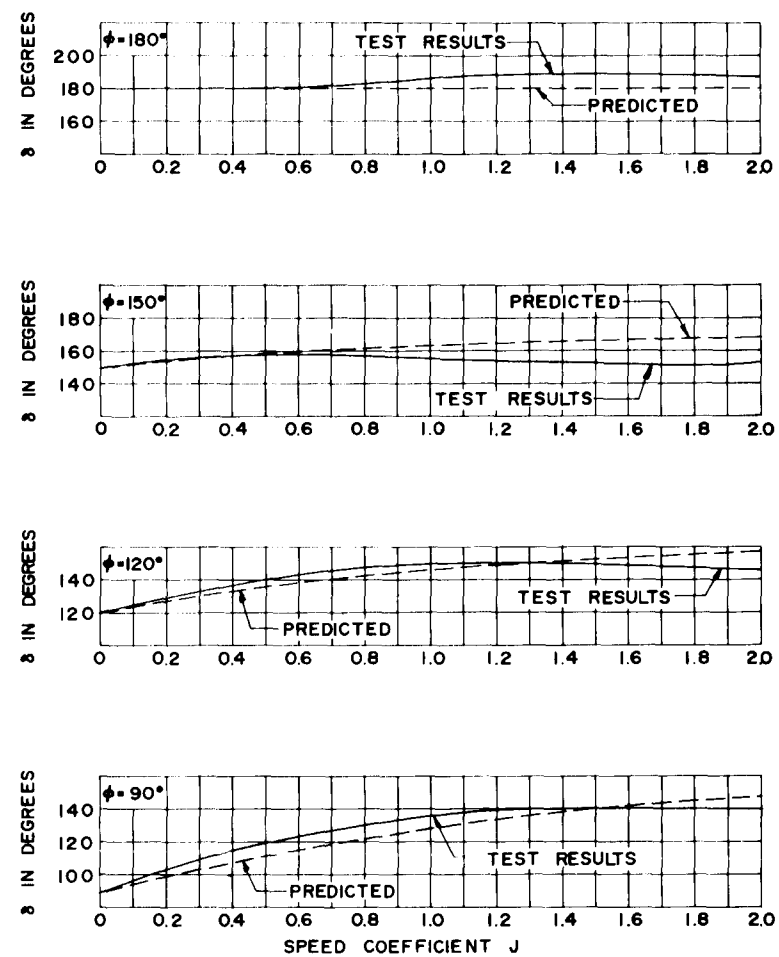

Figure 28b - Steering Angles in Second Quadrant

0.4π Pitch Ratio

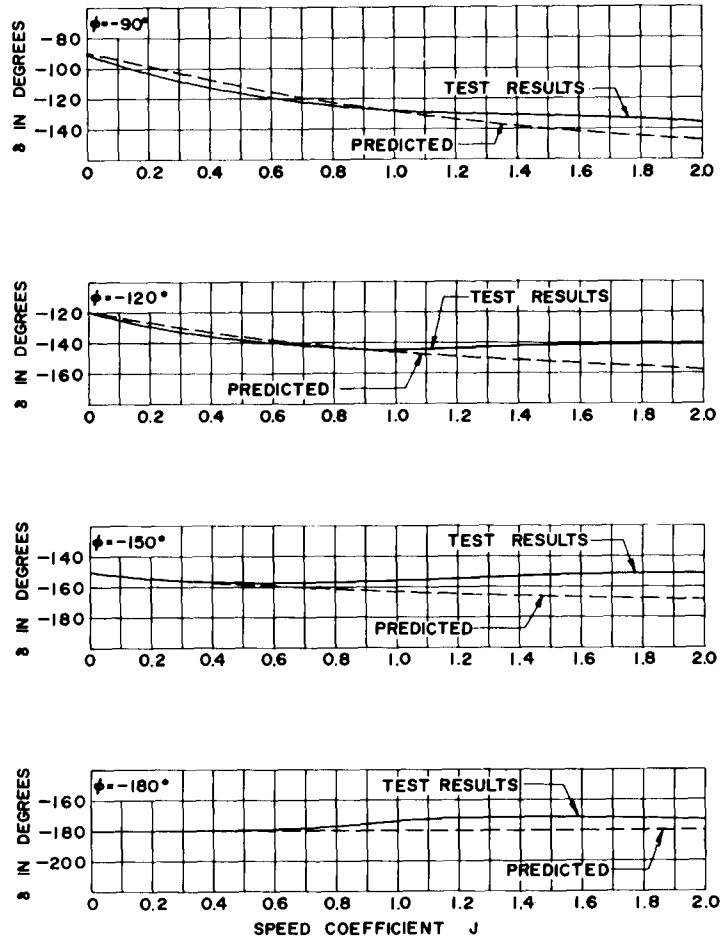

Figure 28c - Steering Angles in Third Quadrant

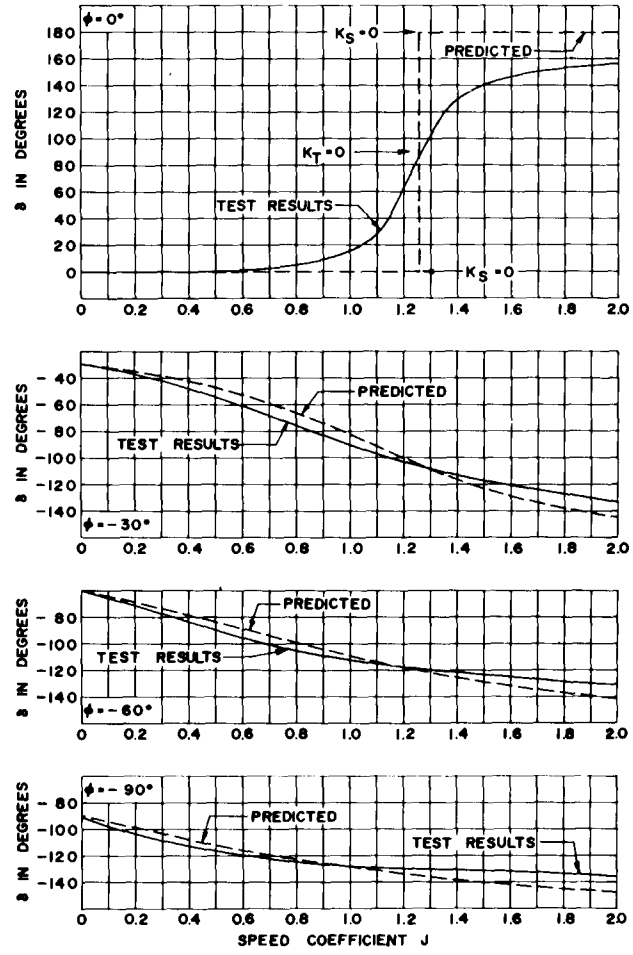

Figure 28d - Steering Angles in Fourth Quadrant

Figure 29 - Angle of Resultant Force Vector for 0.5π Pitch Ratio

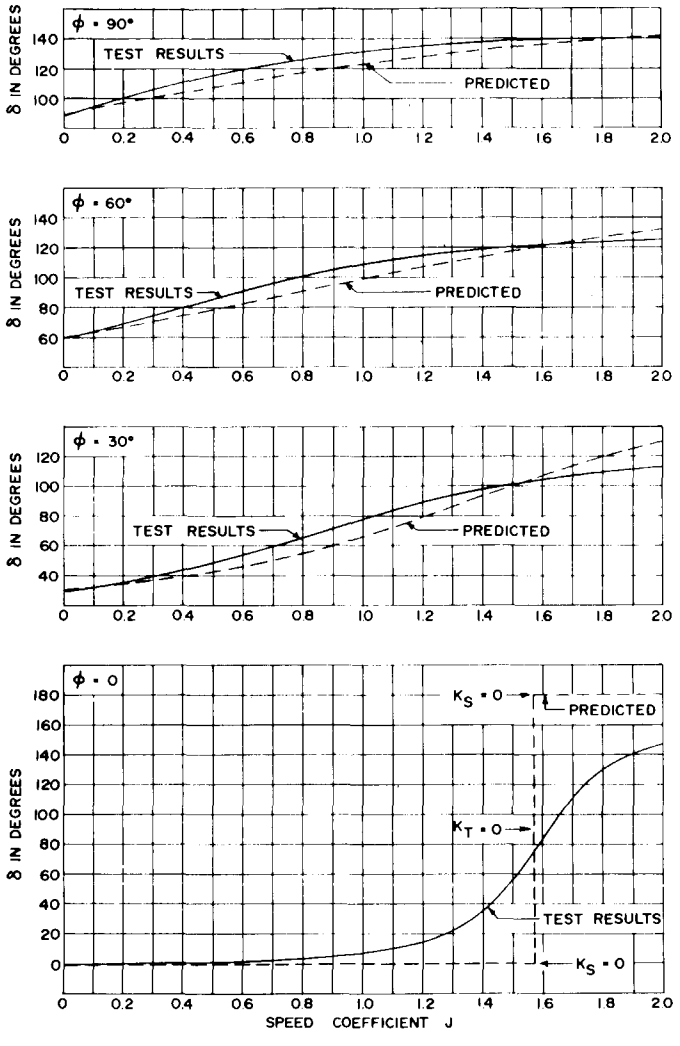

Figure 29a - Steering Angles in First Quadrant

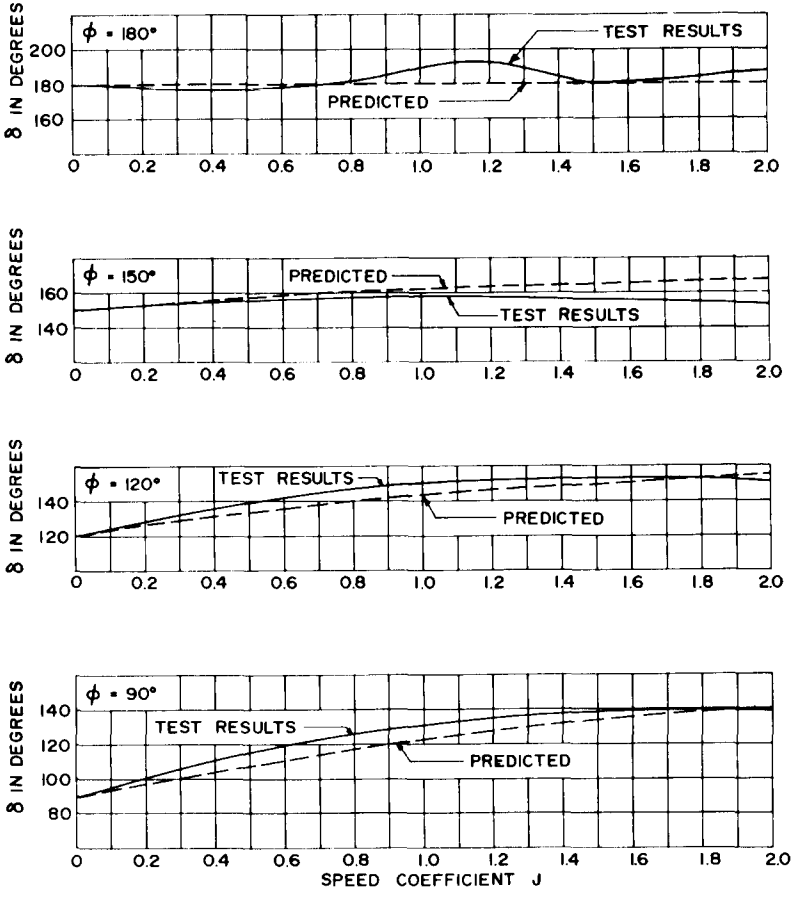

Figure 29b - Steering Angles in Second Quadrant

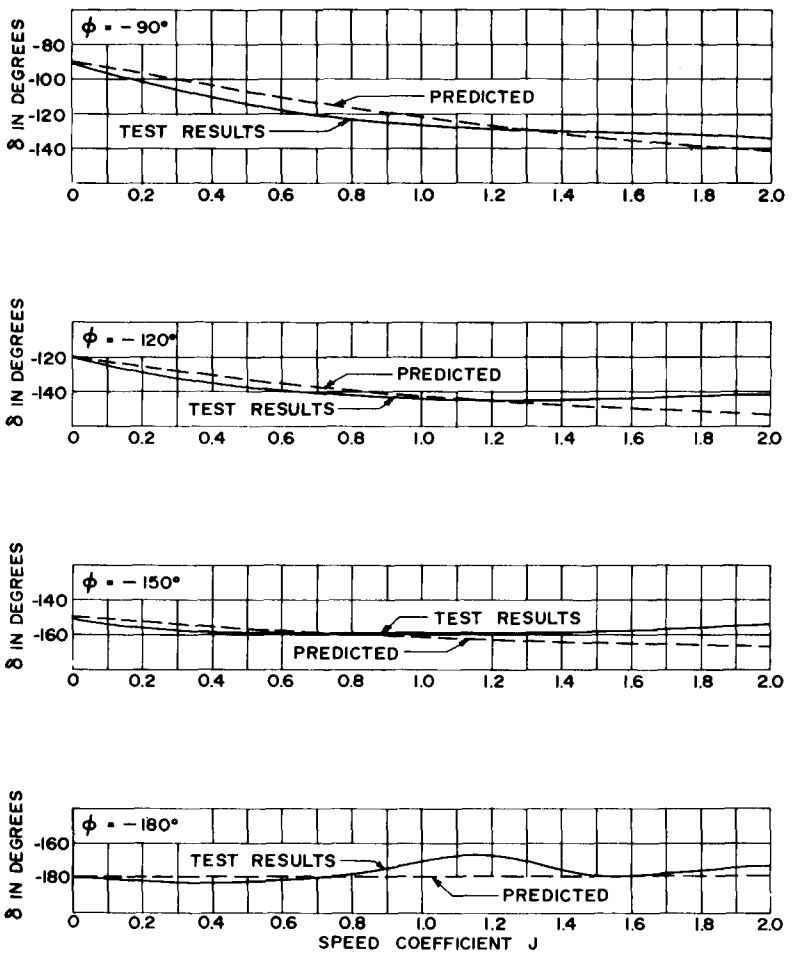

Figure 29c - Steering Angles in Third Quadrant

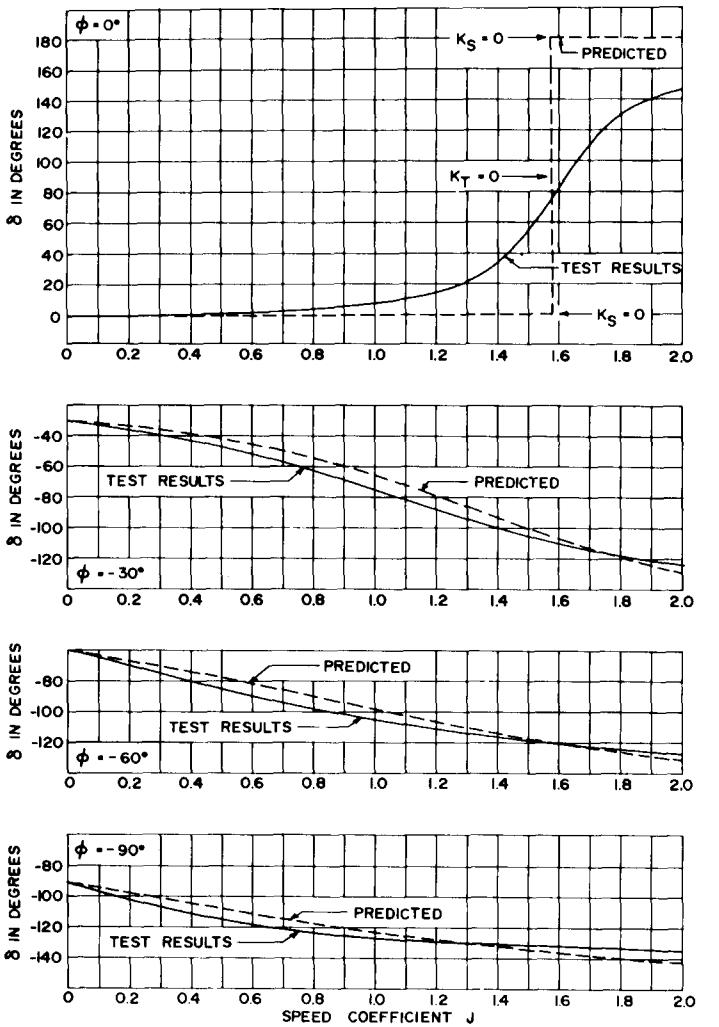

Figure 29d - Steering Angles in Fourth Quadrant

Figure 30 - Angle of Resultant Force Vector for 0.6π Pitch Ratio

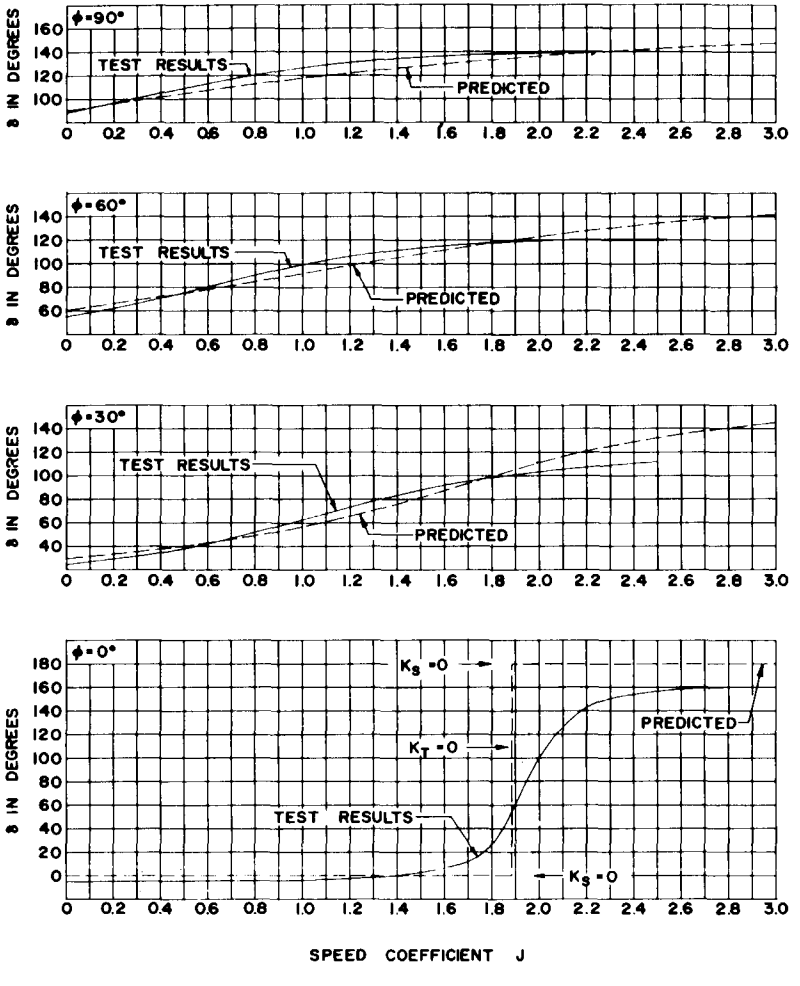

Figure 30a - Steering Angles in First Quadrant

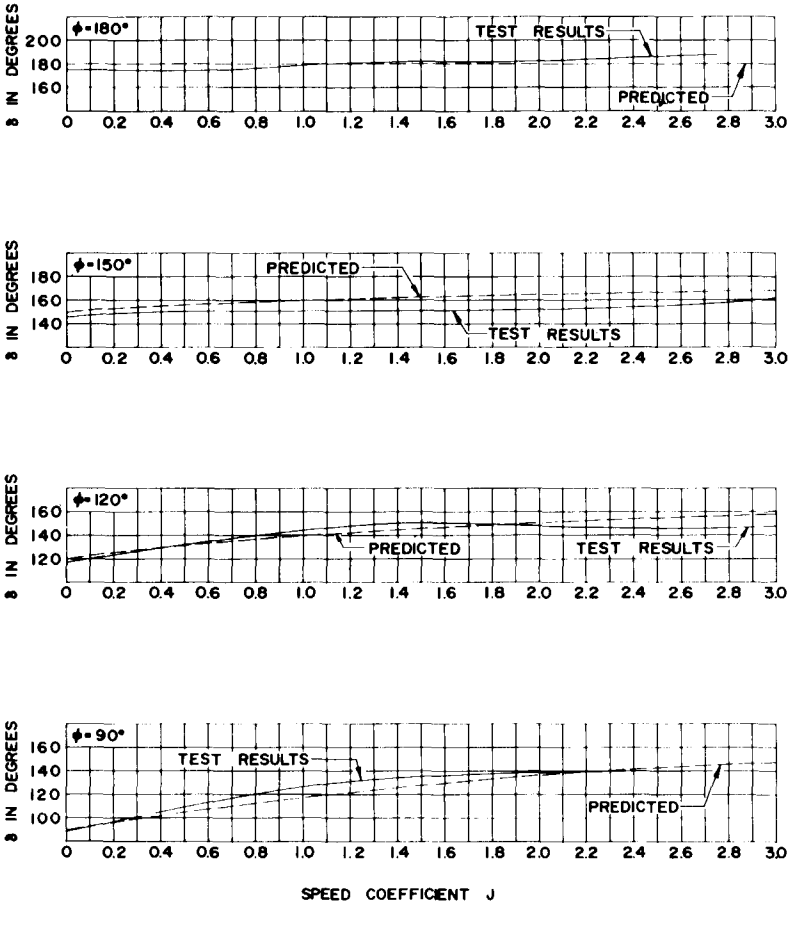

Figure 30b - Steering Angles in Second Quadrant

0.6π Pitch Ratio

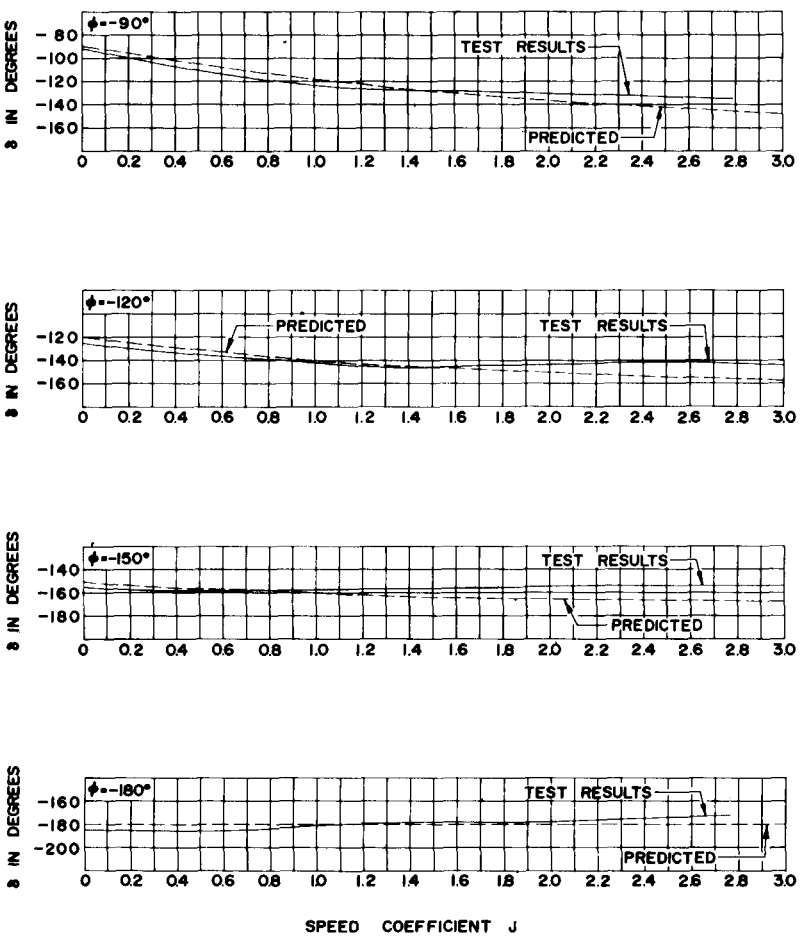

Figure 30c - Steering Angles in Third Quadrant

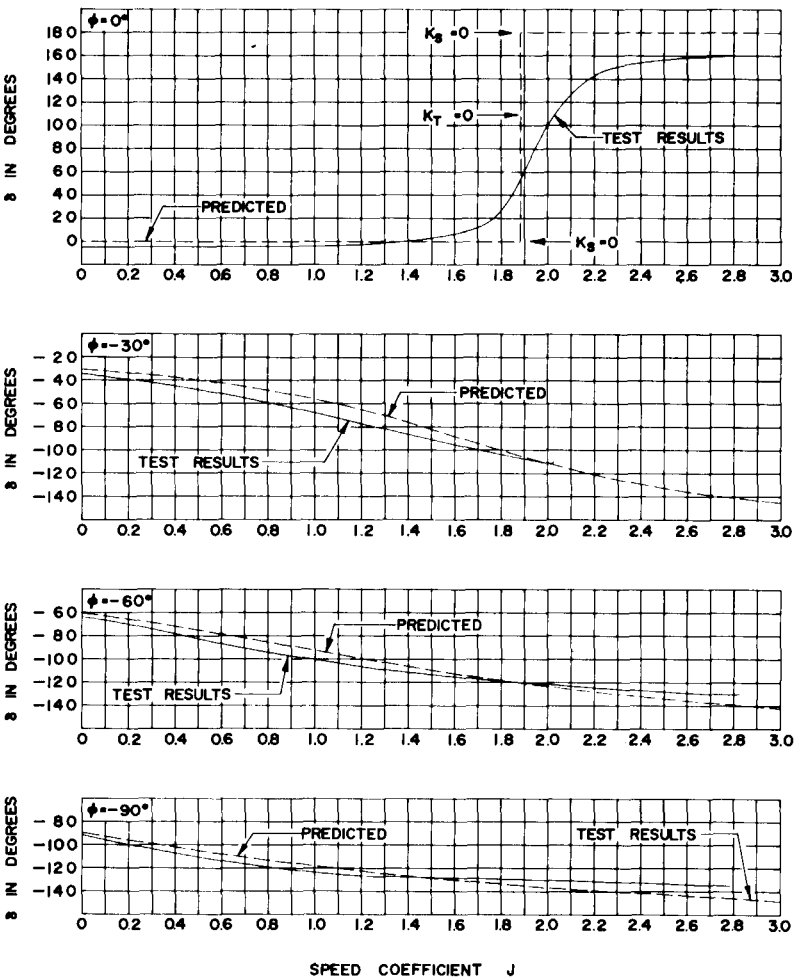

Figure 30d - Steering Angles in Fourth Quadrant

Figure 31 - Angle of Resultant Force Vector for 0.7π Pitch Ratio

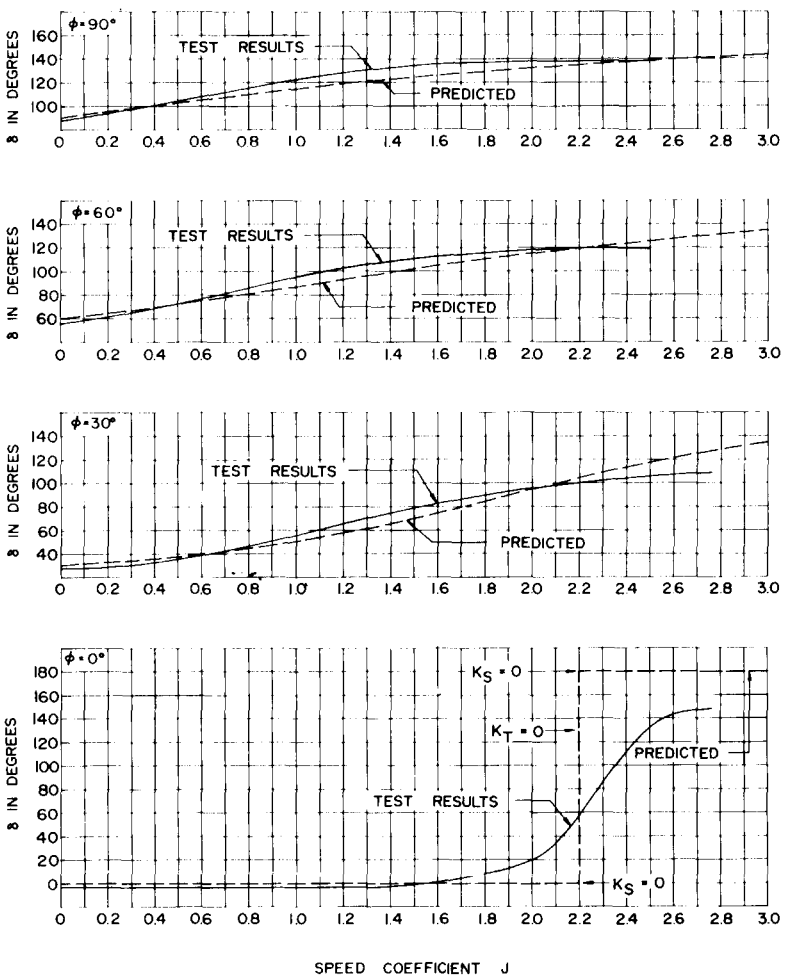

Figure 31a - Steering Angles in First Quadrant

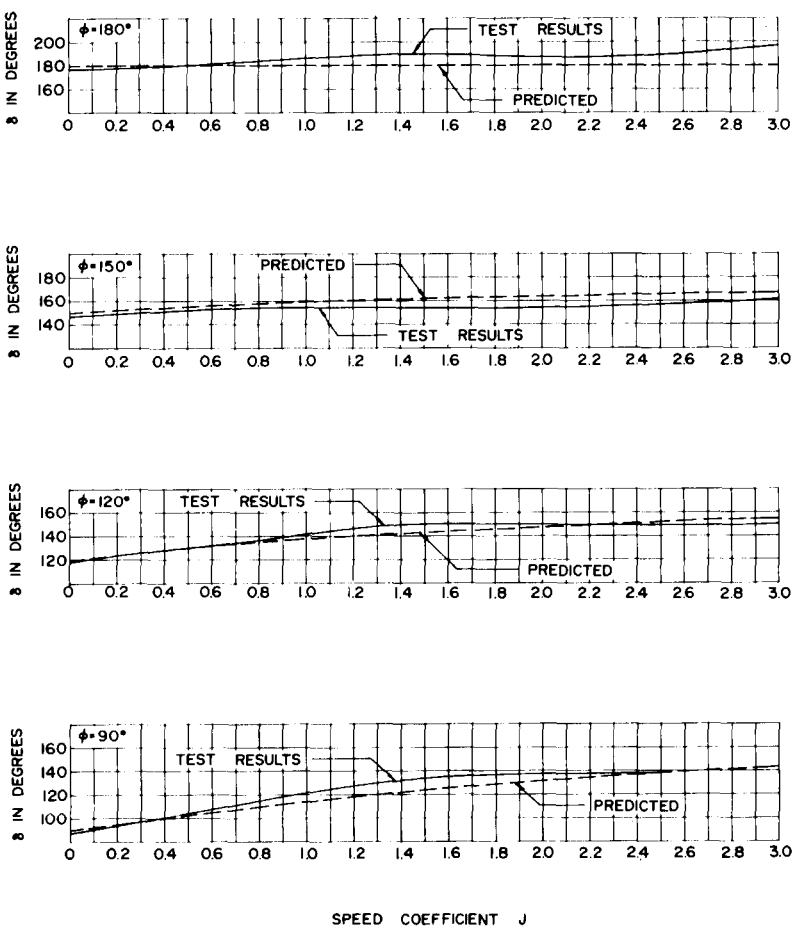

Figure 31b - Steering Angles in Second Quadrant

0.7π Pitch Ratio

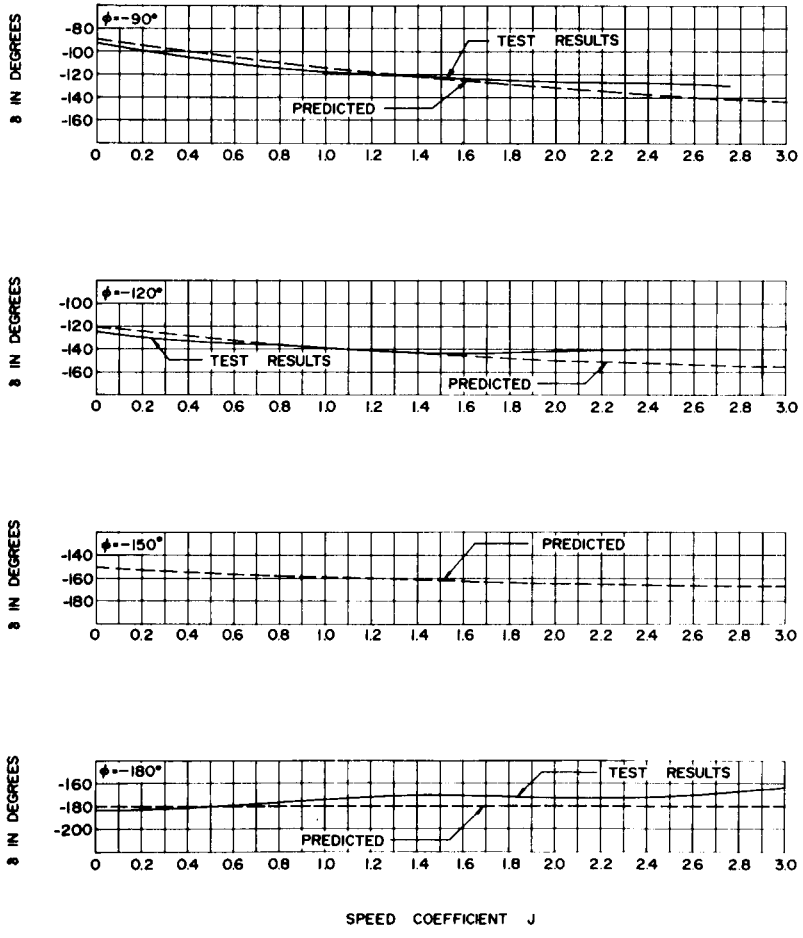

Figure 31c - Steering Angles in Third Quadrant

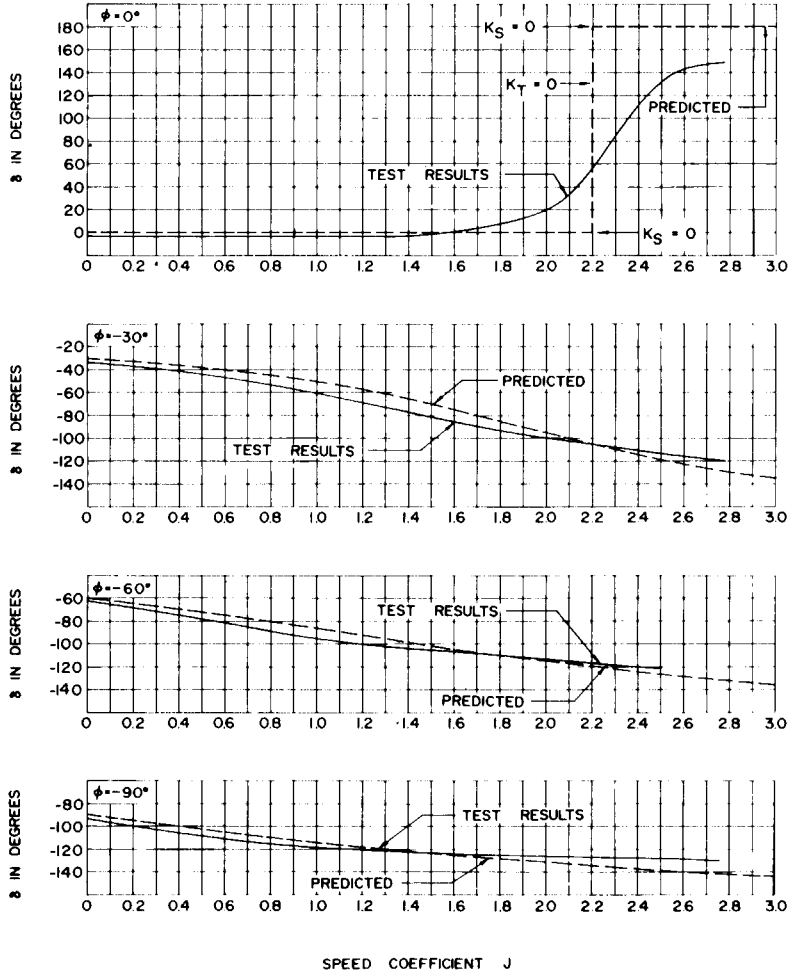

Figure 31d - Steering Angles in Fourth Quadrant

Figure 32 - Angle of Resultant Force Vector for 0.8π Pitch Ratio

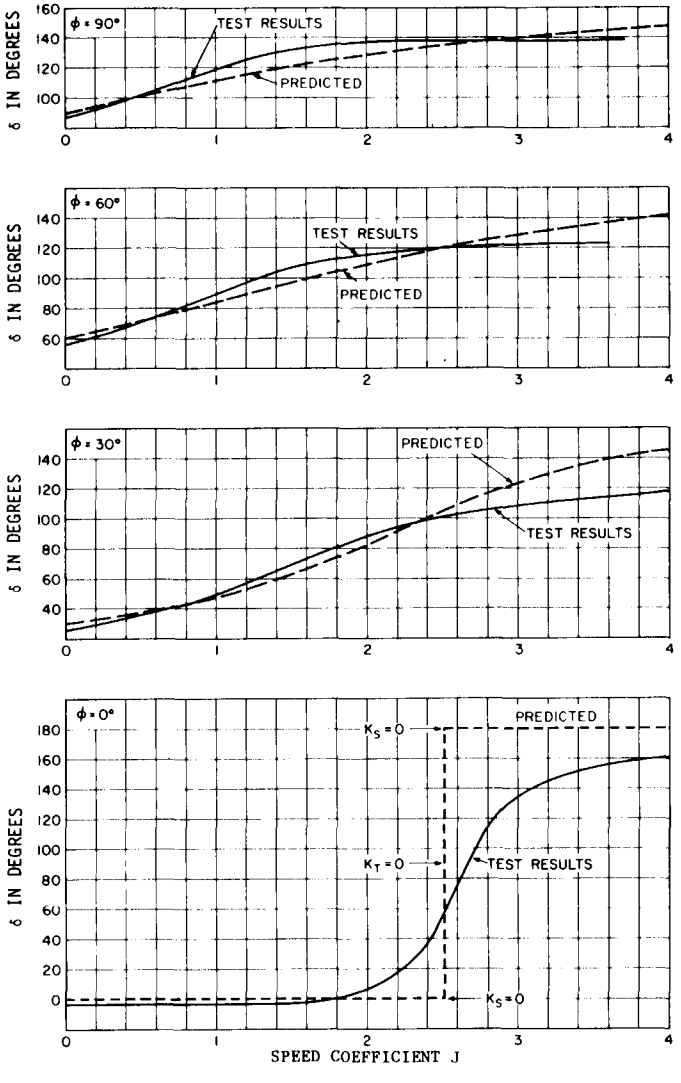

Figure 32a - Steering Angles in First Quadrant

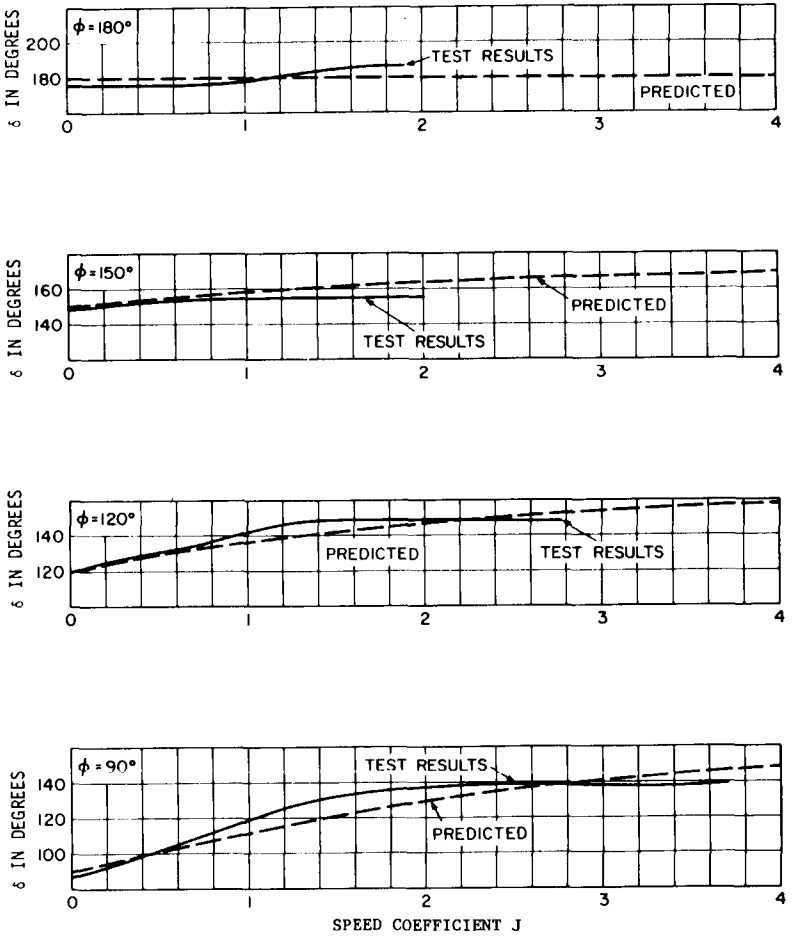

Figure 32b - Steering Angles in Second Quadrant

0.8π Pitch Ratio

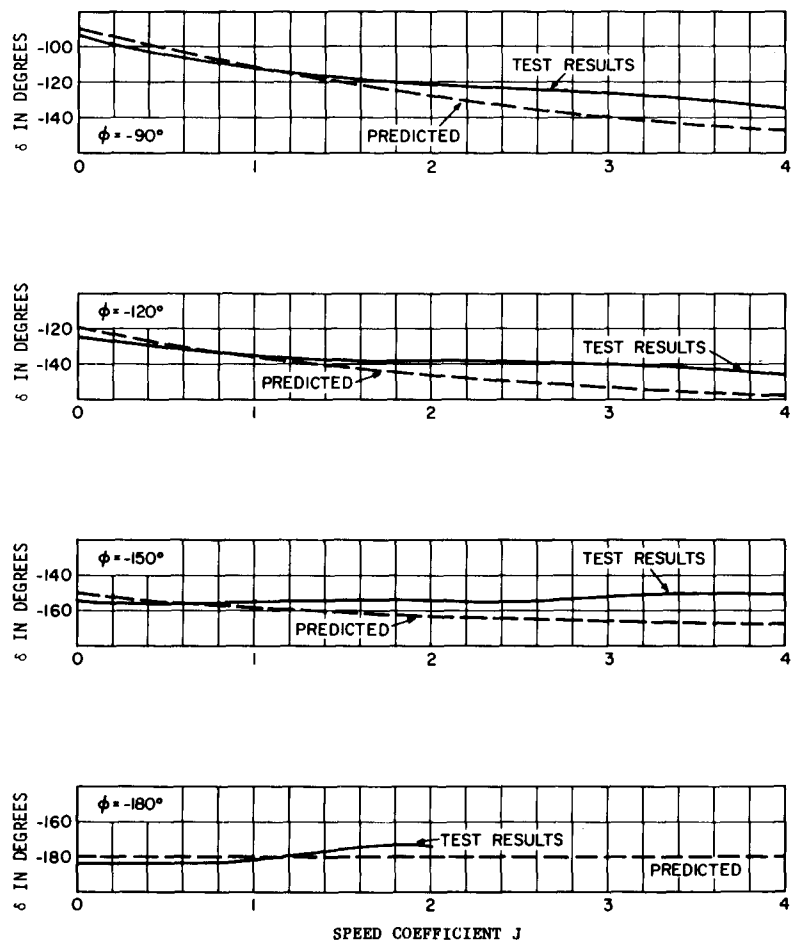

Figure 32c - Steering Angles in Third Quadrant

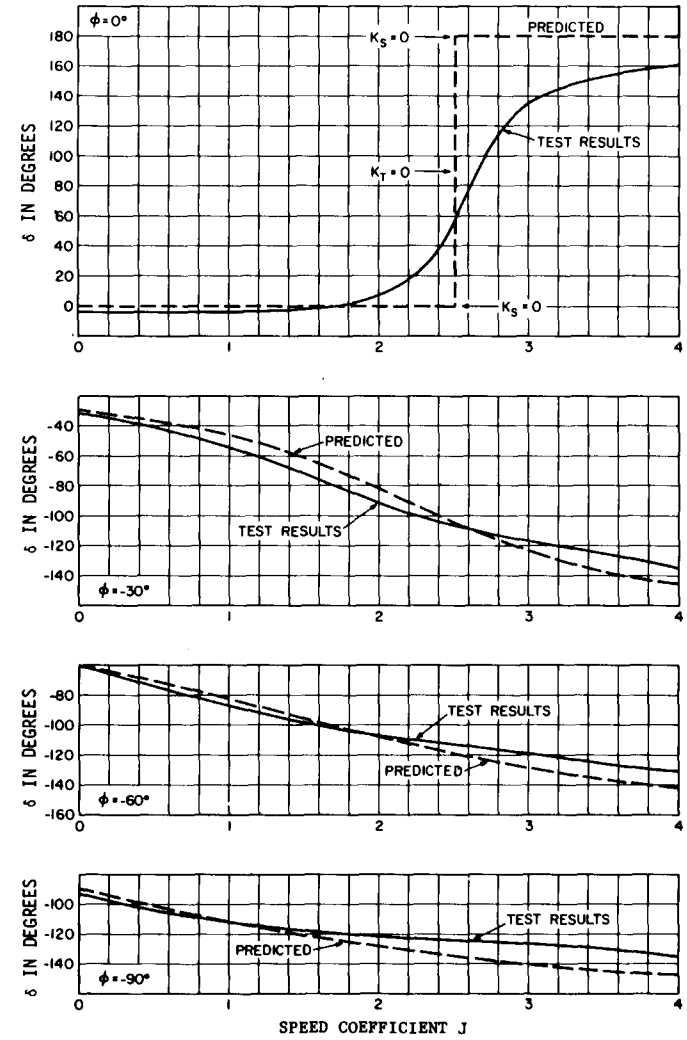

Figure 32d - Steering Angles in Fourth Quadrant

Figure 33 - Angle of Resultant Force Vector for 0.9π Pitch Ratio

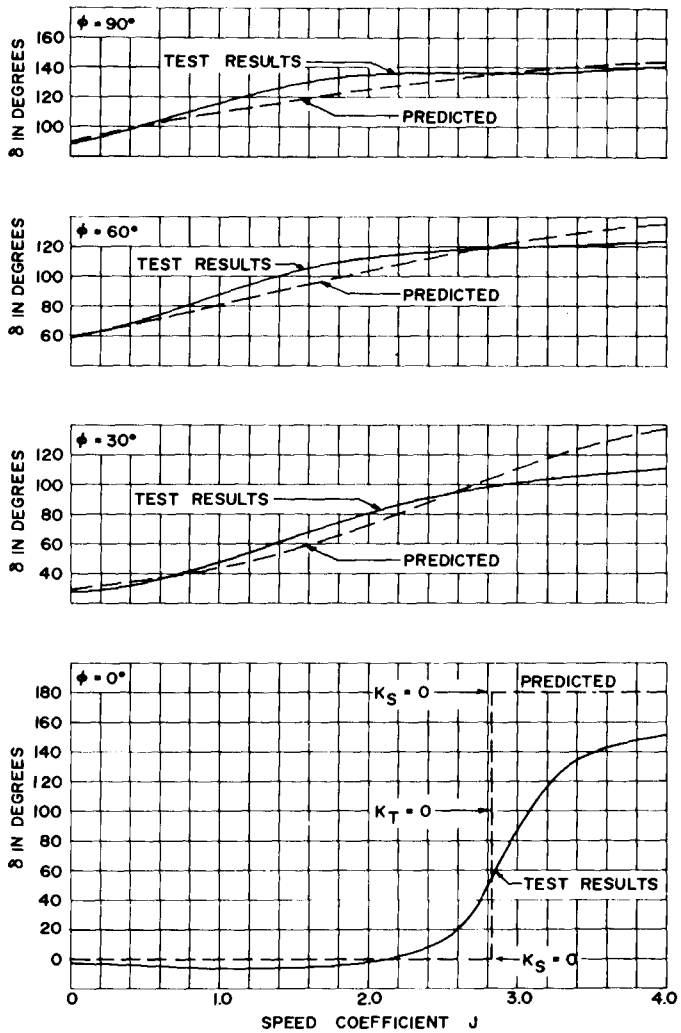

Figure 33a - Steering Angles in First Quadrant

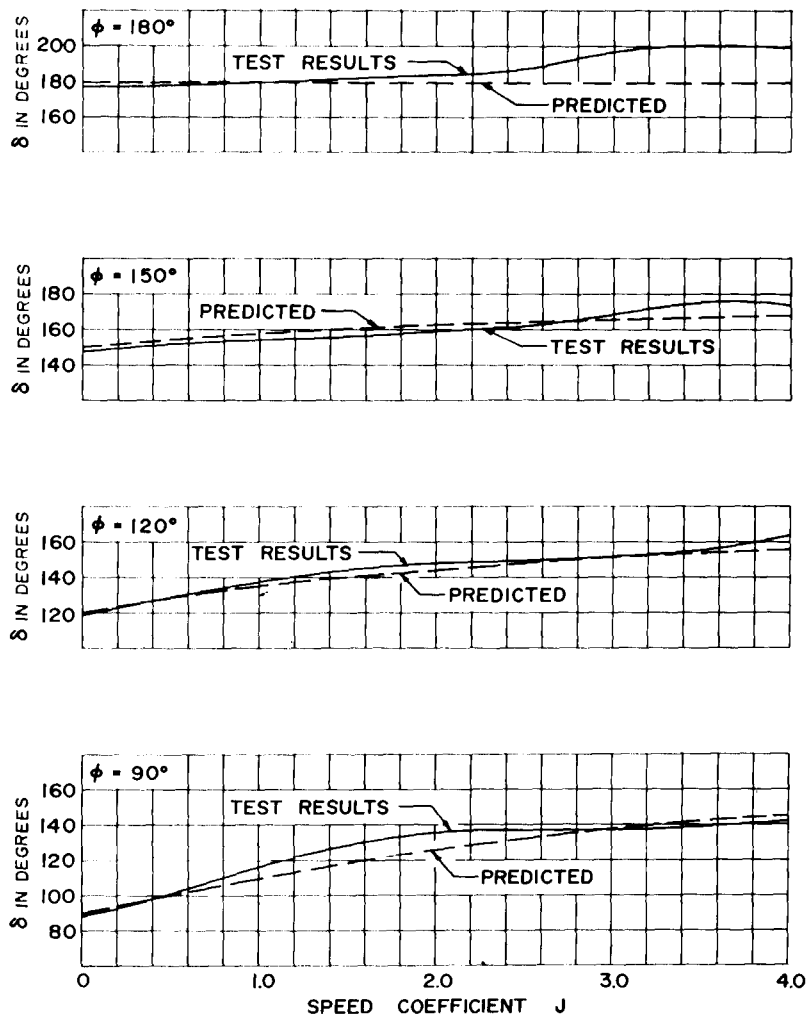

Figure 33b - Steering Angles in Second Quadrant

0.9π Pitch Ratio

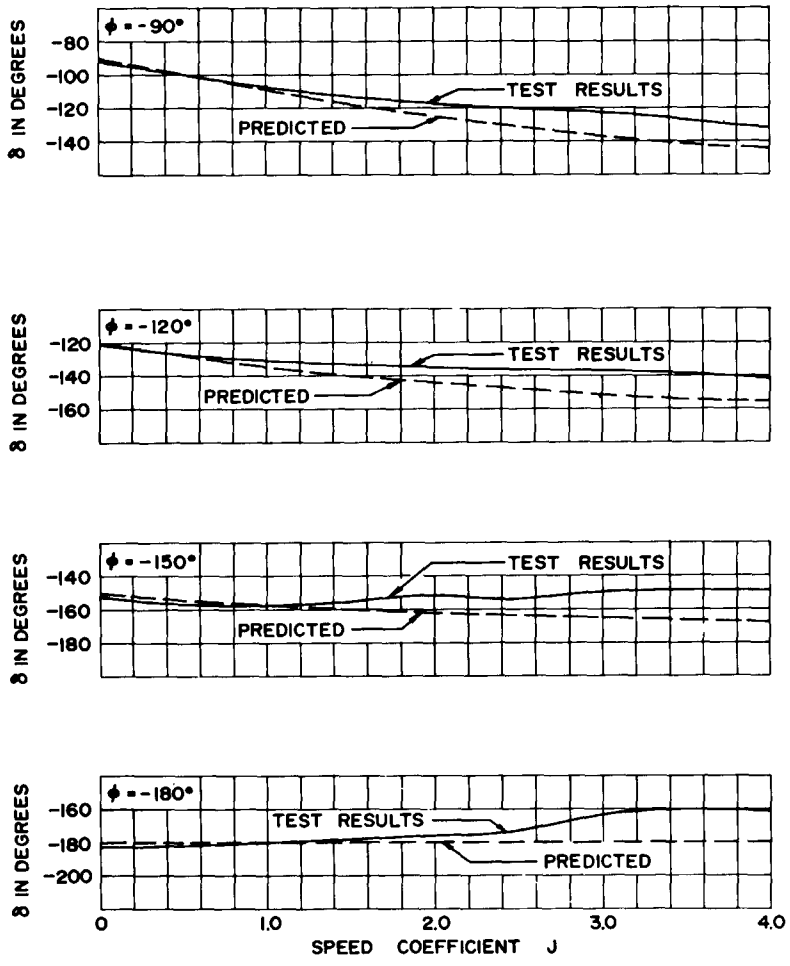

Figure 33c - Steering Angles in Third Quadrant

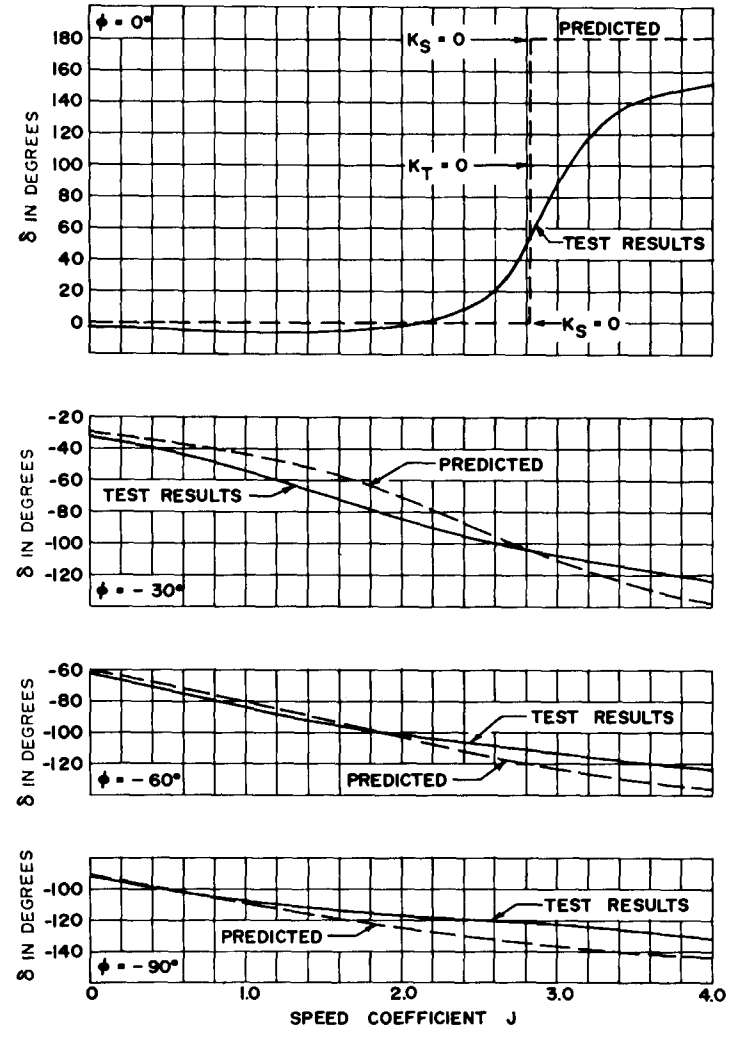

Figure 33d - Steering Angles in Fourth Quadrant

REFERENCES

1. Mueller, H.F., "Recent Developments in the Design and Application of the Vertical Axis Propeller," Transactions of Society of Naval Architects and Marine Engineers (SNAME), Vol. 63, pp. 4-30 (1955).

2. Goldsworthy, E.C., "Transverse Propulsion Using Voith-Schneider Propellers," Shipbuilding and Shipping Record (5 Sep 1963).

3. "Principles of Naval Architecture," (revised) Edited by John P. Comstock, SNAME, New York, (1967) pp. 431, 432, 418.

4. Kingsley, D.M., "Vertical Axis Propellers," presented to Northern California Section of SNAME (12 Dec 1957).

5. Nakonechny, B.V., "Experimental Performance of a Six-Bladed Vertical Axis Propeller," David Taylor Model Basin Report 1446 (Jan 1961).

6. Nakonechny, B.V., "Design of a 9-Inch Cycloidal Propeller-Model Unit and Some Experimental Results," NSRDC Report 3150 (in preparation).

7. Ficken, N.L., "Conditions for the Maximum Efficiency Operation of Cycloidal Propellers," presented to Chesapeake Section of SNAME (Apr 1966).

8. Bourne, J., "A Treatise on the Screw Propeller with Various Suggestions of Improvement," Longman, Brown, Green, and Longmans, London, (1855) pp. 4-5.

9. Kirsten, F.K., "A New Type of Propeller," Journal SAE (Jan 1928).

10. Sarchin, T.H., "The Hull-Propeller Relationship of the Oceanographic Research Ship T-AGOR," Third Annual Technical Symposium, Association of Senior Engineers, Bureau of Ships (Mar 1966).

11. Isay, W.H., "On the Treatment of the Flow Through a Voith-Schneider Propeller Having a Small Advance Coefficient," Bureau of Ships Translation 655C (Jun 1958). Ing. Archiv. Vol. 23, pp. 379-401 (1955).

12. Isay, W.H., "Zur Berechnung der Strönumg durch Voith-Schneider Propeller," Ing. Archiv. Vol. 24, pp. 148-170 (1956).

13. Isay, W.H., "Der Voith-Schneider Propeller in Nachstrom eines Schiffrumpfes," Ing. Archiv. Vol. 25, pp. 308-318 (1957).

14. Isay, W.H., "Ergänzungen zur Theorie des Voith-Schneider Propellers," Ing. Archiv. Vol. 26, pp. 220-232 (1958).

15. Taniguchi, K., "An Approximate Solution of the Voith-Schneider Propeller," Journal Zosen Kokai (Society of Naval Architects in Japan), Vol. 74, pp. 153-161 (1944).

16. Taniguchi, K., "Hydrodynamic Investigations of the Blade Wheel Propeller," Journal Zosen Kokai, Vol. 88, pp. 63-74 (1950).

17. Taniguchi, K., "Studies on a Trochoidal Propeller," Doctor of Engineering Thesis, Tokyo University (1960).

18. Haberman, W.L. and Caster, E.B., "Performance of Vertical Axis (Cycloidal) Propellers According to Isay's Theory," International Shipbuilding Progress, Vol. 9, No. 90, pp. 81-90 (Feb 1962).

19. Haberman, W.L. and Harley, E.E., "Performance of Vertical Axis (Cycloidal) Propellers Calculated by Taniguchi's Method," David Taylor Model Basin Report 1564 (Nov 1961).

20. Sparenberg, J.A., "On the Efficiency of a Vertical-Axis Propeller," Trans. Third Symposium on Naval Hydrodynamics, pp. 45-60 (Sep 1960).

21. van Manen, J.D., "Results of Systematic Tests with Vertical Axis Propellers," International Shipbuilding Progress, Vol. 13, pp. 382-398 (Dec 1966).

22. Voith, J.M., "Voith-Schneider Propulsion,"GMBH Heidenheim, Germany (undated).

23. Ficken, N.L. and Gawlik, S.G., "Model Flow Studies to Investigate Propeller Excited Vibrations on U.S. Army Ship LT. COL. JOHN V.D. PAGE (BDL-1X) Equipped with Vertical Axis Propellers," David Taylor Model Basin Report 1412 (Mar 1960).

24. McKillop, J.A., "A Study of the Flow Through a Vertical Axis Propeller," Engineering Research Associates Report 60/1 (Apr 1965).

UNCLASSIFIED

Security Classification

DOCUMENT CONTROL DATA - R & D

(Security classification of title, body of abstract and indexing annotation must be entered when the overall report is classified)

1. ORIGINATING ACTIVITY *(Corporate author)*

Naval Ship Research and Development Center
Washington, D.C. 20007

2a. REPORT SECURITY CLASSIFICATION

Unclassified

2b. GROUP

3. REPORT TITLE

EXPERIMENTAL PERFORMANCE AND STEERING CHARACTERISTICS OF CYCLOIDAL PROPELLERS

4. DESCRIPTIVE NOTES *(Type of report and inclusive dates)*

Research and Development Report

5. AUTHOR(S) *(First name, middle initial, last name)*

Norman L. Ficken
Mary C. Dickerson

6. REPORT DATE	7a. TOTAL NO. OF PAGES	7b. NO. OF REFS
July 1969	73	24

8a. CONTRACT OR GRANT NO.	9a. ORIGINATOR'S REPORT NUMBER(S)
b. PROJECT NO. S-F013 07 10, Task 3744 and	2983
c. S4632001, Task 12499	9b. OTHER REPORT NO(S) *(Any other numbers that may be assigned this report)*
d.	

10. DISTRIBUTION STATEMENT

This document is subject to special export controls and each transmittal to foreign governments or foreign nationals may be made only with prior approval of Naval Ship Research and Development Center, Code 500.

11. SUPPLEMENTARY NOTES	12. SPONSORING MILITARY ACTIVITY
	Naval Ship Systems Command

13. ABSTRACT

This report presents performance and steering characteristics of cycloidal propellers obtained from model tests for a series of cycloidal motions with pitch ratios ranging from 0.4π to 0.9π. Measured quantities included the thrust, torque, and side force. The tests showed that the direction and magnitude of the resultant force varies with loading and steering. For small steering angles, no significant effect of steering was observed on thrust or on efficiency. Most of the results presented here are for a six-bladed cycloidal propeller. Some performance characteristic curves obtained for a propeller with two and three blades are also included for comparison.

DD FORM 1 NOV 65 1473 (PAGE 1)

S/N 0101-807-6801

UNCLASSIFIED

Security Classification

14. KEY WORDS	LINK A		LINK B		LINK C	
	ROLE	WT	ROLE	WT	ROLE	WT
Propellers						
Cycloidal Propeller						
Vertical axis Propellers						
Maneuvering Capabilities						